Computer Aided Analysis and Design of Off-Road Motorcycle Suspensions

Mark van Vliet

A Thesis

in

The Faculty

of

Engineering

Presented in Partial Fulfillment of the Requirements
for the degree of Doctor of Philosophy at
Concordia University
Montreal, Quebec, Canada

October 1983

ABSTRACT

Computer Aided Analysis and Design of Off-Road Motorcycle Suspensions

Mark van Vliet
Concordia University, 1983

In this dissertation, a design methodology is developed to effectively analyze and improve the performance of off-road motorcycle suspensions. The methodology utilizes mathematical models which are developed from basic principles. A typical front fork and rear shock absorber are mathematically modeled to independently express the damper force equations and suspension system characteristics, in both compression and extension strokes. The damper force models are intended primarily for experimental verification using existing industrial procedures, whereas the suspension system model is used in innovative design procedures.

Fundamental laws of fluid flow and dynamics are used to develop the non-linear expressions for damper force. A digital and an analog computer are used for simulating the damper force models of the front fork and rear shock absorber, respectively. Laboratory experiments are carried out to verify the results obtained by simulation. The results indicate good correlation between theoretical and experimental work.

A mathematical model of the suspension system characterized by a second order non-linear differential equation is developed. The non-linearities in the model include: slip-stick motion due to seal friction, quadratic damping due to the orifices, and an air spring due to the

entrapped column of air. Theoretical responses of the suspension system for harmonic and velocity step excitation are obtained using a numerical integration technique. Laboratory experiments are carried out and the results are correlated to those obtained by computer simulation. The results show excellent agreement. Suspension performance indices are then introduced in the frequency and time domains. Each performance index is used to formulate an objective function, for each domain, and a numerical optimization method is applied. The results are discussed and an existing suspension is modified using a set of optimal design parameters. The predicted optimal performance is verified in the laboratory using the modified suspension.

The investigation is extended to include the stochastic response of the motorcycle suspension. The excitation spectrum is obtained from field measurements. Once the nature of the excitation and system model is known, analytical techniques for obtaining the stochastic response are reviewed. A suitable technique (equivalent linearization) is selected and the performance of various innovative techniques is compared. The most suitable technique (discrete-harmonically linearized force method) is then applied and the stochastic response of the suspension system is obtained. A performance criteria is formulated and a numerical technique is applied, yielding a set of optimal design parameters. The procedure is verified in the laboratory by comparing the predicted response of the optimized suspension with the response of a modified hardware model.

ACKNOWLEDGEMENTS

The author is deeply indebted to his supervisor, Dr. S. Sankar, for his dedicated guidance, encouragement, and expertise throughout the course of this investigation.

The author is grateful to Mrs. I. Crawford for typing the manuscript and to Mr. R. Guevara for drafting assistance.

Thanks are due to the numerous faculty members, Computer Centre personnel, and technical support staff for their contributions to this effort.

The financial support provided by the assistantships, fellowships, and scholarships, funded by the Department of Mechanical Engineering, Concordia University, and the Natural Sciences and Engineering Research Council is gratefully acknowledged.

Finally, the author would like to express his appreciation for the personal encouragement provided by his wife, members of his family, fellow students, and friends, during the course of this undertaking.

TABLE OF CONTENTS

LIST OF FIGURES

LIST OF TABLES

NOMENCLATURE

a	outer annular diameter, m
A_{hyd}	flow area at hydraulic stop, m^2
A_i	i^{th} flow area, m^2
A_p	cross-sectional piston area, m^2
A_r	cross-sectional rod area, m^2
A_{tube}	stanchion tube area, m^2
A_{vi}	i^{th} valve ball area, m^2
A_i^*	orifice area at i^{th} location on damper rod, m^2
$\hat{A}_i^*$	orifice area at i^{th} location on piston, m^2
b	inner annular diameter, m
c	damping coefficient, N-s/m
C_d	orifice discharge coefficient
d_i	i^{th} orifice diameter, m
d_p	diameter of piston, m
d_{vi}	i^{th} valve ball diameter, m
D	weighing factor
$E[\ ]$	expected value of [ ]
f	excitation frequency, Hz
f_n	natural frequency, Hz
f_p	frequency at which the peak transmissibility occurs, Hz
F	force, N
F_{coul_1}	fork leg coulomb friction, N
F_{coul_2}	guidance bearing coulomb friction, N
F_d	damper force, N
F_g	ground load, N

F_{hyd}	effective hydraulic stop force, N
F_k	spring force, N
F_{opt}	optimal force, N
F_p	peak force; N
F_{seal_1}	fork leg seal stiction, N
F_{seal_2}	guidance bearing seal stiction, N
F_t	transmitted force, N
g_i	i^{th} constraint
h	fluid height, m
H	binary constant
H_a	absolute transmissibility
H_r	relative transmissibility
I	performance index
I_f	frequency domain performance index
I_r	random domain performance index
I_t	time domain performance index
k	helical spring constant, N/m
k_i	i^{th} relief valve spring constant, N/m
ℓ	piston ring length, m
L	laminar flow coefficient, N-s/m
m	mass, kg
$\hat{MRT}$	constant, N-m
n_i	i^{th} geometric constant
p	pressure, Pa
p_a	pressure on accumulator side of piston, Pa
p_{at}	atmospheric pressure (absolute), Pa
p_b	pressure on rod side of piston, Pa

p_i	i^{th} control volume pressure, Pa
p_o	initial gas pressure, Pa
$\hat{p}$	pressure (absolute), Pa
q	response quantity
Q	flowrate, m^3/s
Q_p	flowrate through piston, m^3/s
Q_i^*	flowrate through i^{th} orifice, m^3/s
S_a	absolute acceleration power spectrum, m^2/s^4
S_i	input acceleration power spectrum, m^2/s^4
S_z	relative displacement power spectrum, m^2
t	time, s
T	turbulent flow coefficient, kg/m
T_{hyd}	turbulent flow coefficient for the hydraulic stop, kg/m
T_{or}	turbulent flow coefficient for the damper rod orifice, kg/m
T_p	turbulent flow coefficient for the piston, kg/m
TR	transmissibility
TR_h	transmissibility in the higher range
TR_p	peak transmissibility
u_j	j^{th} relief valve displacement, m
$u_{j,i}$	preloaded displacement of j^{th} relief valve, m
$u_{j,max}$	maximum displacement of j^{th} relief valve, m
U	objective function
U_f	frequency domain objective function, m
U_m	modified objective function
U_t	time domain objective function, m/s
v_i	initial velocity, m/s
v_i^ℓ	lower bound on initial velocity, m/s

v_i^u	upper bound on initial velocity, m/s
V	volume, m^3
V_o	initial volume, m^3
x	displacement of mass, m
$\underset{\sim}{X}$	vector containing optimization parameters
y	input displacement, m
Y	excitation amplitude, m
Y^ℓ	lower bound on excitation amplitude, m
Y^u	upper bound on excitation amplitude, m
z	relative displacement, m
z_{max}	maximum allowable travel, m
Z_c	location of hydraulic stop, m
Z_i	location of i^{th} damper rod orifice, m
α	perturbation parameter
ϵ	velocity increment, m/s
γ	specific weight of the damper fluid, N/m^3
μ	dynamic viscosity of the damper fluid, $N\text{-}s/m^2$
ρ	mass density of the damper fluid, kg/m^3
$\dot{}$	a dot represents differentiation with respect to time

CHAPTER 1

INTRODUCTION

CHAPTER 1

INTRODUCTION

1.1 General

The popularity of motorcycles has grown steadily over the years. This increase can be attributed to many sources, but one reason for the growth is the steady technical evolution of the motorcycle. Motorcycles have become very sophisticated vehicles which appeal to a large cross-section of people, and like other vehicles, have become more and more specialized. Each type has its own technical history. In many cases technological improvements in one type of motorcycle have led to improvements in other types. An example of this process is the recent overall improvement in motorcycle suspension design due to the development of motorcycles specifically designed for motocross racing.

Motocross involves racing the motorcycle over a closed loop natural terrain course. The terrain can consist of sand, grass, mud, rocks, clay, silt or any possible combination of natural environment. The course contour can vary from rolling hillsides to square-edged bumps. Motocross motorcycles represent a particularly interesting type of vehicle because they are required to negotiate such difficult terrain at the limits of control while maintaining an environment for the rider which is not overly fatiguing. The suspension system on such motorcycles is vital and its effectiveness is highlighted by the racing environment. Since the early 1970's motocross suspensions have seen increasing innovation and improvement. The benefits of this development is permeating the other types of motorcycles.

At present, in most of the motorcycle industries, suspension

development is carried out based on the subjective assessment of the rider in field testing. There has been very little analytical and/or numerical work done in this area. It is the objective of this investigation to establish a computer-aided design procedure using analytical and numerical techniques.

1.2 Literature Review

Previous investigations in suspension research include a diversity of topic areas. The literature in the area of motorcycle suspension contributes a small sector in the field of suspension research, however since it is the focus of this investigation it is reviewed as a separate topic in the following Subsection 1.2.1. Extensive research has been performed in related topic areas such as automotive, aircraft, and railway suspensions. Whenever possible the methods used in such areas and the concepts presented in theoretical work are employed in this investigation. A review of the literature in related topic areas is given in Subsection 1.2.2.

1.2.1 Motorcycle Suspensions

The telescopic front fork found on virtually every mass produced motorcycle today dates back to the late 1930's [1]. Three other configurations were also popular in the 1930's; the girder, leading link, and trailing link, as illustrated in Fig. 1.1. The leading link design was popular on American built machines whereas the girder design was much more common on European built motorcylces [2]. The linkage designs employed adjustable friction dampers to control the relative motion between the links, whereas telescopic forks used hydraulic dampers to control suspension travel [3]. The development of oleo-pneumatic

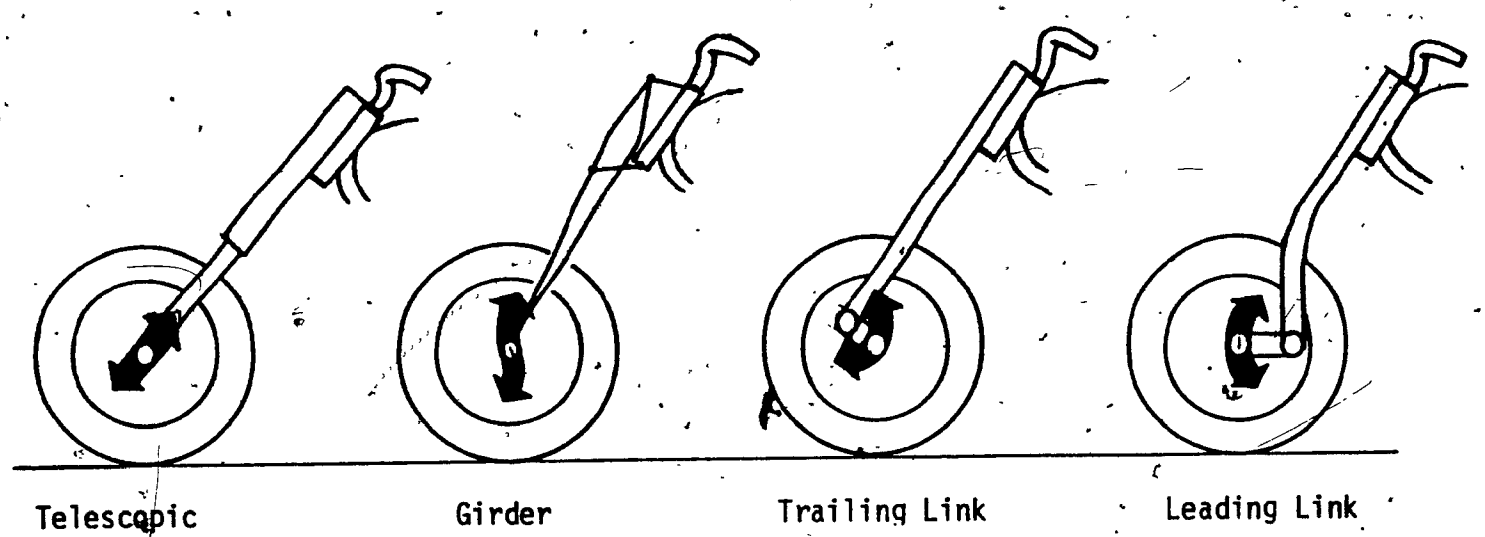

Fig. 1.1: Front Suspension Configurations

suspension struts during World War II brought significant advances to the industry so that by the mid 1950's the telescopic front fork could be found on nearly every production motorcycle [4]. The next two decades saw little improvement in motorcycle suspension until the popularization of off-road racing in the early 1970's [5].

The majority of the literature published in the last decade is descriptive in nature. Some articles [6-12] update the enthusiast about the developments in motorcycle suspension technology, whereas others [13-16] supply information regarding modifications so that the suspension might meet the individuals requirements. A comprehensive design text which includes practical considerations for suspension design has been published by Irving [2]. Although somewhat out-dated, the text offers the reader an overview of the engineering highlights of the motorcycles from the 1950's. An experimental investigation into motorcycle suspension damping characteristics has been published by Jennings [17]. The damping characteristics of various suspensions were recorded in a laboratory and then correlated with test rider results. The significant contribution of the paper is the physical insight obtained by correlating the laboratory data with rider feedback.

The use of analytical and/or numerical techniques by the motorcycle industry appears to be very limited regarding suspension developement. Harley-Davidson Motor Co. (USA) is reportedly [18] using extensive computer simulation in the power-train department, however there haven't been any reports of suspension simulation. Bombardier Ltd. (Canada) has investigated rear suspension geometry [19] with the aid of a desk top computer. Works Performance Inc. (USA), a major aftermarket suspension

component manufacturer, also uses a desk top computer to generate static suspension characteristics and estimate damping requirements (based on empirical formulae) for individual customer requirements [20]. Kayaba Industries Co. (Japan), manufacturer of suspension components used by all four Japanese motorcycle manufacturers, appears to be the only industry employing analytic and numerical techniques in suspension development. Obata [21] reports the use of a simplified analytic model in conjunction with test rider reports as part of a suspension development flowchart at Kayaba Industries, however no results are published.

Several investigators [22-25] have studied motorcycle handling characteristics as influenced by a variety of factors, however only Roe [26] considers the influence of front fork flexibility. He shows that the inherent low lateral stiffness of the telescope fork is the most important parameter limiting the maximum stable road speed. He then proposes a leading-link design possessing high lateral stiffness. Other investigators [2,27] show agreement with his observations. The leading-link design is commercially available on the aftermarket [28], however it is not offered on any mass produced motorcycle.

A four-degree-of-freedom model of the motorcycle has been investigated by Black and Taylor [29]. The salient points of the model are:

i) Non-linear geometry.

ii) Non-linear damping and stiffness.

iii) Variable ratio of compression to rebound damping.

iv) Limited suspension travel and wheel deflection.

v) Wheel lift-off.

vi) Tire models which produce horizontal forces and roll over

obstacles in the sense of behaving like a low pass filter. They present the results of a computer simulation. However, this study does not experimentally verify the non-linear parameters or the results, nor does it show the effect of a change in the system parameters on the response. Consequently, it doesn't propose any design guidelines regarding motorcycle suspension.

1.2.2 Related Topics

In this section the literature in areas related to motorcycle suspension is reviewed. The review is comprehensive with respect to those areas only in the sense of advances which contributed to this investigation.

1.2.2.1 Ground Vehicles

Much of the literature in the area of automotive suspension, like motorcycle suspension, is descriptive in nature [30-32]. Another major portion of automotive literature is concerned with the handling aspects of automobiles [33-35]. Unlike the motorcycle suspension area, there have been several significant analytical developments in the automotive suspension area. Lang [36] has presented a detailed model of the automotive shock absorber (damper) as an isolated component. Salient points of the model include:

i) Compressible fluid flow.

ii) Elastic cylinder wall.

iii) Unsteady flow through the orifices.

iv) Valve dynamics.

v) Leakage flow.

The damper force is simulated on an analog computer and verified by experiment. Unfortunately, the type of excitation used in the simulation does not represent the actual suspension environment [37] and hence the range of applicability of the model is limited. Dinca and Teodosiu [38-40] have presented a detailed model of the shock absorber. In addition to modelling non-linearities, they consider the response of the vehicle to a random road profile. Where possible, the equations are simplified and a closed form solution presented. Ariaratnam [41] has applied the Fokker-Planck equation to a non-linear vehicle model to obtain the exact response to a "white" road input. The limitation of these two approaches is that the range of practical problems to which exact methods can be applied is very restricted [42]. A comprehensive review of the literature regarding automobile ride quality has been given by Smith [43]. Strikeleather et al [44] have pioneered work in the classification of ride comfort. Of particular relevance to this investigation is the treatment of random measurements by Strikeleather as well as Butkumas [45] and Healey [46,47]. Corbin and Kaufman [48] have stated guidelines for using power spectral densities as applied to railway measurements. A comprehensive literature survey in railway vehicle dynamics has been given by Law and Cooperrider [49]. Other relevant work regarding the laboratory simulation of road conditions has been published by Cryer et al [50] and Dodds [51]. Cryer et al introduce a unique road profiling technique so that a particular roadway can be used as the input, or the statistics of a class of roadways can be used. Dodds has shown how synthesized random displacements can be obtained from a single traverse along the road. Both works show excellent agreement between laboratory and field measurements.

The optimization of vehicle suspensions subject to random input is a vast topic in itself, however there are several outstanding works which have been extensively used as support work for this investigation. Thompson [52] has used analog computer studies to obtain the optimal ratio of bump to rebound damping rates using an integral-square criterion. Dahlberg [53] optimized vehicle suspension parameters using numerical techniques. He has also introduced elaborate performance indices (to be used in the optimization) and demonstrated the practical limitations of multi-parameter optimization verses computer costs [54].

The interesting possibility of using active suspension components is beyond the scope of this investigation, however a brief overview of the possibilities is admissible. Bender [55] has shown that a reduction in the rms acceleration response level of 16 to 1 over passive systems is theoretically possible while still maintaining low tire loads. The theoretical advantages verses the practical disadvantages of active suspensions has been discussed by Karnopp [56], Bender [57], and Sutton [58]. An extensive literature review on active suspensions has been presented by Hedrick and Wormley [59].

1.2.2.2 Aircraft

The relevant literature in the area of aircraft studies falls into two categories; analysis of aircraft landing gear during touchdown, and during taxying over the runway surface. Habekil [60] has presented a detailed mathematical model of aircraft landing gear. A more detailed model including the effects of fluid compressibility has been presented by Wahi [61]. He has used analog simulation supported by drop test data

to verify some of his work [62]. Venkatesan and Krishnan [63] have shown that the application of dual phase damping to an aircraft landing gear yields significant performance increases during touchdown over fixed orifice damping. Venkatesan has also shown [64] that non-linear damping gears are more practical than intricate, truely linear, damping gears. Venkatesan and Nagara have optimized the non-linear parameters [65] and have suggested the use of dual rate stiffnesses to obtain maximum performance from the landing gear.

The earliest results of runway roughness studies were presented by Walls et al [66]. A very comprehensive elaboration of Walls work was performed by Thompson [67]. Thompson's paper contains 80 pages of power spectral density plots from runways around the world. Houbolt [68] has outlined steps for practical measurement as well as analog and digital roughness simulation schemes. Silby [69] appears to be the first investigator to use an analytic (linear) model of the airplane in runway roughness studies. A very in depth analysis and simulation has been performed by Tung et al [70]. Tung applied numerical integration routines to a non-linear suspension model to obtain the deterministic response. He then used a combination of linearization techniques to obtain statistics of the random response. A simulation of a non-linear model in the time domain using time histories for input data has been presented by Gerardi and Lohasser [71].

1.3 Scope of the Investigation

In this investigation, a computer aided analysis and design methodology is presented. The material is developed with the introduction of mathematical models for the damper units found on the off-road

motorcycle. The remaining suspension components in the front suspension are also modeled and a suspension system model is formulated.

In Chapter 3 the damper force models are used in both digital and analog computer simulation. The results are compared to in-house laboratory results. The computer simulation is extended in Chapter 4 to the mathematical model of the suspension system. Results are obtained using the non-linear model in both the frequency and time domains. As with the damper force model, experimental verification of the results is carried out in both domains.

In Chapter 5, performance criteria are developed in the frequency and time domains based on the interrelationship of the dynamic quantities of interest. These performance criteria are used to formulate objective functions in Chapter 6. Suitable numerical optimization methods are then applied, yielding an optimally designed suspension in each domain. The optimal design procedure is verified by modifying an existing suspension with the optimally found design parameters, and comparing the performance in the laboratory with that predicted by the optimal design procedure.

The analysis is extended for the stochastic excitation in Chapter 7. The statistics of terrain-induced excitation are measured and presented. The various analytical techniques and their applicability to the present investigation are discussed. A suitable technique is selected and several variations of the technique are applied to the problem. The results are compared and the most suitable approach is used together with a numerical optimization scheme in order to obtain an optimal suspension design based on the stochastic response. The optimal design procedure is then verified using a suitably modified suspension and comparing the

results obtained in the laboratory with those previously obtained in the optimization procedure. Finally, a discussion of the results, conclusions, and recommendations for future work are presented in Chapter 8. To gain confidence in the computer aided design methodology developed for motorcycle suspensions, extensive validation of the mathematical models has been carried out with appropriate experimental data. The validation is discussed in various Chapters and Appendix IV.

CHAPTER 2

DEVELOPMENT OF MATHEMATICAL MODELS

CHAPTER 2

DEVELOPMENT OF MATHEMATICAL MODELS

2.1 Introduction

In this chapter, mathematical models are formulated for the front and rear suspension elements of an off-road motorcycle. The motorcycle suspension normally consists of a telescopic front fork and rear swinging arm as shown in Fig. 2.1, Various suspension configurations are presently in use, however they all stem from the same basic design. Table 2.1 contains comparative data on commercially available motorcycle suspensions during the 1980 production year.

The telescopic front fork typically consists of a pair of frame mounted stanchion tubes which slide into wheel mounted sliders. The relative displacement is controlled by internal springing and damping units as shown in Fig. 2.2. The springing is achieved by a helical spring and pressurized air column. The damping is effected by stiction (seal friction) and the restriction of oil flow through several passageways. When the motorcycle encounters a bump, the slider moves up the stanchion tube, storing energy in the helical spring and air column. At the same time, energy is dissipated by stiction and oil-flow restrictions. As the slider moves up the stanchion tube, the oil trapped beneath the piston lifts the piston valve off its seat and passes through the piston. In addition to the flow past the piston, oil flows through the damper rod orifice due to the volume of stanchion tube entering the slider. The flow is further restricted at large relative displacements when the hydraulic stop is encountered. On the return or extension stroke the oil that is trapped above the piston causes the valve to drop onto its

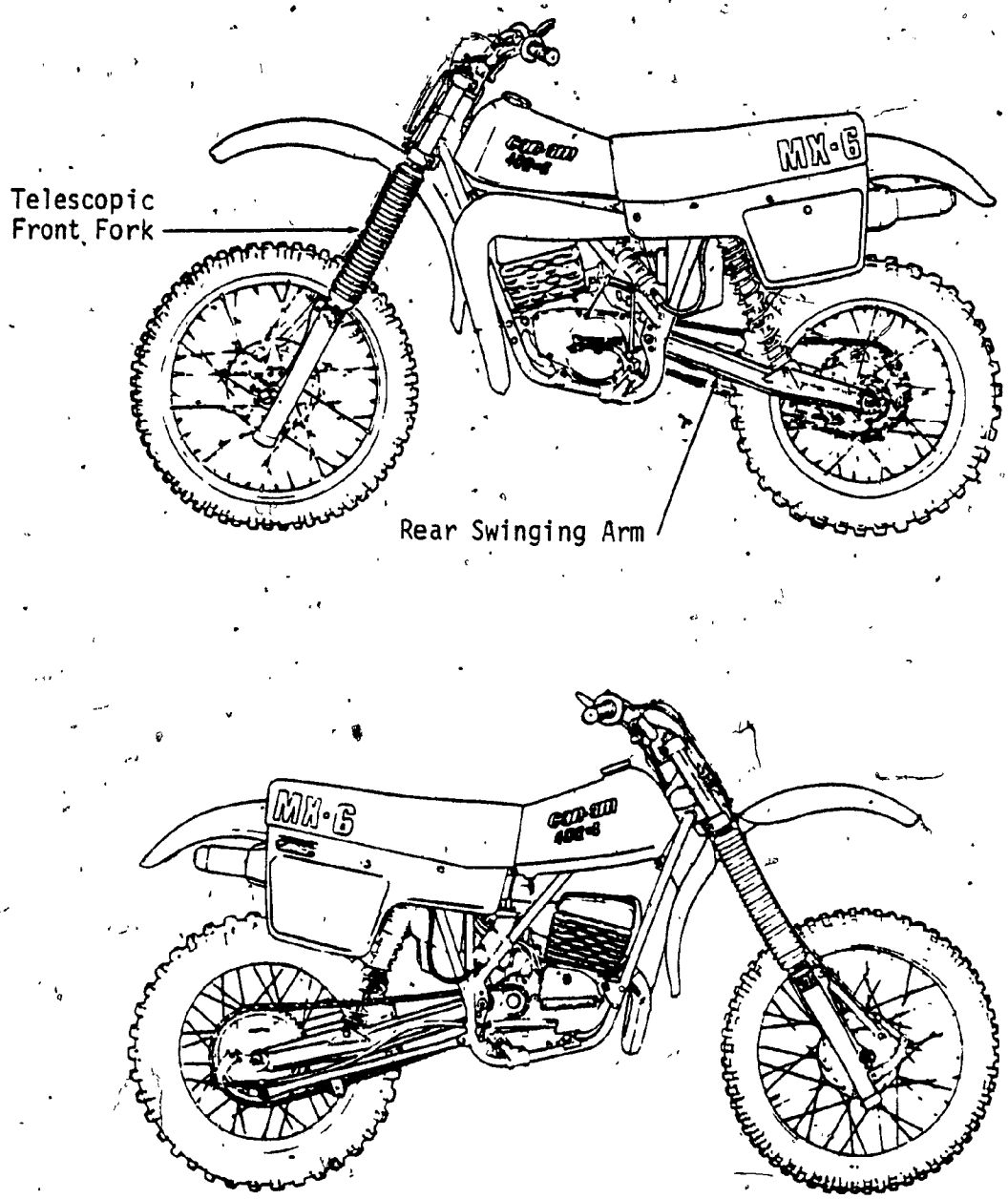

Fig. 2.1: An Off-Road Motorcycle (Reproduced with the Permission of Bombardier Ltd.)

TABLE 2.1: Commercially Available Motorcycle Suspensions
(sample only)

Motorcycle Manufacturer	Front Suspension				Rear Suspension		
	Manufacturer	Type	Wheel Travel, mm	Tube Dia, mm	Manufacturer	Type	Rear Wheel Travel mm
Can Am (Canada)	Marzocchi (Italy)	air/spring	292	38	Ohlins (Sweden)	Dual shock	274
Can Am (Canada)	Betor (Spain)	air/spring	203	35	Monroe (Canada)	Dual shock	165
Honda (Japan)	KYB[1] (Japan)	air/spring	300	41	Showa (Japan)	Single shock linkage	317
Husqvarna (Sweden)	Husqvarna (Sweden)	air/spring	300	40	Ohlins (Sweden)	Dual shock	315
Kawasaki (Japan)	KYB (Japan)	air/spring	287	38	KYB (Japan)	Single shock linkage	284
Maico (Germany)	Maico (Germany)	air/spring	312	42	Corte Cossa (Italy)	Dual shock	315
Montessa (Spain)	Marzocchi (Italy)	air/spring	292	38	Marzocchi (Italy)	Dual shock	279
Suzuki (Japan)	KYB (Japan)	air/spring	284	38	KYB (Japan)	Dual shock	300
Yamaha (Japan)	KYB (Japan)	air/spring	289	43	KYB (Japan)	Single shock	305

[1]Kayaba Industries

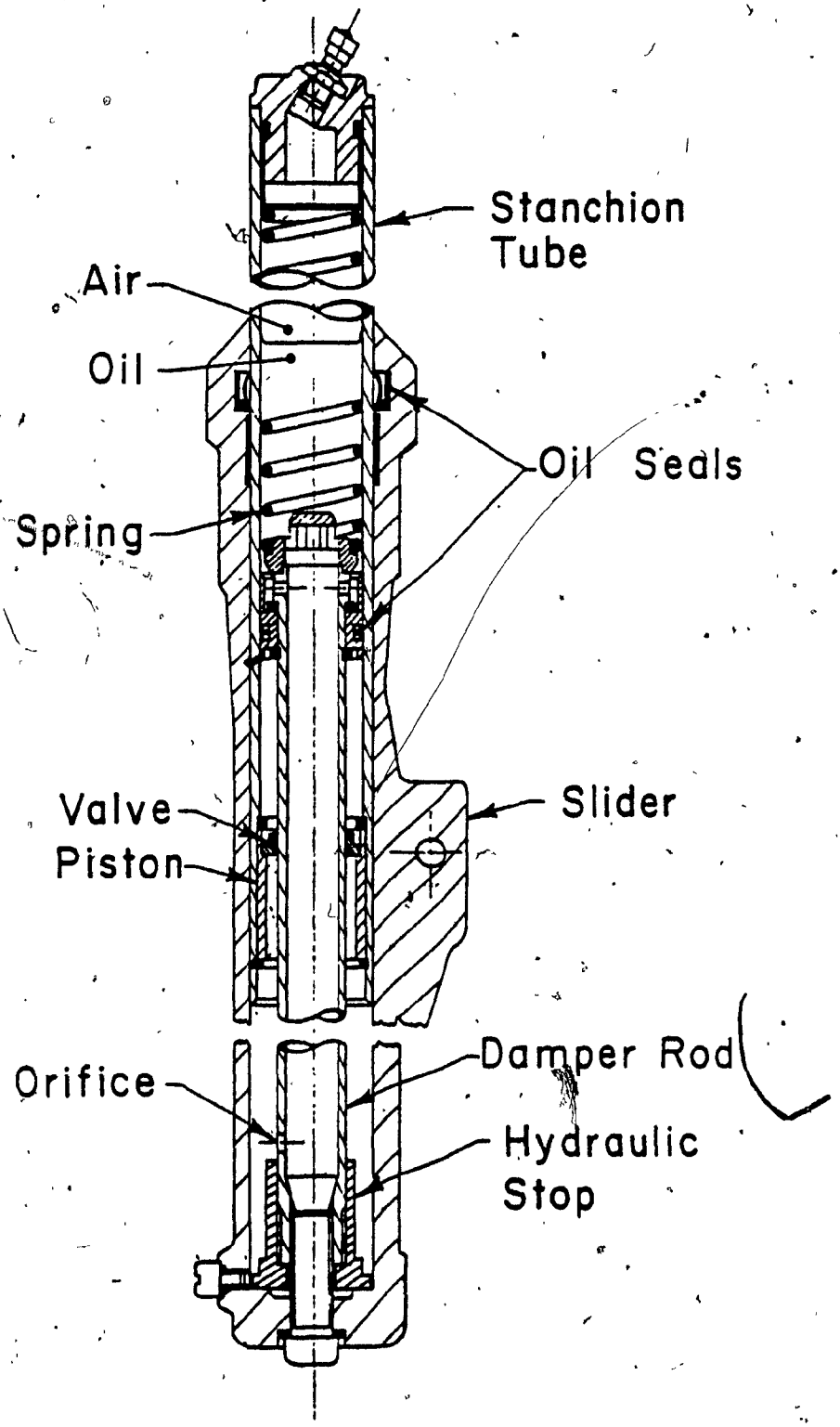

Fig. 2.2: Cross-Sectional View of a 38 mm Marzocchi Fork Leg

seat, providing an added restriction.

Without exception the rear suspension consists of a swinging arm pivoting on a frame member (near the countershaft sprocket) to which the rear wheel is attached. The arc of wheel travel is roughly vertical as shown in Fig. 2.3. At present, several shock absorber (damper) and spring configurations are used to control the swing arm motion. The most common configuration is a "dual shock" setup in which a shock absorber with external spring is mounted on each side of the motorcycle. The shock absorbers are often cantered forward from the vertical so that a rising spring rate with wheel travel is experienced at the rear wheel [19]. Recently several manufacturers have employed linkages to transmit the swing arm motion to a single shock absorber and external spring [6;10]. The principle advantages of the linkage systems are: increased frame stiffness, decreased unsprung mass, and reduced shock absorber speeds. These attributes are offset by increased complexity and decreased cooling due to the inboard location of the shock absorber [72-74].

A schematic of several rear shock absorbers is shown in Fig. 2.4. In order to accommodate the piston rod volume, a gas charged accumulator or freon-cell is used. These devices provide springing in addition to the external helical spring. Some manufacturers charge the accumulators to a high pressure (about 1 MPa) to reduce cavitation, however this also increases the spring pre-load, which raises the static ride height of the motorcycle. The damping is effected by stiction and the restriction of oil flow past the piston. Typically the piston contains a set of hydraulic valves which respond to the pressure drop across the piston and the direction of relative velocity.

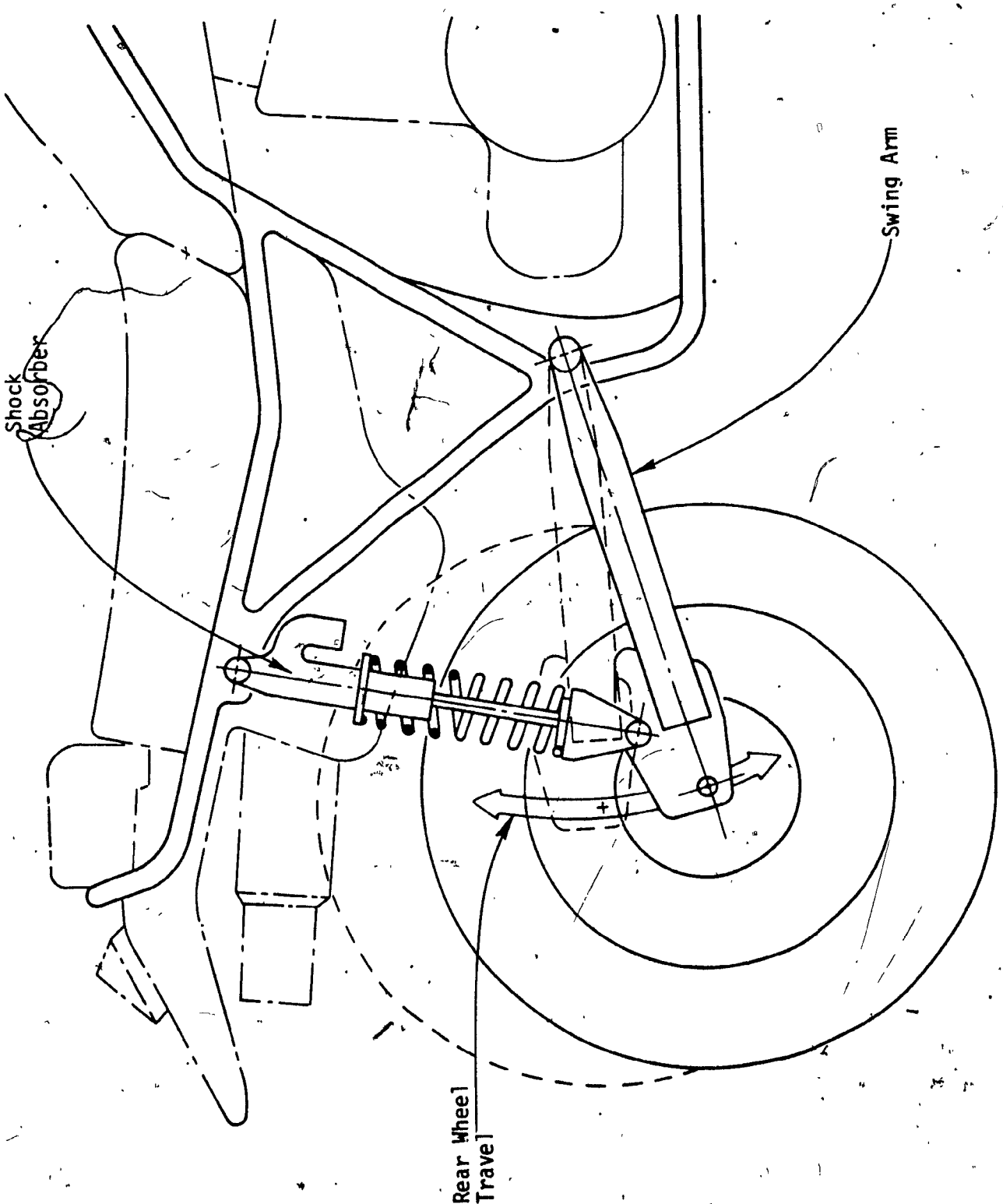

Fig. 2.3: Rear Suspension

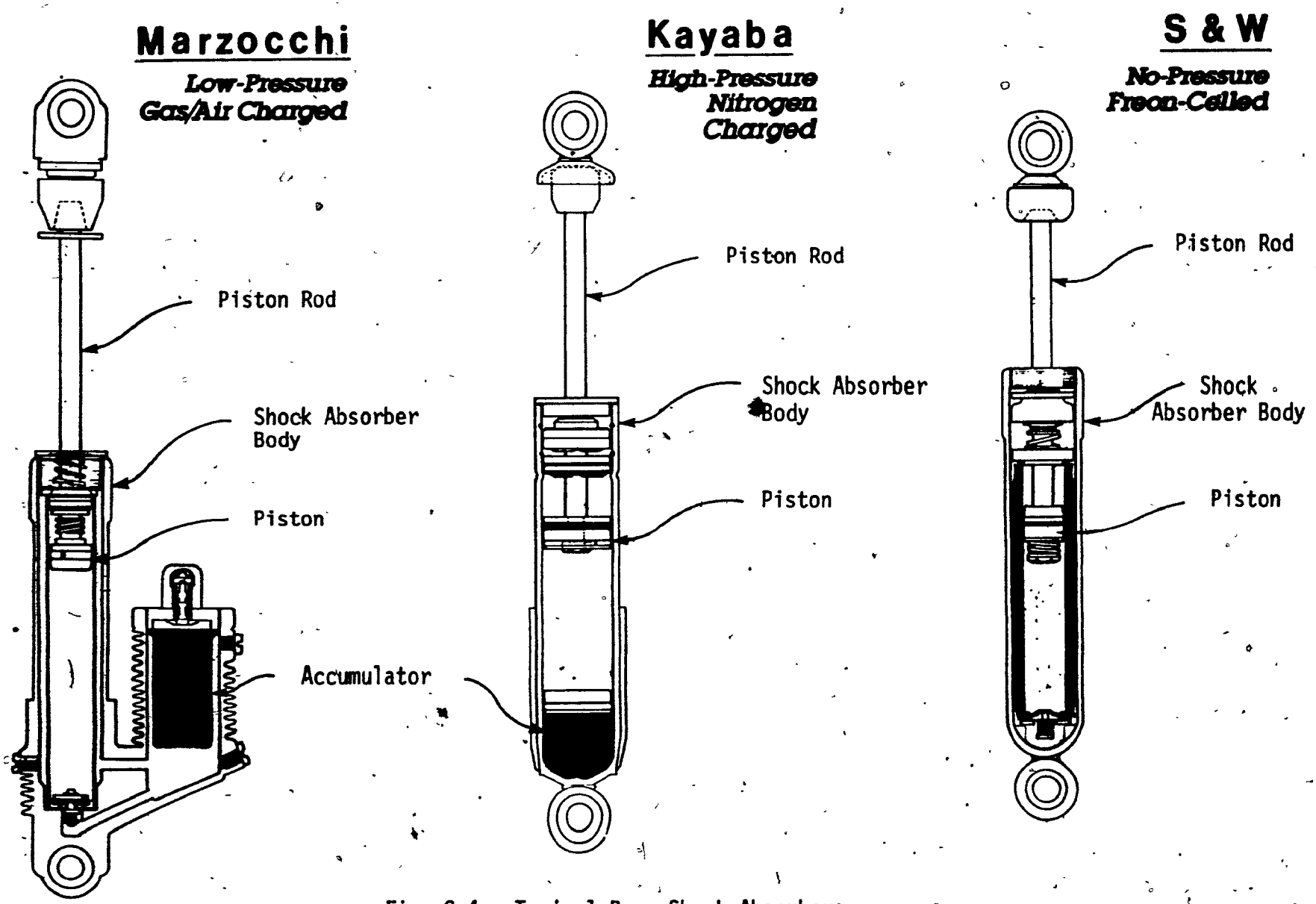

Fig. 2.4: Typical Rear Shock Absorbers

2.2 Damper Force Models

In this section, the components which affect the damping in the front and rear suspension are modelled. The objective is to provide mathematical models which can be experimentally verified using conventional testing procedures [7].

2.2.1 Front Fork

When this investigation was initiated there were a number of private discussions with the research personnel involved in the design and manufacturing of off-road motorcycles at Bombardier Ltd.. Bombardier Ltd. is the only Canadian manufacturer of off-road motorcycles. Based on these discussions, a front fork manufactured by Betor and used on the 1980 production models was selected as the representative unit for this part of the investigation. A schematic of the 35 mm Betor unit is shown in Fig. 2.5. Although very similar in performance, the Betor unit differs from the schematic of the front fork shown in Fig. 2.2 because it contains two damper rod orifices above the piston (during normal operation).

In the development of the mathematical model for the damping characteristics, the effects of the relatively small stanchion tube and hydraulic stop areas are neglected because they do not contribute to the response at the intended low excitation levels.

The damping characteristics of the front fork depend on the nature of the fluid flow through the valves and orifices. As a first step in the analysis, the flow of fluid in the front fork has to be classified as either laminar or turbulent.

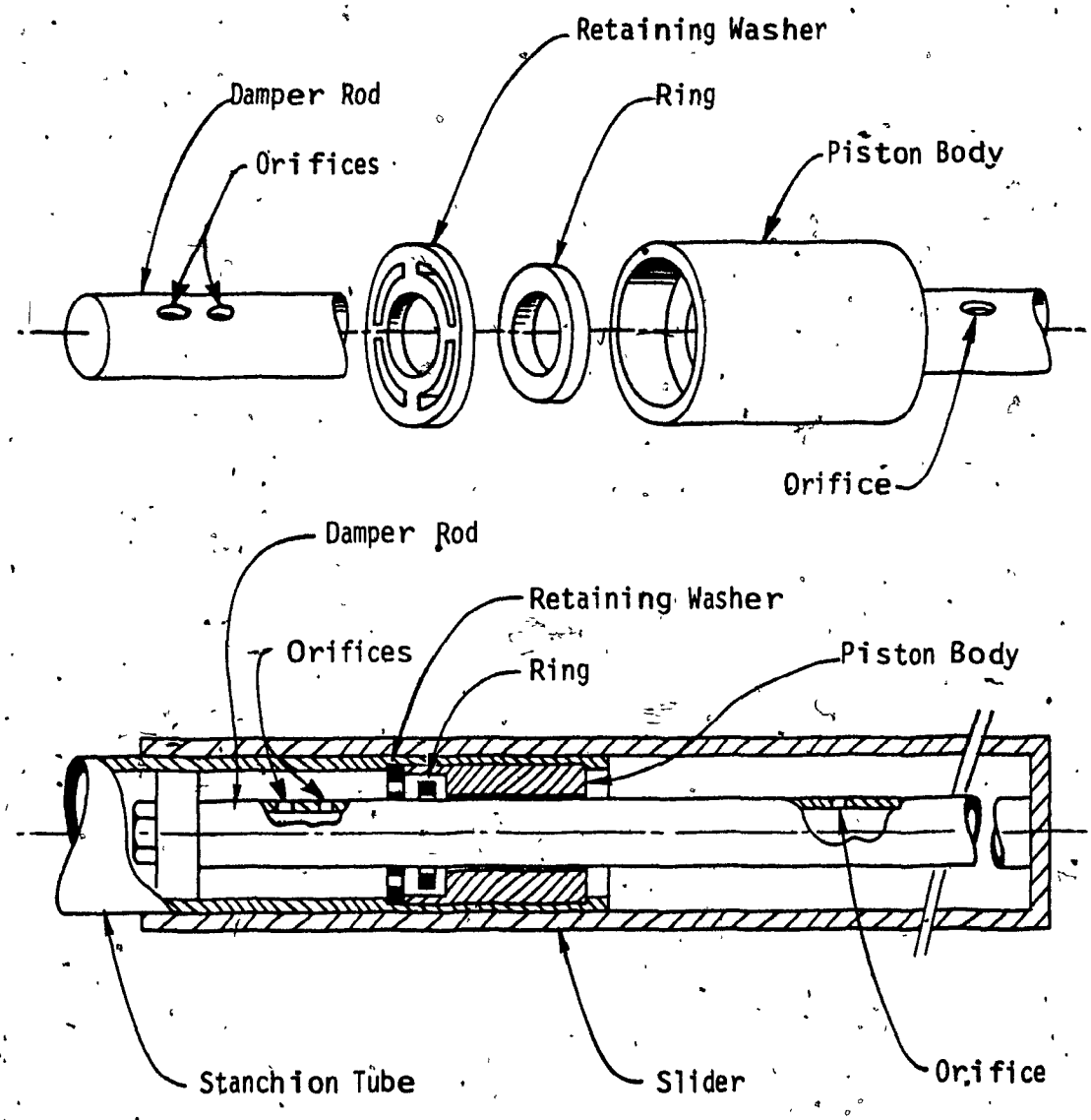

Fig. 2.5: Valving Mechanism of a 35 mm Betor Fork Leg

Case 1: *Laminar Flow Conditions*

In laminar flow, the damping force is generated mainly because of shearing of the oil. A schematic of possible flow paths is shown in Fig. 2.6. The oil flowing through the piston ring has a much larger area exposed to shear than the area corresponding to the oil flowing through the orifices located in the damping rod. Hence, only the laminar flow through the piston is considered. Although the annular area through which the oil flows is not the same during the compression and extension strokes, it remains annular so a form of the Hagen-Poiseuille equation [76], as shown below, can be used to express the fluid flow characteristics, (aspect ratio is 50:1)

$$Q = -\frac{\pi}{8\mu}\frac{d}{d\ell}(p + \gamma h)\left[a^4 - b^4 - \frac{(a^2 - b^2)^2}{\ell n \frac{a}{b}}\right] \qquad (2.1)$$

where Q is the flowrate,

a and b are the respective outer and inner annular diameters,

μ is the dynamic viscosity of the fluid,

$d(p + \gamma h)$ is the pressure difference across the annular section,

$d\ell$ is the elemental length of the annular section.

If F is the force acting on a piston of cross-sectional area A_p and length ℓ, then the fluid flow through the piston body can be obtained from equation (2.1):

$$Q_p = \frac{\pi F}{8\mu\ell A_p}\left[a^4 - b^4 - \frac{(a^2 - b^2)^2}{\ell n \frac{a}{b}}\right] \qquad (2.2)$$

The effect of oil compressibility and container compliance can be modelled [36,61], however their influence on the system's response is

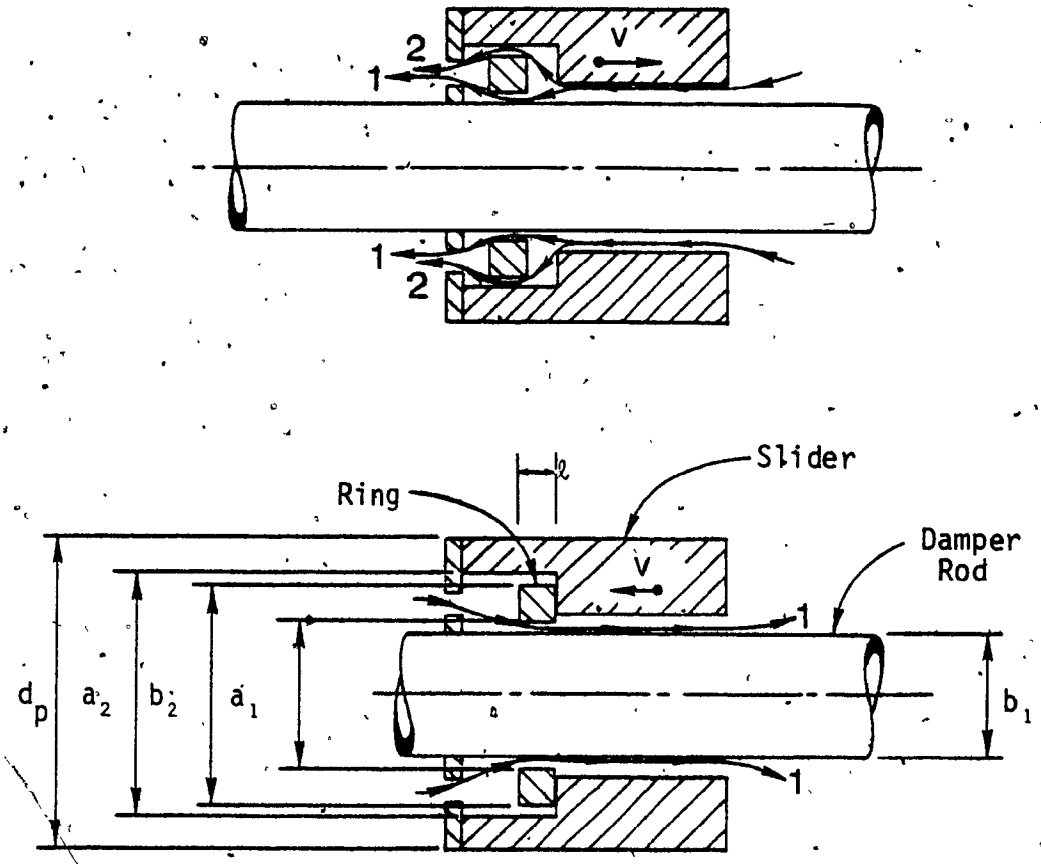

Fig. 2.6: Laminar Flow Path Schematic

usually insignificant. In the literature [38-40, 62-65], the flow of oil through the damper is normally considered as an incompressible flow. If $\dot{z}$ is the relative velocity of the piston with respect to the slider body, then by assuming an incompressible flow, the flowrate can be expressed as:

$$Q_p = \dot{z} A_p \tag{2.3}$$

By combining equations (2.2) and (2.3), the force acting on the piston (and hence exerted by the fork leg) is:

$$F = L \dot{z} \tag{2.4}$$

where L is the laminar flow coefficient given by:

$$L = 8\mu\ell A_p^2/\pi \left[a^4 - b^4 - \{(a^2 - b^2)^2/\ell n(a/b)\}\right] \tag{2.5}$$

Referring to Fig. 2.6, the fluid flows along paths 1 and 2 during compression and only along path 1 during extension. Therefore the laminar flow coefficient, L, is different for compression and extension strokes. Using equation (2.5) they can be expressed as:

Compression Stroke

$$L = 8\mu\ell A_p^2/\pi \sum_{i=1}^{2} \left[a_i^4 - b_i^4 - \{(a_i^2 - b_i^2)^2/\ell n(a_i/b_i)\}\right]$$

where a_i and b_i represent outer and inner annular diameters, respectively, for the i^{th} flow path.

Extension Stroke

$$L = 8\mu\ell A_p^2/\pi \left[a_1^4 - b_1^4 - \{(a_1^2 - b_1^2)^2/\ell n(a_1/b_1)\}\right]$$

Case 2: *Turbulent Flow Conditions*

In turbulent flow, the damping force results from the fluid flow through the piston and orifices in the damper rod. The possible flow paths are shown in Fig. 2.7. The flow paths are in parallel and are subject to change depending upon the relative displacement and direction of relative velocity. Considering the fully extended position as a datum for the relative displacement, the location of the orifices can be designated as Z_1, Z_2, and Z_3 as shown in Fig. 2.7. The characteristic equation for turbulent flow through an orifice is:

$$Q = C_d A^* [2(\Delta p)/\rho]^{\frac{1}{2}} \tag{2.6}$$

where C_d is the discharge coefficient of an orifice

A^* is the orifice area

Δp is the pressure drop across the orifice

ρ the mass density of the fluid.

The pressure drop across the piston can be expressed in terms of the pressures in control volumes 1 and 2, and the force acting on the piston:

$$p_2 - p_1 = \frac{F}{A_p} \tag{2.7}$$

Assuming an incompressible fluid flow, the total flow rate, Q, out of control volume 2 can be expressed in terms of the relative velocity of the piston as:

$$Q = \dot{z} A_p \tag{2.8}$$

The expressions for turbulent flow depend on piston position and velocity direction. Referring to Fig. 2.7 they can be obtained as

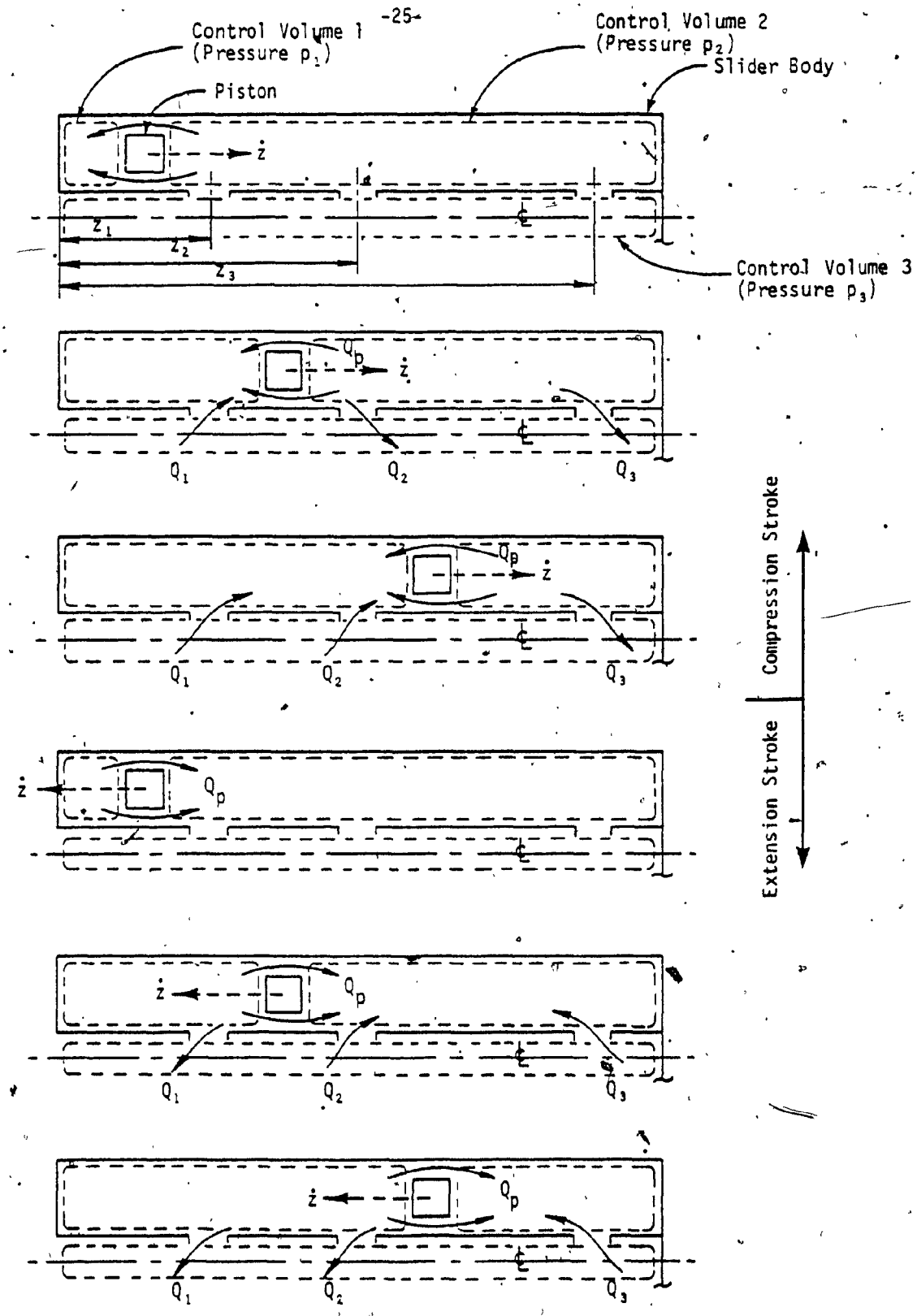

Fig. 2.7: Turbulent Flow Path Schematic

follows:

Compression Stroke

(i) For $0 \leq z \leq Z_1$

In this region the fluid can only flow through the piston. Equation (2.6) can be expressed as:

$$Q = C_d (A_1 + A_2) [2(p_2 - p_1)/\rho]^{\frac{1}{2}} \tag{2.9}$$

where A_1 and A_2 are the cross-sectional annular areas corresponding to flow paths 1 and 2 in Fig. 2.6.

Combining equations (2.7), (2.8) and (2.9), the damping force can be obtained as:

$$F = T \dot{z}^2 \, \mathrm{sgn}(\dot{z}) \tag{2.10}$$

where T is the turbulent flow coefficient given by:

$$T = \frac{A_p^3 \rho}{2 C_d^2 (A_1 + A_2)^2}$$

(ii) For $Z_1 \leq z < Z_2$

The total flowrate out of control volume 2 can be expressed as:

$$Q = Q_p + Q_2 + Q_3 \tag{2.11}$$

where $Q_p = C_d (A_1 + A_2) [2(p_2 - p_1)/\rho]^{\frac{1}{2}}$

$Q_2 = C_d A_2^* [2(p_2 - p_3)/\rho]^{\frac{1}{2}}$

$Q_3 = C_d A_3^* [2(p_2 - p_3)/\rho]^{\frac{1}{2}}$.

The equation of flow continuity for the system is:

$$Q_2 + Q_3 = Q_1 \qquad (2.12)$$

where $Q_1 = C_d A_1^* [2(p_3 - p_1)/\rho]^{\frac{1}{2}}$.

Combining equations (2.7), (2.8), (2.11) and (2.12) yields equation (2.10):

$$F = T \dot{z}^2 \, \mathrm{sgn}(\dot{z}) \qquad (2.10)$$

where

$$T = \frac{A_p^3 \rho}{2 C_d^2 [A_1 + A_2 + \{(A_2^* + A_3^*)/(1 + n_1)^{\frac{1}{2}}\}]^2}$$

and $n_1 = [(A_2^* + A_3^*)/A_1^*]^2$.

(iii) For $Z_2 \leq z \leq Z_3$

The total flowrate out of control volume 2 is:

$$Q = Q_p + Q_3 \qquad (2.13)$$

where $Q_p = C_d (A_1 + A_2) [2(p_2 - p_1)/\rho]^{\frac{1}{2}}$

$Q_3 = C_d A_3^* [2(p_2 - p_3)/\rho]^{\frac{1}{2}}$.

From flow continuity:

$$Q_3 = Q_1 + Q_2 \qquad (2.14)$$

where $Q_1 = C_d A_1^* [2(p_3 - p_1)/\rho]^{\frac{1}{2}}$

$Q_2 = C_d A_2^* [2(p_3 - p_1)/\rho]^{\frac{1}{2}}$.

Combining equations (2.7), (2.8), (2.13) and (2.14) again yields equation (2.10):

$$F = T \dot{z}^2 \, \mathrm{sgn}(\dot{z}) \qquad (2.10)$$

where

$$T = \frac{A_p^3 \rho}{2 C_d^2 [A_1 + A_2 + [A_1^* + A_2^*]\{(n_2/(1+n_2))\}^{\frac{1}{2}}]^2}$$

and $n_2 = [A_3^*/(A_1^* + A_2^*)]^2$.

Extension Stroke

Proceeding in a similar manner and recalling that during extension the total flow is into control volume 2 and the flow through the annular area A_2 is zero, the governing equation is still:

$$F = T \dot{z}^2 \, sgn(\dot{z}) \qquad (2.10)$$

where the turbulent flow coefficient, T, is expressed as follows:

$0 \leq z < Z_1$

$$T = \frac{A_p^3 \rho}{2 C_d^2 A_1^2}$$

$Z_1 < z < Z_2$

$$T = \frac{A_p^3 \rho}{2 C_d^2 [A_1 + [(A_2^* + A_3^*)/(1 + n_1)^{\frac{1}{2}}]]^2}$$

where $n_1 = [(A_2^* + A_3^*)/A_1^*]^2$.

$Z_2 \leq z < Z_3$

$$T = \frac{A_p^3 \rho}{2 C_d^2 [A_1 + [A_1^* + A_2^*]\{(n_2/(1+n_2))\}^{\frac{1}{2}}]^2}$$

where $n_2 = [A_3^*/[A_1^* + A_2^*]]^2$.

Summary

The foregoing set of equations describe the damping force generated

by the flow of fluid through the valves and orifices in the front fork. Depending on the laminar or turbulent flow conditions, the form of equation (2.4) or (2.10) is used as the mathematical model for damping force. This is accomplished by checking whether the Reynolds number, R_e, is greater than $(R_e)_{critical}$. No transitional flow is considered and the hydraulic diameter of the piston is used as the smallest characteristic dimension [76] for the Reynolds number calculation.

In addition to considering the damping of the front fork, an entrapped column of air above the fluid has to be accounted for in the expression for damper force. The effect of the air column is that of a spring working in parallel with the damper.

The cyclic stroking of the fork can be considered to be an isothermal process. At low pressures, air will behave as an ideal gas [77]:

$$\hat{p}V = M\hat{RT} \tag{2.15}$$

where $\hat{p}$ is the absolute pressure of the gas

V is the volume

$M\hat{RT}$ is a constant.

The air column volume decreases linearly with relative displacement:

$$V = V_o - A_p z \tag{2.16}$$

where V_o is the initial gas volume.

The additional spring force, F_k, due to the entrapped air column is:

$$F_k = A_p p_3 \tag{2.17}$$

Using equations (2.15) and (2.16), equation (2.17) can be rewritten as:

$$F_k = \left[\frac{MR\hat{T}}{V_o - A_p z} - p_{at}\right] A_p \qquad (2.18)$$

To summarize, the models for damper force are:

$$F = L\dot{z} + \left[\frac{MR\hat{T}}{V_o - A_p z} - p_{at}\right] A_p \quad \text{for laminar flow}$$

$$F = T\dot{z}^2 + \left[\frac{MR\hat{T}}{V_o - A_p z} - p_{at}\right] A_p \quad \text{for turbulent flow}$$

where the laminar and turbulent flow coefficients (L and T) take on values depending on the relative displacement and direction of relative velocity.

2.2.2 Rear Shock Absorber

The rear shock absorber modelled in this section is a state-of-the-art unit manufactured by Works Performance. The damping is controlled by a piston moving through a volume of pressurized oil. The piston contains four orifices as shown in Fig. 2.8. The governing equations are very similar to those of a front fork except this unit contains a set of one-way and relief valves which control the flow through the orifices.

Referring to Fig. 2.8, the first orifice remains open during both compression and extension strokes while the second orifice uses a check valve that allows fluid to flow through it only during compression. If only these two orifices were used, the shock absorber would display damping characteristics very similar to those of the front fork. The

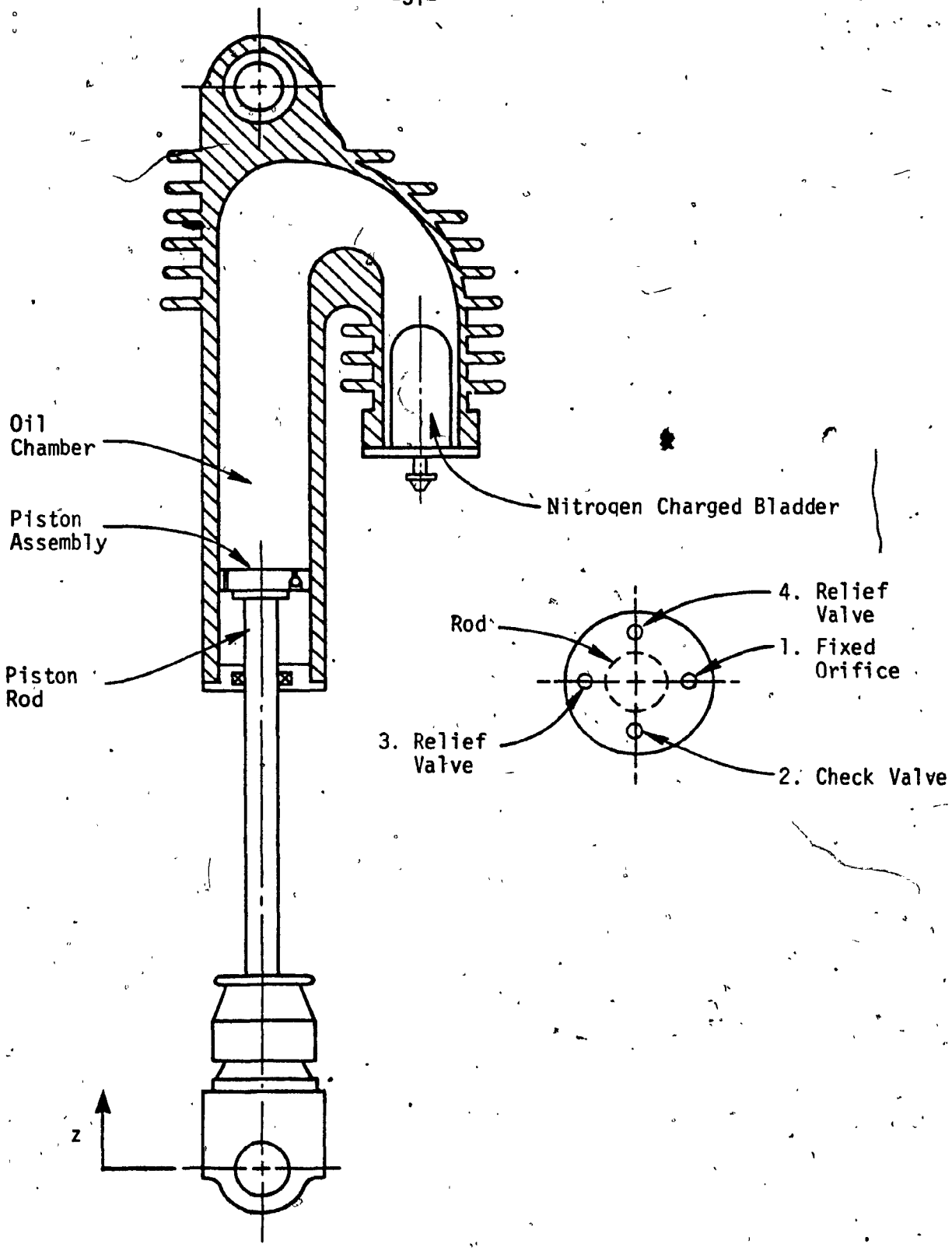

Fig. 2.8: Works Performance Shock Absorber

principal advantage of this design is due to orifices 3 and 4 during the compression stroke. Orifices 3 and 4 each contain a relief valve. The relief valves consist of a ball restrained by a preloaded spring. The purpose of these valves is to reduce the maximum force which would be transmitted to the frame. There are three stages of relief valve operation. They can be identified as follows:

1) The force on the relief valve due to the pressure differential across it is not sufficient to overcome the preload on the spring. In this case, there will not be any flow of fluid through the relief valve.

2) The pressure differential lifts the relief valve off its seat but the preloaded spring is not fully compressed. Under these conditions the flow of fluid through the relief valve is dependent upon the relief valve response. In this case the valve is modelled as a mass-spring-damper system.

3) The preloaded spring is fully compressed and the relief valve is fully open. The flow of fluid through the valve is governed by the open valve or upstream orifice, whichever has a smaller flow area.

Extension Stroke

During extension, only orifice 1 is open. The orifice diameter is small, so only the turbulent flow condition is considered, as given by equation (2.6). The piston area during extension differs from the area during compression due to the rod area. The force acting on the piston during extension can be expressed in terms of the piston area, A_p, and rod area, A_r:

$$F = p_a A_p - p_b (A_p - A_r) \qquad (2.19)$$

where p_a and p_b are the pressures on the accumulator and rod sides of the piston, respectively.

Since $p_a - p_b$ is the pressure drop, Δp, across the orifice, equation (2.19) can be rewritten as:

$$\Delta p = (F - p_a A_r)/(A_p - A_r) \tag{2.20}$$

For incompressible flow:

$$Q = \dot{z} (A_p - A_r) \tag{2.21}$$

Substitution of equations (2.20) and (2.21) into equation (2.6) yields:

$$F = T \dot{z}^2 \, \mathrm{sgn}(\dot{z}) + p_a A_r \tag{2.22}$$

where T is the turbulent flow coefficient in extension given by:

$$T = \frac{(A_p - A_r)^3 \rho}{2 C_d^2 \hat{A}_1^{*2}}$$

where $\hat{A}_1^*$ is the cross-sectional area of the first orifice.

Under the assumption of incompressible flow, the pressure term in equation (2.22) simply denotes the pressure in the accumulator. This pressure is due to the rod volume entering the shock. The volume of the accumulator changes linearly with relative displacement as:

$$V = V_o - A_r z \tag{2.23}$$

Assuming ideal gas behavior, equations (2.15), (2.22) and (2.23) can be combined to give the expression for damper force during extension:

$$F = T \dot{z}^2 \, \mathrm{sgn}(\dot{z}) + \left[\frac{M R \hat{T}}{V_o - A_r z} - p_{at} \right] A_r \tag{2.24}$$

Compression Stroke

During part of the compression stroke the valves may be neither fully open nor fully closed. Hence no explicit relationship between damper force and relative velocity and/or displacement is possible. Instead, the governing equations can be formulated as implicit relationships and are readily handled using computer simulation techniques.

Recalling equations (2.15), (2.19) and (2.23), the damper force can be expressed as:

$$F = (p_a - p_b)(A_p - A_r) + \left[\frac{MR\hat{T}}{V_o - A_r z} - p_{at}\right] A_r \qquad (2.25)$$

Equation (2.25) is solved (implicitly) by recalling equation (2.21) and expressing the total flow, Q, in terms of $(p_a - p_b)$. From continuity:

$$Q = Q_1 + Q_2 + Q_3 + Q_4 \qquad (2.26)$$

where Q_i is the flow through the i^{th} orifice.

The flowrates through orifices 1 and 2 are given in terms of $(p_a - p_b)$ as:

$$Q_1 = C_d \hat{A}_1^* [2(p_a - p_b)/\rho]^{\frac{1}{2}} \qquad (2.27)$$

$$Q_2 = C_d \hat{A}_2^* [2(p_a - p_b)/\rho]^{\frac{1}{2}} \qquad (2.28)$$

where $\hat{A}_1^*$ and $\hat{A}_2^*$ are the cross-sectional areas of orifices 1 and 2, respectively.

The flowrate through orifices 3 and 4 is implicit in terms of $(p_a - p_b)$ and relief valve displacement, u. The three stages of valve operation are modelled as follows:

Orifice 3

First stage: $(p_a - p_b) < \frac{k_3 u_{3,i}}{\hat{A}_3^*}$

where k_3 is the spring constant of the relief valve

$\hat{A}_3^*$ is the area of the third orifice

$u_{3,i}$ is the preloaded displacement of the third valve spring.

During this stage the valve remains shut, thus:

$$Q_3 = 0 \tag{2.29}$$

Second stage: $\frac{k_3 u_{3,i}}{A_3^*} \leq (p_a - p_b) < \frac{k_3 (u_{3,i} + u_{3,max})}{A_3^*}$

$u_{3,max}$ represents the maximum lift of the relief valve (measured from $u = 0$) and is determined by the upstream restriction. The maximum lift occurs when the valve flow area equals that of the orifice. From Fig. 2.9:

$$\hat{A}_3^* = \pi d_3 u_{3,max}$$

where d_3 is the diameter of the third orifice.

Since; $\hat{A}_3^* = \pi d_3^2/4$,

$u_{3,max} = d_3/4$

The relief valve can be modelled as a mass-spring-damper system [78]. The equation of motion is given by:

$$m_3 \ddot{u}_3 + c_3 \dot{u}_3 + k_3 u_3 = (p_a - p_b) A_{V_3} \tag{2.31}$$

where

m_3 is the valve mass

c_3 is the damping coefficient

u_3 is the valve displacement

A_{V_3} is the valve ball area.

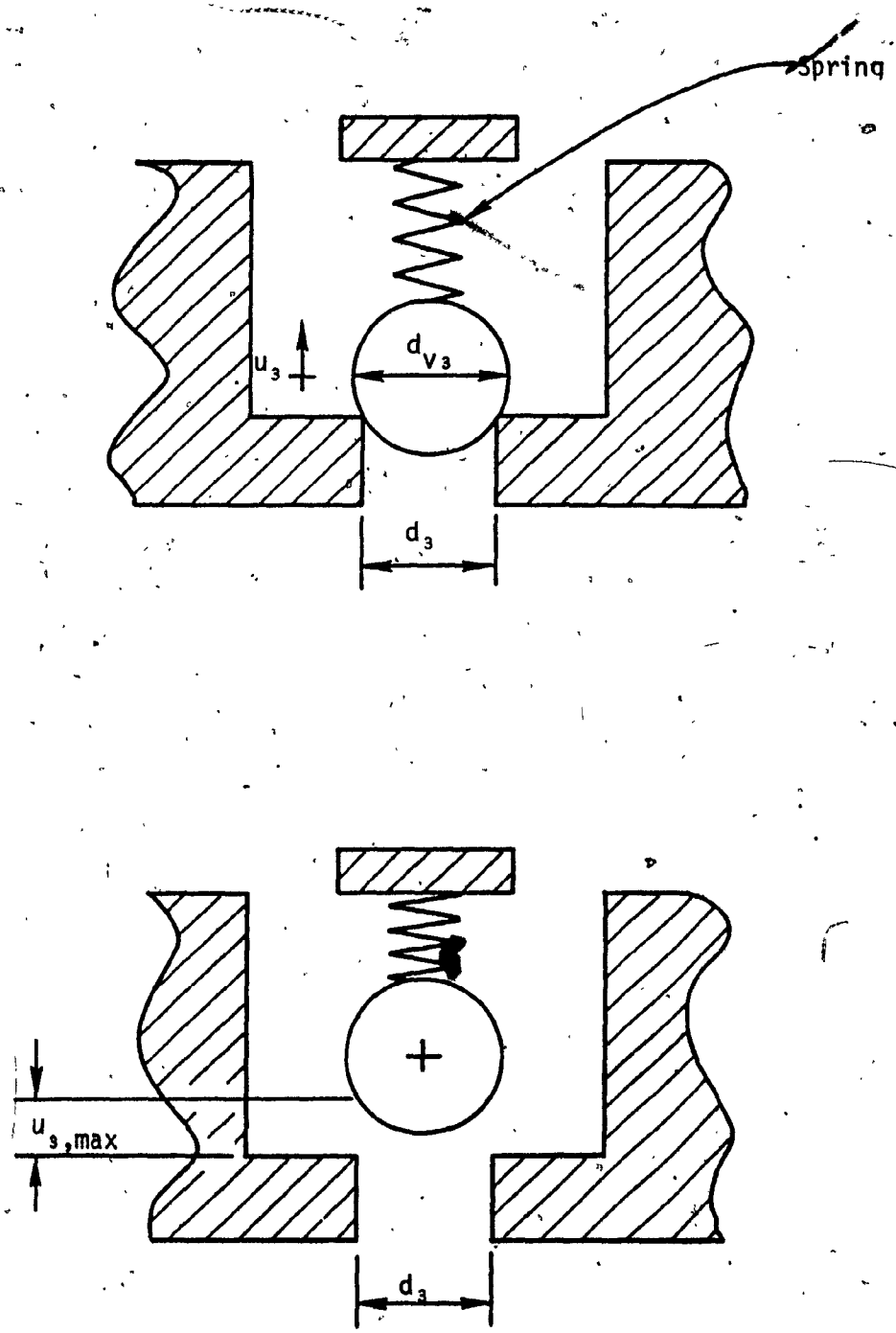

Fig. 2.9: Valving Mechanism (third orifice)

The flow through orifice 3 may be expressed as:

$$Q_3 = \pi d_3 u_3 C_d \left[2(p_a - p_b)/\rho\right]^{\frac{1}{2}} \tag{2.32}$$

Third stage: $(p_a - p_b) \geq \dfrac{k_3(u_{3,i} + u_{3,max})}{\hat{A}_3^*}$

The valve is fully open in this stage. The flowrate is given by:

$$Q_3 = \pi d_3 u_{3,max} C_d \left[2(p_a - p_b)/\rho\right]^{\frac{1}{2}} \tag{2.33}$$

Orifice 4

The form of the flow equations governing the fourth orifice are identical to those developed for the third orifice. They are;

First stage: $(p_a - p_b) < \dfrac{k_4 u_{4,i}}{\hat{A}_4^*}$

where

k_4 is the spring constant of the relief valve

$\hat{A}_4^*$ is the area of the fourth orifice

$u_{4,i}$ is the preloaded displacement of the fourth valve spring.

$$Q_4 = 0 \tag{2.34}$$

Second stage: $\dfrac{k_4 u_{4,i}}{\hat{A}_4^*} \leq (p_a - p_b) < \dfrac{k_4(u_{4,i} + u_{4,max})}{\hat{A}_4^*}$

$$m\ddot{u}_4 + c\dot{u}_4 + k_4 u_4 = (p_a - p_b) A_{V_4} \tag{2.35}$$

where

m_4 is the valve mass

c_4 is the damping coefficient.

u_4 is the valve displacement.

$$Q_4 = \pi d_4 u_4 C_d [2(p_a - p_b)/\rho]^{\frac{1}{2}} \tag{2.36}$$

Third stage: $(p_a - p_b) > \dfrac{k_4(u_{4,i} + u_{4,max})}{\hat{A}_4^*}$

$$Q_4 = \pi d_4 u_{4,max} C_d [2(p_a - p_b)/\rho]^{\frac{1}{2}} \tag{2.37}$$

To summarize, the rear shock absorber model in compression; equations (2.21) and (2.26), are used to express the flowrates in terms of the relative velocity. Flowrates through the first and second orifices are given by equations (2.27) and (2.28). The flowrate through the third and fourth orifices are implicit in $(p_a - p_b)$, u_3, and u_4. Using an iterative procedure, equations (2.29), (2.31) and (2.32), or (2.33) are used for the third orifice, and equations (2.34), (2.35) and (2.36), or (2.37) are used for the fourth orifice. Once $(p_a - p_b)$, u_3 and u_4 are known, equation (2.25) is solved for the damper force.

2.3 Suspension System Model

To study the suspension system, a lumped mass analysis is typically performed [35,79,80]. In some of the previous work [35,81,82] the suspension parameters are assumed linear. In this manner the total vehicle response is obtained. Unfortunately, the low excitation requirement of the linearized model is violated as soon as realistic inputs are considered. In fact, it is the strong nonlinear nature of the suspension components (i.e. hydraulic stop and air column) which prevent damage to the machine at high excitation levels [64]. In this investigation, the nonlinear nature of the various components is exploited by modelling the front suspension system as a single degree of freedom system with nonlinear elements. The sample fork used in the modelling

procedure is a 38 mm diameter fork manufactured by Marzocchi.

Due to the growing popularity of the Marzocchi fork in the current production models, it is justifiable to use this unit instead of the Betor fork used in the damper force model. It should be noted that the performance of the Marzocchi and Betor units is similar, although the units have dimensional differences.

The system can be modelled with linear and non-linear elements as shown in Fig. 2.10. The mass, m, represents an equivalent mass due to the rider and vehicle, realized at each fork leg. However, in practice the effective mass is not a constant, due to the rider dynamics. A constant effective mass reflects ideal suspension operation. In this investigation, a value of 1/6 the total mass (vehicle and average rider; 100 kg + 73 kg) is used in the model. A helical spring, generating a restoring force due to its stiffness, represents the linear element in the model. The non-linear elements are: the pneumatic spring due to the pressurized air column, the coulomb friction due to seal striction, and the damping due to the restriction of oil flow.

Referring to Fig. 2.2, it is evident that there are two paths for oil flow: flow through the valve in the piston and flow through the damper rod orifice. The latter flow is independent of the former and depends only on the volume of stanchion tube entering the slider. The effect of these two independent flows is that of two non-linear dampers acting in parallel. Since the intended excitation levels are much higher than those of the Betor fork model, only turbulent flow conditions are considered. The governing equations characterizing the force generated due to oil flow are similar to those of the Betor fork. Referring to

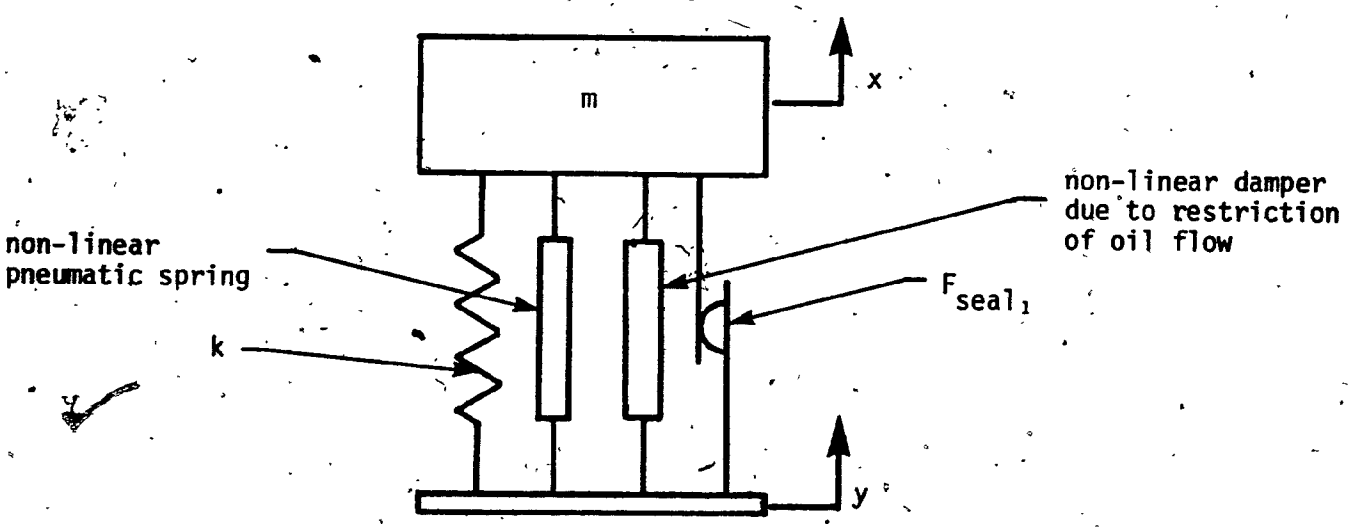

Fig. 2.10: Suspension System Model

the flow schematic shown in Fig. 2.11, the damper force will be given by:

$$F = A_p (p_2 - p_1) + A_{tube}\, p_2 + F_k \tag{2.38}$$

where

A_p and A_{tube} are the cross-sectional areas of the piston and stanchion tube, respectively.

F_k is the force due to the compressed air column.

Assuming an incompressible fluid flow, the flow through the piston, Q_p, and through the damper rod orifice, Q_1, can be expressed in terms of the relative velocity as:

$$Q_p = A_p \dot{z} \tag{2.39}$$

$$Q_1 = A_{tube} \dot{z} \tag{2.40}$$

Compression Stroke

During the compression stroke, equation (2.6) describes the flows as:

$$\begin{aligned} Q_p &= C_d (A_1 + A_2) [2(p_2 - p_1)/\rho]^{\frac{1}{2}} \\ Q_1 &= C_d A_1 [2(p_2 - p_3)/\rho]^{\frac{1}{2}} \end{aligned} \tag{2.41}$$

Combining equations (2.38) to (2.41) yields:

$$F = T_p \dot{z}^2 \operatorname{sgn}(\dot{z}) + T_{or} \dot{z}^2 \operatorname{sgn}(\dot{z}) + A_{tube} p_3 + F_k \tag{2.42}$$

where T_p and T_{or} are the turbulent flow coefficients for the piston and damper rod orifice given by:

$$T_p = \frac{A_p^3 \rho}{2 C_d^2 (A_1 + A_2)^2}$$

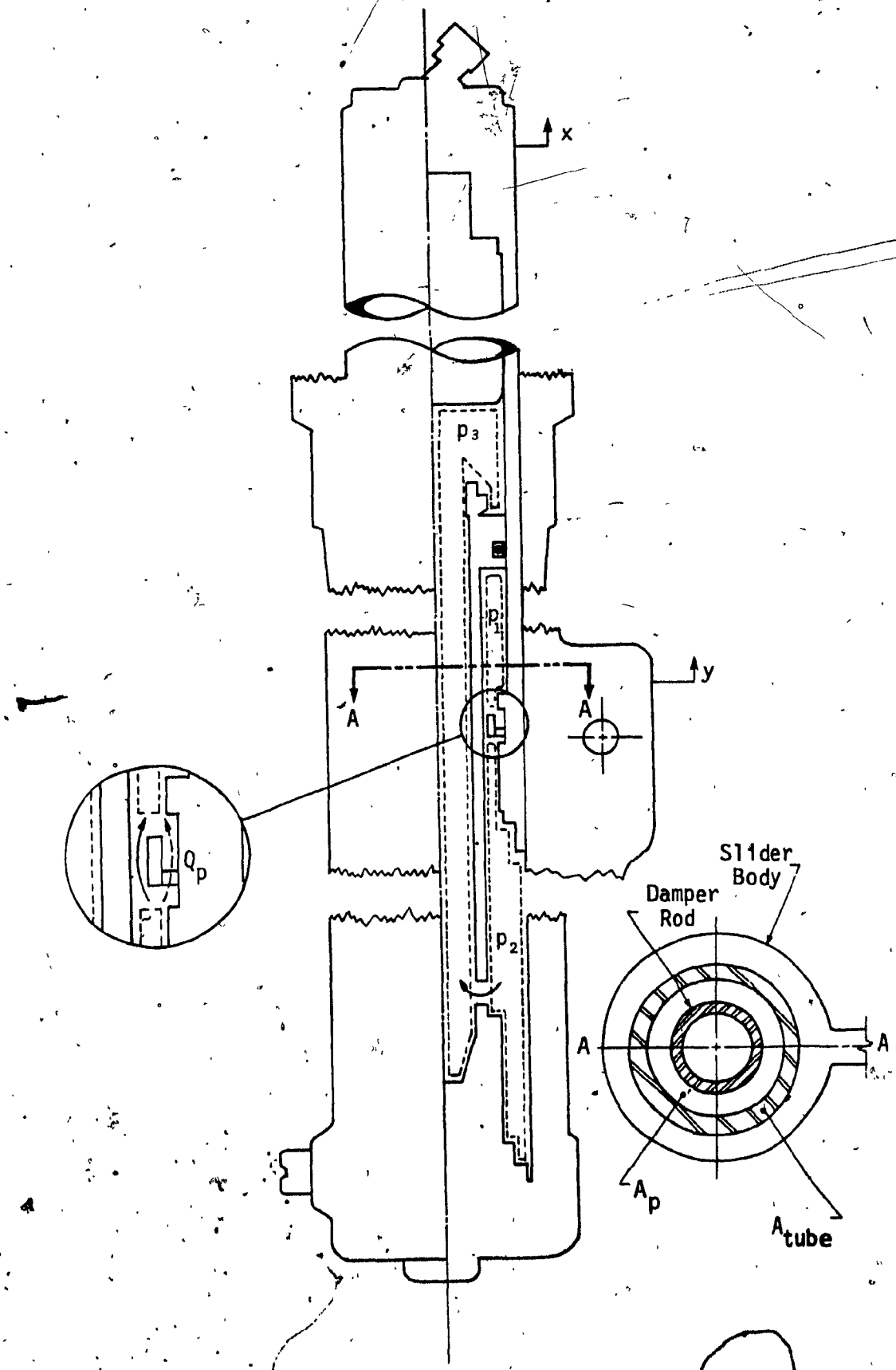

Fig. 2.11: Flow Schematic for the 38 mm Marzocchi Fork

$$T_{or} = \frac{A_{tube}^3 \rho}{2 C_d^2 A_{or}^{2\,1}}$$

Extension Stroke

During the extension stroke, the piston valve restricts the flow of oil through the piston. Equation set (2.41) becomes:

$$Q_p = C_d A_1 [2(p_1 - p_2)/\rho]^{\frac{1}{2}}$$
$$Q_1 = C_d A_1 [2(p_3 - p_2)/\rho]^{\frac{1}{2}} \qquad (2.43)$$

Combining equations (2.38), (2.39), (2.40) and (2.43) once again yields equation (2.42) with the exception that the turbulent flow coefficient of the piston is expressed as:

$$T_p = \frac{A_p^3 \rho}{2 C_d^2 A_1^2}$$

The equation for damper force, (2.42), contains four terms. The first two terms depend on the square of the relative velocity and can be identified as non-linear damping terms. The third and fourth terms are non-linear stiffness terms.

Considering the contribution of the stanchion tube area, equations (2.16) and (2.17) become:

$$V = V_o - (A_p + A_{tube})z \qquad (2.44)$$

$$F_k = A_p p_3 \qquad (2.45)$$

Recalling equation (2.15) and applying equations (2.44) and (2.45) to (2.43) yields:

$$F = (T_p + T_{or})\dot{z}^2 \operatorname{sgn}(\dot{z}) + \left[\frac{MR\hat{T}}{V_o - (A_p + A_{tube})z} - p_{at}\right](A_p + A_{tube}) \quad (2.46)$$

A hydraulic stop (Fig. 2.2), is used to reduce the possibility of the fork bottoming at the end of the stroke. The hydraulic stop acts as an additional parallel damper at large relative displacements. If Z_c is the critical relative displacement above which the hydraulic stop is effective, then its damping force is:

$$F_{hyd} = T_{hyd}\, \dot{z}^2\, \operatorname{sgn}(\dot{z}) \quad (2.47)$$

$$T_{hyd} = \frac{A_{tube}^3\, \rho}{2\, C_d^2\, A_{hyd}^2} \qquad \text{for } z > Z_c$$

where A_{hyd} is the flow area at the hydraulic stop.

$$T_{hyd} = 0 \qquad \text{for } z \leq Z_c$$

In addition to the damping due to the restriction of oil flow, the fork contains seals which exert a stiction force. This stiction can be considered to be a slip-stick mechanism in the model [83]. The mechanism requires the system excitation and response to be identical for an inertial force less than the breakaway seal friction force, i.e. $|m\ddot{X}| < F_{coul_1}$. The governing equations of the system in the sticking mode are:

$$\ddot{x} = \ddot{y}$$

$$\dot{x} = \dot{y} \quad (2.48)$$

$$x = y$$

For inertial force greater than breakaway seal friction, the system is in the sliding mode. The stiction is modelled as coulomb friction depending on the sign of the relative velocity, $\dot{z}$. Since numerical difficulties arise when $\dot{z}$ is zero, the stiction is modelled as viscous damping for small $\dot{z}$ [84].

$$F_{seal_1} = F_{coul_1}\, sgn[\dot{z}] \qquad \text{for } |\dot{z}| > \epsilon$$
$$F_{seal_1} = F_{coul_1}\left(\frac{\dot{z}}{\epsilon}\right) \qquad \text{for } |\dot{z}| \leq \epsilon \tag{2.49}$$

where

F_{coul_1} is the coulomb friction force

ϵ is a small predetermined velocity.

Recalling equations (2.46), (2.47) and Fig. 2.10, the governing equation of the system in the sliding mode ($|m\ddot{x}| \geq F_{coul_1}$) is:

$$m\ddot{x} + \left[T_p + T_{or} + T_{hyd}\right]\dot{z}^2\, sgn[\dot{z}] + F_{seal_1}$$
$$+ kz + \left[\frac{MR\hat{T}}{V_o - (A_p + A_{tube})z} - p_{at}\right](A_p + A_{tube}) = 0 \tag{2.50}$$

To summarize, equation (2.48) or (2.50) is the governing equation of the suspension system model, depending on whether $|m\ddot{x}|$ is less than or greater than F_{coul_1}, respectively. In the latter case, the magnitudes of T_p and F_{seal_1} depend on the relative velocity according to equations (2.43) and (2.49). In addition, the magnitude of T_{hyd} depends on the relative displacement as given by equation (2.47).

2.4 Summary

In this chapter, a typical front fork and rear shock absorber are

mathematically modelled to independently express the damper force equations and suspension system characteristics, in both compression and extension strokes. The damper force models are intended primarily for experimental verification using existing industrial procedures, whereas the suspension model serves in innovative design procedures which will be introduced in subsequent chapters. Fundamental laws of fluid flow and dynamics are used to develop the non-linear expressions for damper force. The analysis is extended to a suspension system model in which some of the components are represented by the developed expressions whereas others, such as mass and helical spring stiffness, are represented by idealized elements.

CHAPTER 3

COMPUTER SIMULATION AND EXPERIMENTAL VERIFICATION OF DAMPER FORCE MODELS

CHAPTER 3

COMPUTER SIMULATION AND EXPERIMENTAL VERIFICATION OF DAMPER FORCE MODELS

3.1 Introduction

In this chapter, the damper force models are simulated on computer and verified through laboratory testing. The fork model is simulated on a digital computer, whereas the implicit nature of the rear shock absorber is simulated on an analog computer. In each application the objective is to establish the validity of the non-linear damper force models.

In both the front fork and rear shock absorber simulations, the excitation and testing configurations are those presently in use by the industry [17,30,32,36,75,85]. A sinusoidal displacement input of constant amplitude was selected as the input excitation to one end of the suspension with the other end assumed to be fixed. The helical spring elements are removed so that the damping component is isolated as much as possible from the remainder of the suspension system. For this purpose, in the test rig, one end of the damping component is fixed to a load cell while the other end is driven by a sinusoidal displacement signal. The amplitude and frequency are varied to obtain damping characteristics over an excitation range. The measured quantities are relative displacement or velocity, and transmitted force. The displacement or velocity is plotted against the force, resulting in Lissajous diagrams as shown in Fig. 3.1.

The choice of using displacement or velocity is dependent upon the aspect to be investigated. The force vs velocity diagrams, known as "characteristic diagrams" [75,85], are suitable criteria for investigating

(a) F - D Diagram

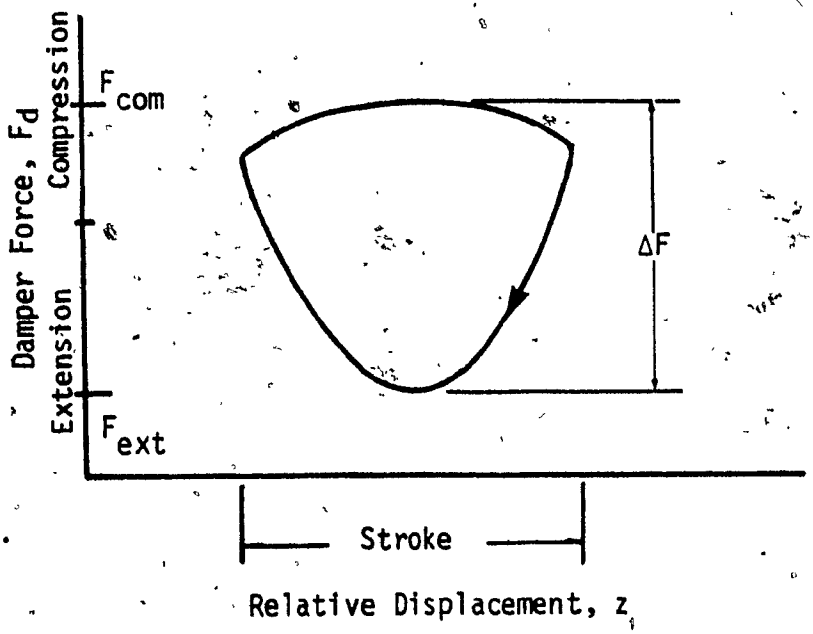

(b) F - V Diagram

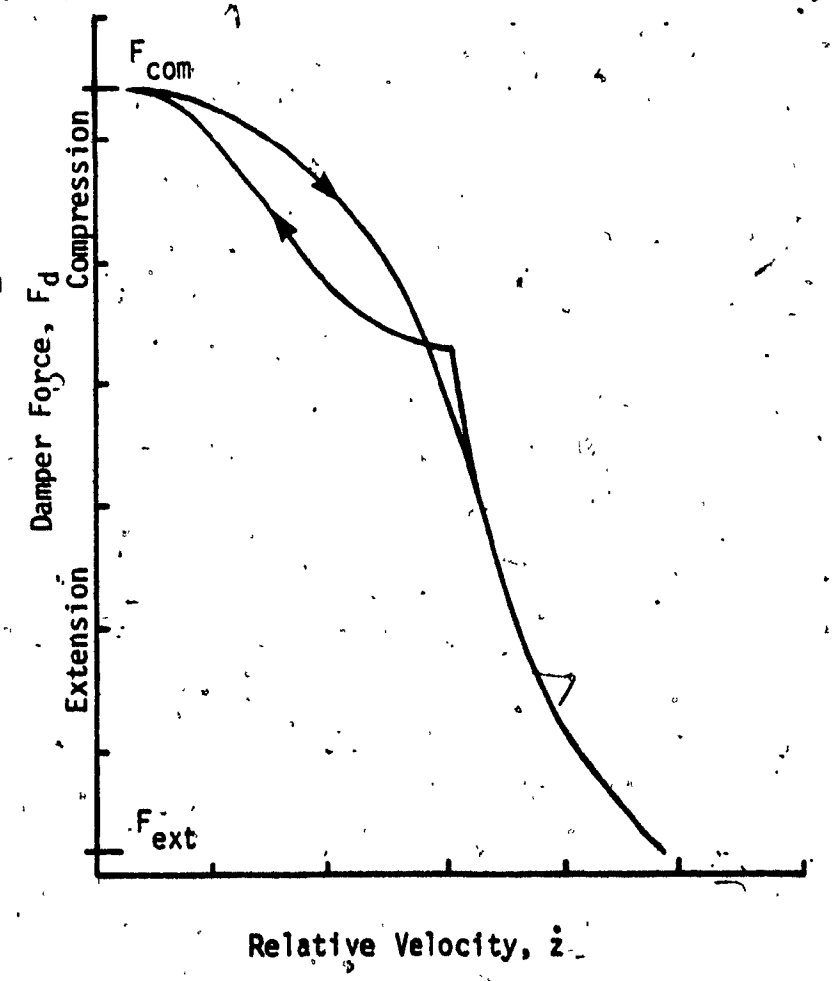

Fig. 3.1: Lissajous Diagrams

heat fade, hysteresis, and other frequency dependent quantities. Ideally the velocity and damper force should be in phase, hence the diagram tends to be difficult to use. For ideal damping, the displacement and damper force are 90 degrees out of phase. When these two quantities are plotted against each other, the details of the damping characteristics are much more vivid. If velocity dependent quantities are desired, they can be measured directly from the force vs displacement (F-D) diagrams because of the sinusoidal nature of the motion. These F-D diagrams are widely used in industries to compare the performance of suspension damping components [17,30,32,36,75]. Referring to Fig. 3.1(a), the horizontal axis represents the damper stroke (displacement) and the vertical axis indicates damping resistance. The top half of the performance chart represents damper force in compression whereas the lower half indicates damper force during extension.

3.2 Computer Simulation

3.2.1 Front Fork

The damper model presented in Section 2.2.1 is highly discontinuous in nature. A digital computer was used for the simulation. Equations (2.4), (2.10) and (2.18), along with the velocity and displacement dependent expressions for the laminar and turbulent flow coefficients, L and T, were programmed on a Control Data Corporation Cyber 172/2 computer. Amplitude and frequency were the independent variables with damper force as the dependent variable.

The results were plotted as F-D diagrams. Typical output plots are shown in Fig. 3.2 and Fig. 3.3. A complete set of results is listed in Table 3.1. The validation of the dynamic quantities of interest is discussed in Appendix IV.

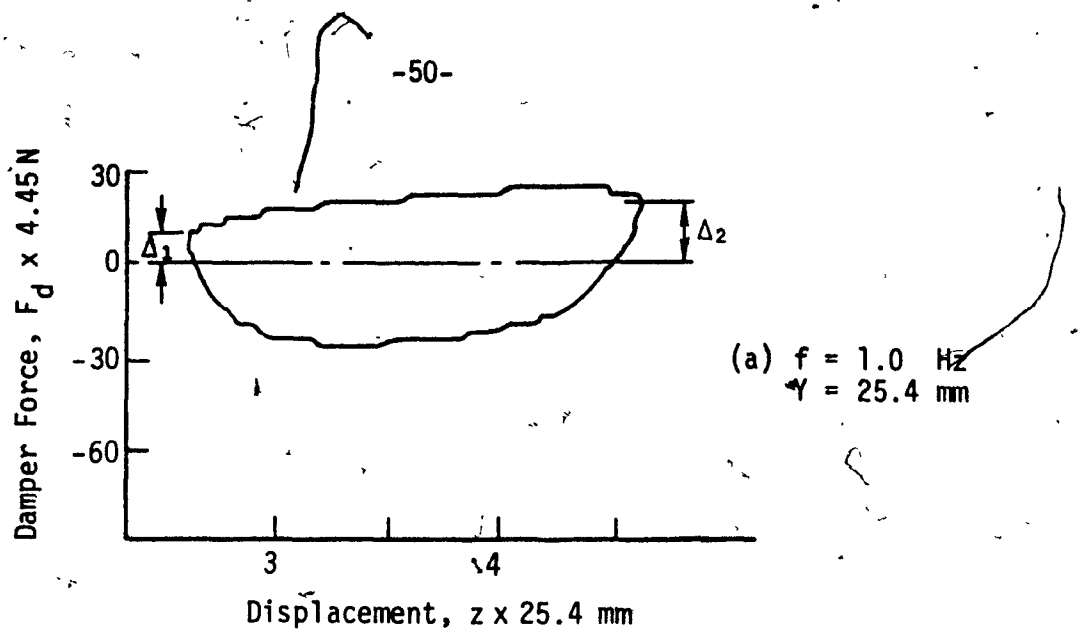

(a) f = 1.0 Hz
Y = 25.4 mm

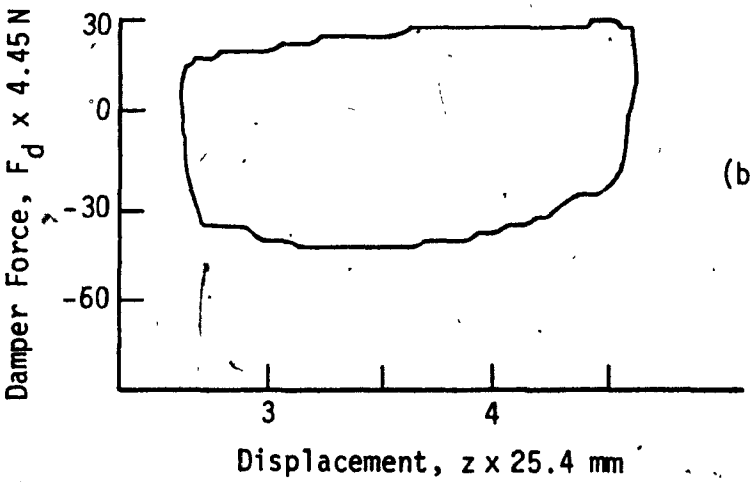

(b) f = 3.0 Hz
Y = 25.4 mm

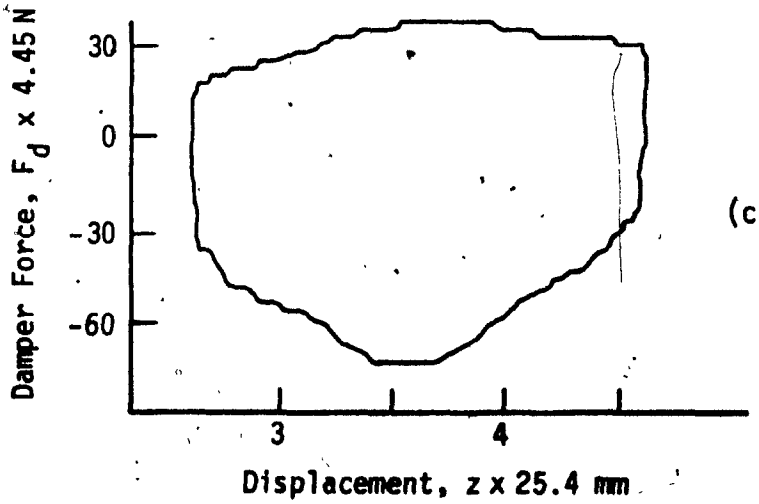

(c) f = 5.0 Hz
Y = 25.4 mm

Fig. 3.2: Front Fork - Simulation Results

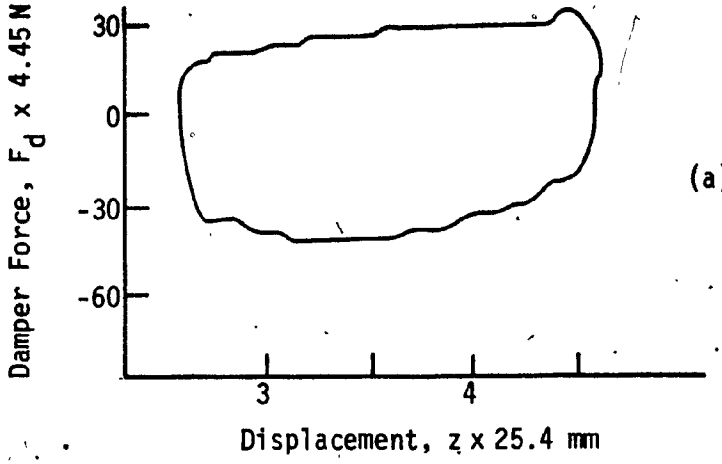

(a) f = 3.0 Hz
Y = 25.4 mm

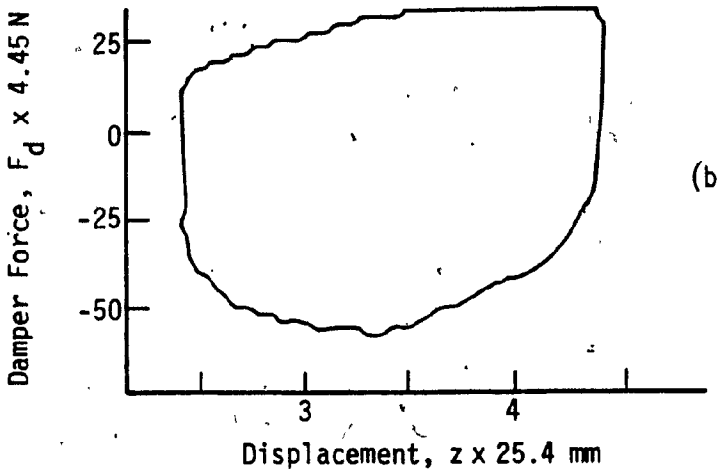

(b) f = 3.0 Hz
Y = 38.1 mm

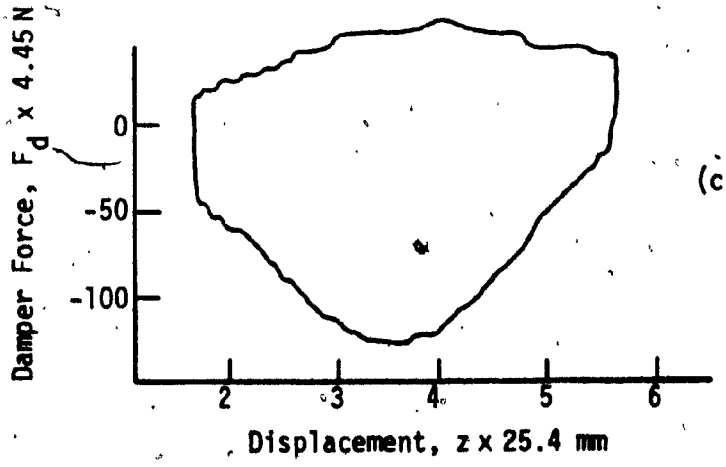

(c) f = 3.0 Hz
Y = 50.8 mm

Fig. 3.3: Front Fork - Simulation Results

TABLE 3.1: Front Fork Results

Excitation Amplitude (mm)	Excitation Frequency (Hz)	Computer Simulation ΔF^c (N)	Experimental Data ΔF^e (N)	% Error = $\left\|\frac{\Delta F^c - \Delta F^e}{\Delta F^e}\right\| \times 100$
12.7	1.0	118.3	121.9	3.0 %
25.4	1.0	223.3	227.7	1.9 %
38.1	1.0	283.8	281.1	0.9 %
25.4	3.0	322.5	322.9	0.1 %
25.4	5.0	492.4	491.1	0.3 %
38.1	3.0	407.4	471.5	13.6 %
50.8	3.0	712.1	706.3	0.8 %

3.2.2 Rear Shock Absorber

The damper model presented in Section 2.2.2 consists of a set of discontinuous equations. The manner in which the equations interact is shown in Fig. 3.4. The implicit nature of the model is amiable to analog computer simulation. Subsequently, an EAI 680 analog computer was used for the simulation of a rear shock absorber.

The differential equations of motion were rewritten, solving for the highest order derivative. The equations were then used for drawing an unscaled computer diagram following the General Method [86]. The unscaled analog circuit diagram is shown in Fig. 3.5.

The maximum anticipated values of the physical parameters were estimated. From these maxima, appropriate scale factors were introduced into the system equations and the circuit elements to form a scaled circuit diagram. The scaled circuit was then patched on an EAI 680 computer.

A static check was then performed. The check consisted of a program check and a circuit check. The program check consisted of two sets of calculations; one based on the original equations and the other on the program. The results from the two sets of calculations were compared and the appropriate circuit corrections were made. A circuit check was then performed. The initial conditions were established and the amplifier outputs were measured. These outputs were compared to previously calculated values, and patching corrections were made. The scaling factors, scaled circuit diagram, potentiometer and voltage settings, and static test data are given in Appendix I.

To effectively use the scaled variables, only the excitation

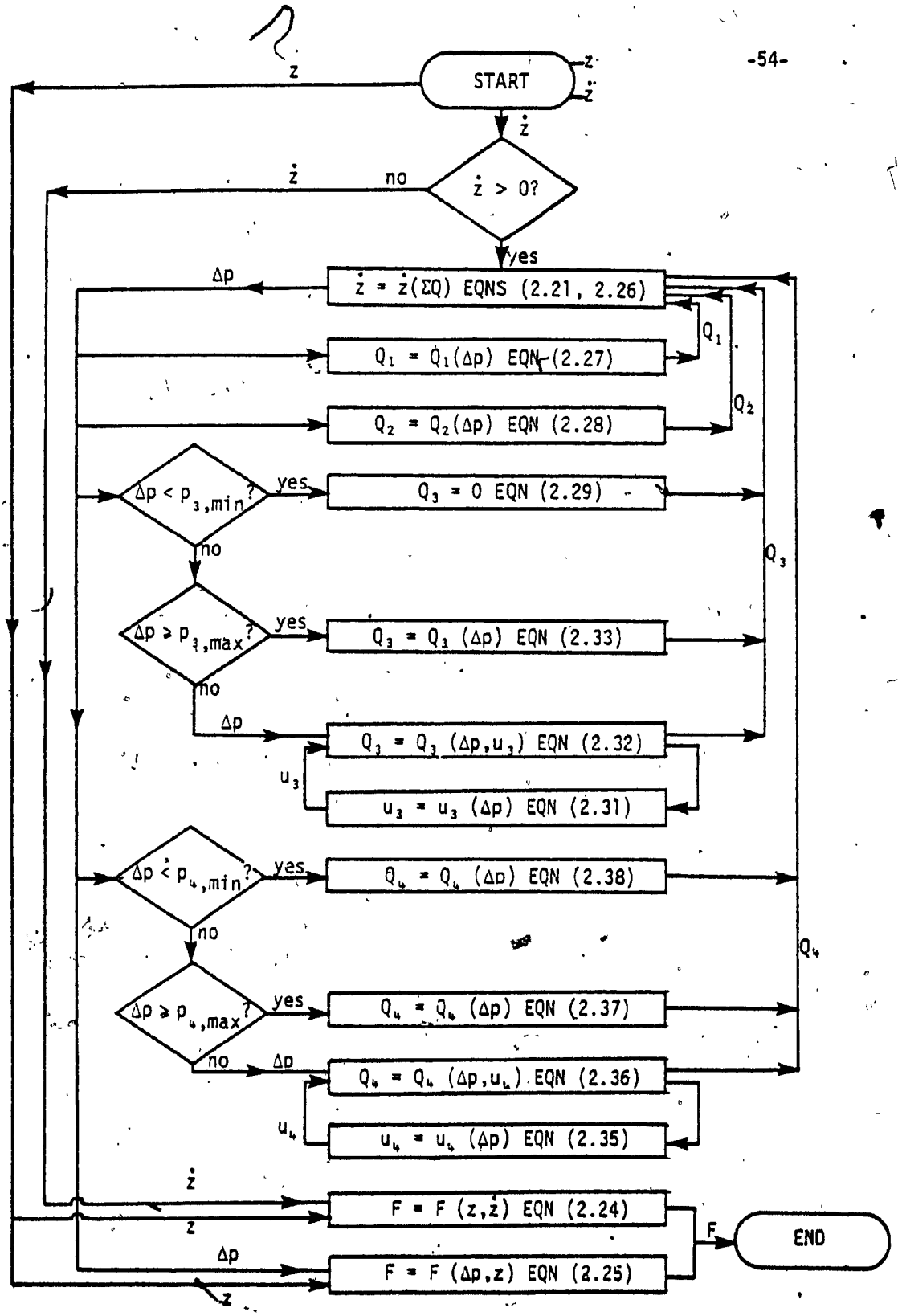

Fig. 3.4: Flowchart for the Rear Shock Absorber Model

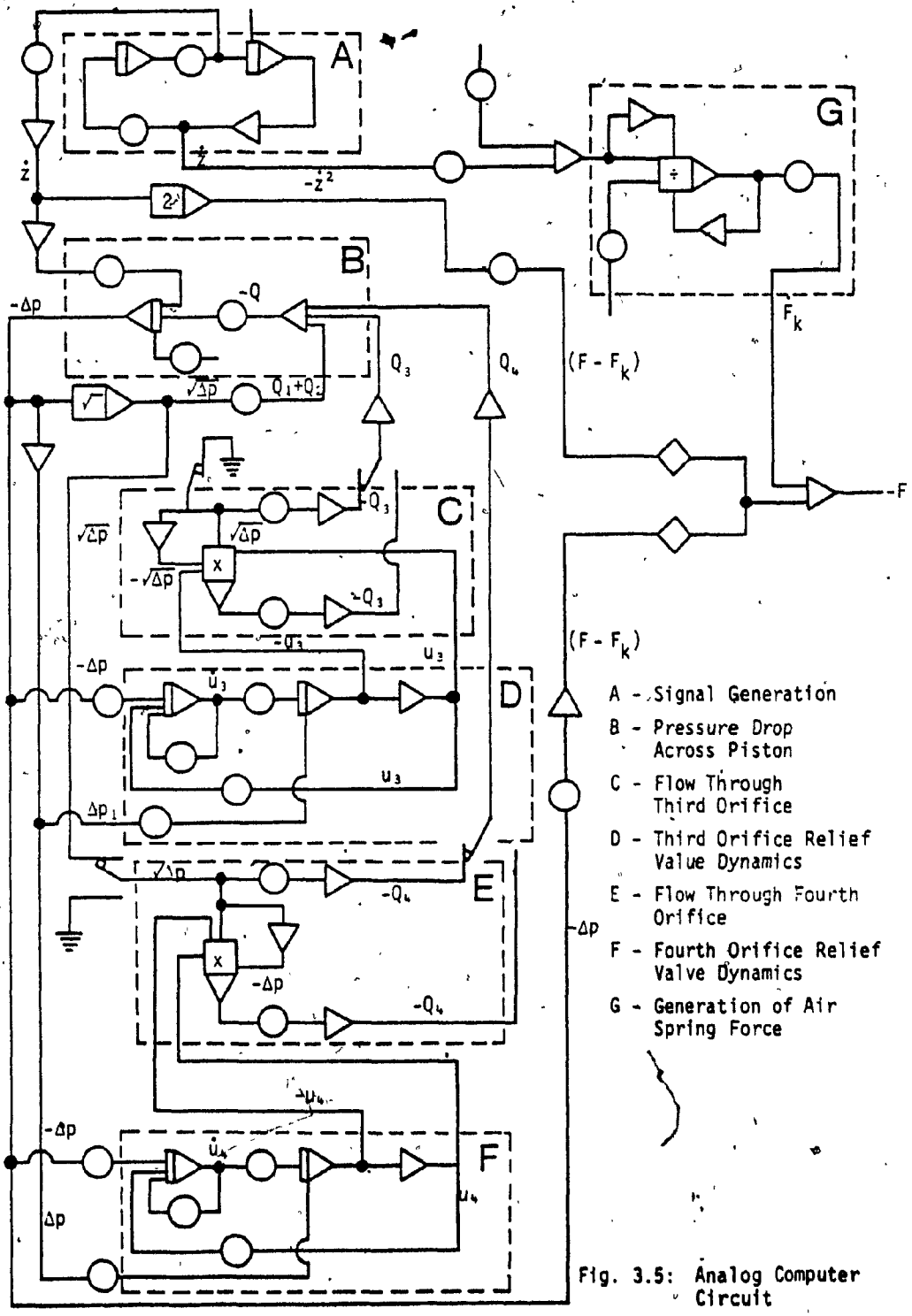

Fig. 3.5: Analog Computer Circuit

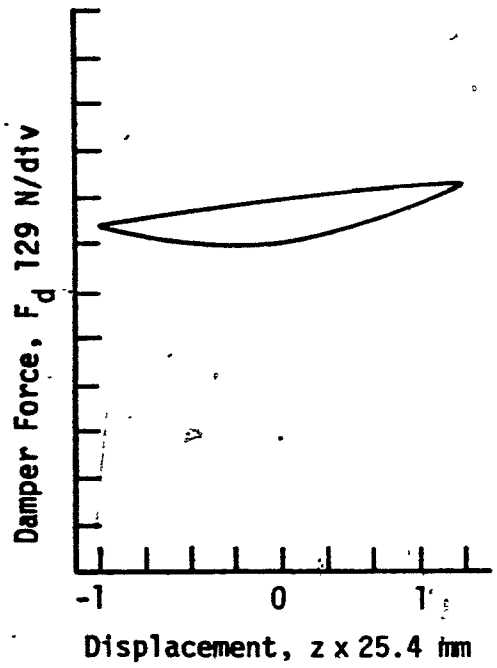

(a) f = 1.0 Hz
Y = 25.4 mm

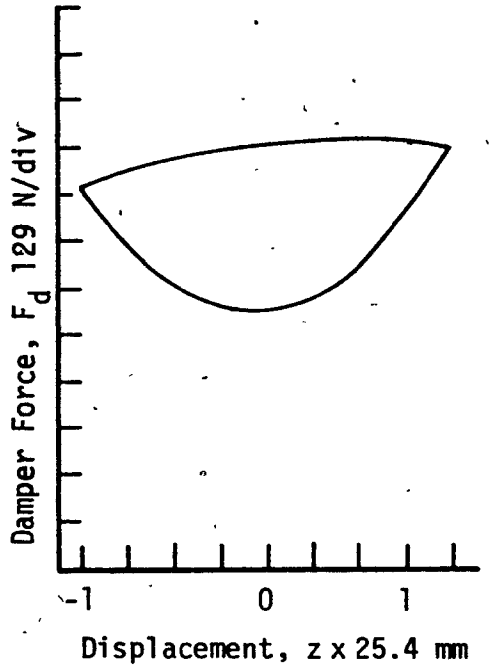

(b) f = 2.0 Hz
Y = 25.4 mm

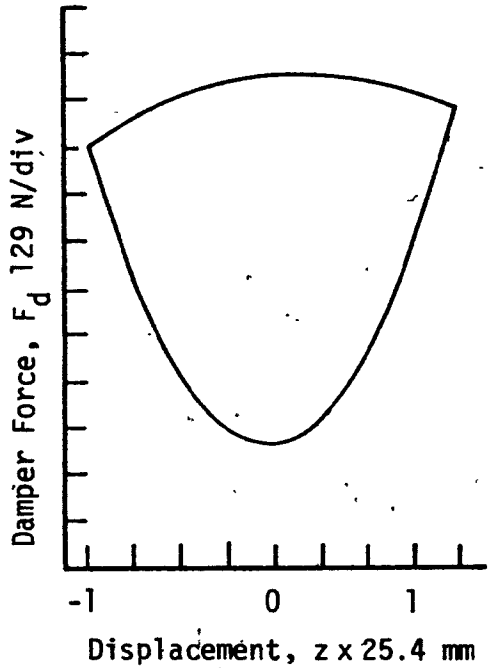

(c) f = 3.0 Hz
Y = 25.4 mm

Fig. 3.6: Rear Shock Absorber - Simulation Results

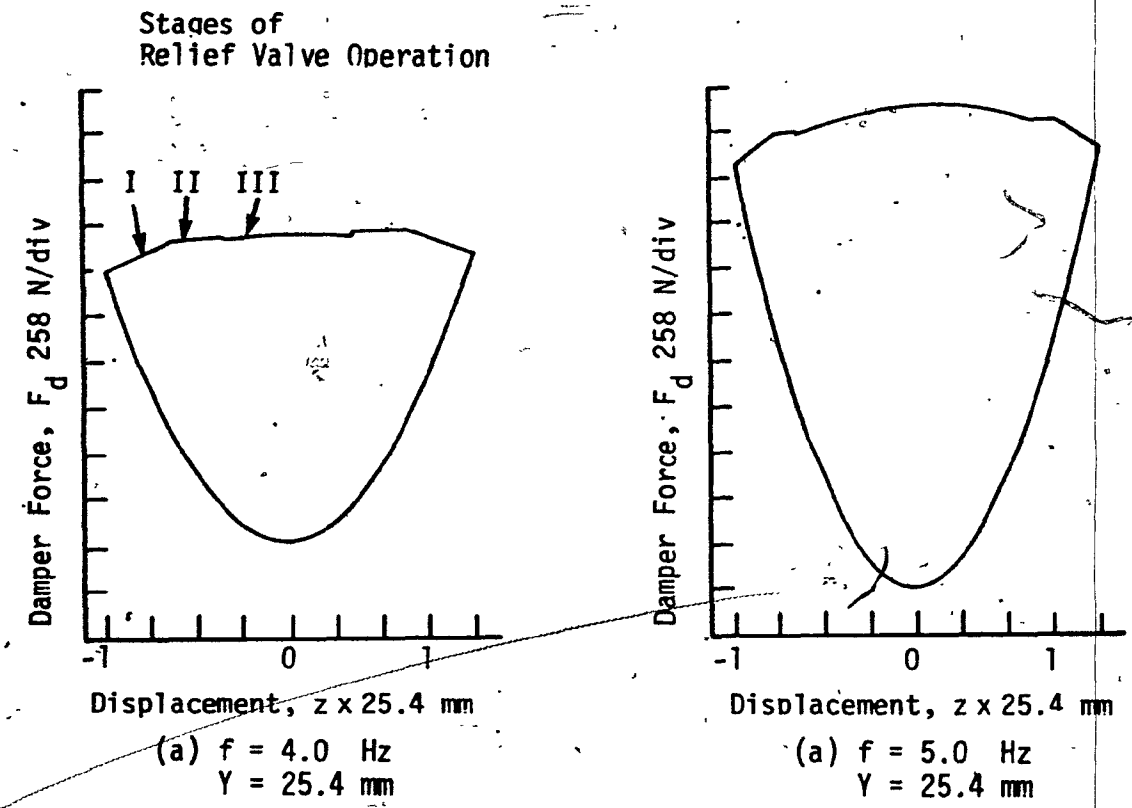

Fig. 3.7: Rear Shock Absorber - Simulation Results

TABLE 3.2: Rear Shock Absorber Results

Amplitude (mm)	Frequency (Hz)	Computer Simulation ΔF^c(N)	Experimental Data ΔF^e(N)	% Error = $\left\|\frac{\Delta F^c - \Delta F^e}{\Delta F^e}\right\| \times 100$
25.4	1.0	163.7	141.9	13.3 %
25.4	2.0	529.3	462.6	12.2 %
25.4	3.0	1001.9	1031.9	5.0 %
25.4	4.0	1721.4	1754.3	1.9 %
25.4	5.0	2757.7	2708.8	1.7 %

frequency was varied in the simulation. Each response was recorded as a F-D diagram on a X-Y plotter. The results are shown in Fig. 3.6 and 3.7, and in tabular form in Table 3.2.

3.3 Experimental Verification

The experimental verification consisted of isolating the front fork and rear shock absorber from the remaining suspension components (i.e. mass and helical spring). This was accomplished by fixing one end of the damping component to an inertial frame and driving the other end with an input signal.

The test rig consists of an electro-hydraulic shaker driving one end of the fork leg, or shock absorber, while the other end is fixed to an inertial frame through a load cell. A pictorial view of the test configuration is shown in Fig. 3.8. The shaker employs displacement and servo-valve feedback so that stable inputs are possible at low excitation levels. It was manufactured by International Scientific Instruments/Ling Co. of Japan. The damping force is measured by a Kyowa 2-ton capacity load cell. The Kyowa unit uses a strain gage piezo-resistive circuit with 2v AC bridge excitation so that a reliable signal is produced even near DC levels. The signal is amplified and conditioned using a Multi-metrics low pass filter with a break frequency of 100 Hz. The signal is then displayed on a Tektronix 5031 series oscilloscope. The X-Y display mode is used with displacement and force plotted on the X and Y axis, respectively. The resulting F-D diagrams are recorded by Polaroid camera.

3.4 Correlation of Results

For sinusoidal excitation, the peak damping force is generated at mid-stroke. The peak damper force may, however, occur elsewhere due to

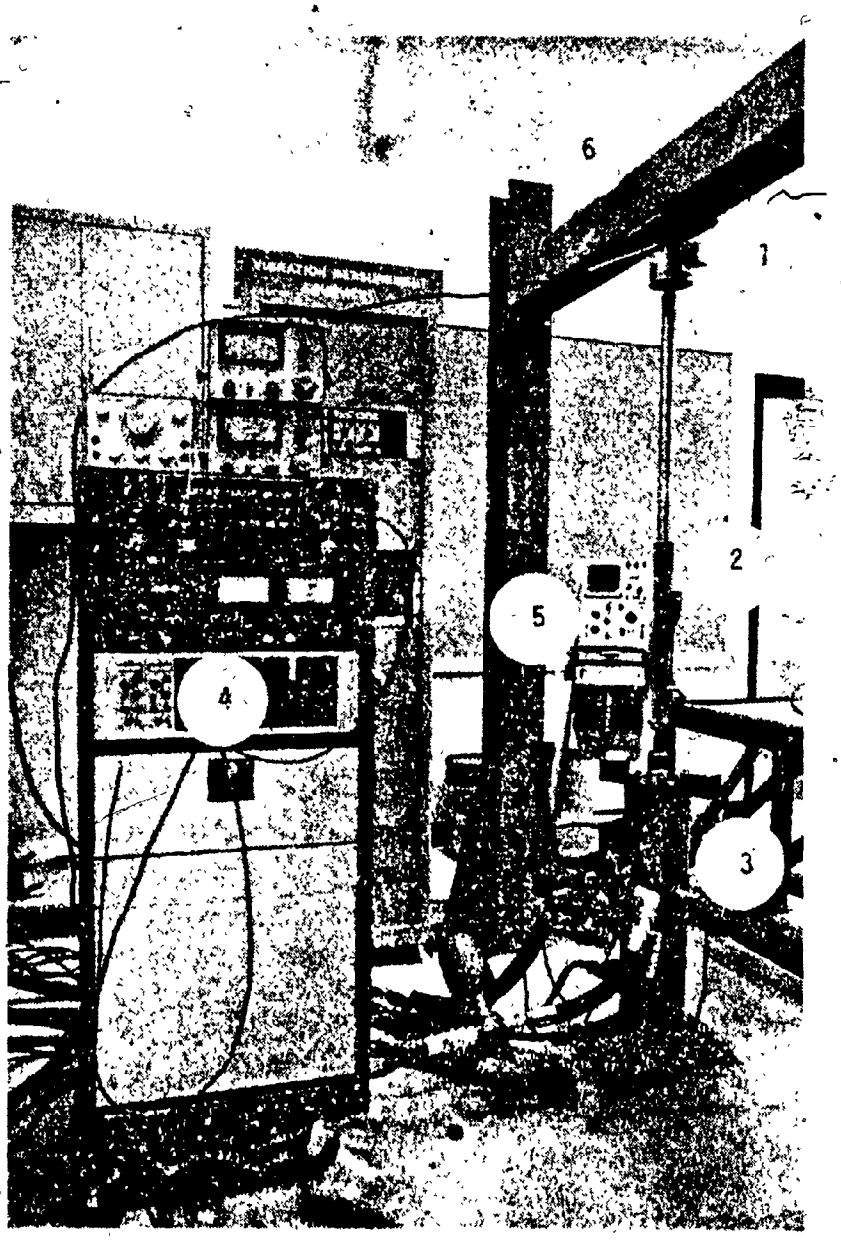

1 - Load Cell
2 - Fork Leg
3 - Electro-Hydraulic Shaker
4 - Signal Conditioner
5 - Oscilloscope
6 - Inertial Frame

Fig. 3.8: Pictorial View of Damper Force Testing Configuration

the skewness of the F-D diagram which results from the compression of the entrapped air column or accumulator. Since the damping force is the principle quantity of interest, the peak to peak damper force measured at mid-stroke is used for correlation.

3.4.1 Front Fork

The experimental results corresponding to the simulated plots in Figs. 3.2 and 3.3 are shown in Figs. 3.9 and 3.10. Qualitatively, the theoretical and experimental F-D diagrams appear to be very similar. Referring to Fig. 3.2(a) the skewness due to the air spring can be noted. Designating the forces at the extremities referred to the indicated datum as Δ_1 and Δ_2 , the contribution of the air spring is clear because of these points the velocity (and hence damping) is zero.

Quantitatively, the experimental and theoretical results along with their percentage errors are listed in Table 3.1. The peak to peak force (ΔF in Fig. 3.1) is generated at a part of the F-D diagram least likely to experience transient behavior. The steady-state nature of the fluid flow equations used in the damper force model development makes ΔF a logical choice for comparing simulated and experimental results. The differences in the F-D diagrams, obtained by simulation and experiment, in particular the behavior near the endpoints (zero relative velocity), is due to the omission of compressible reversed flow, valve dynamics, and other transient inducing considerations in the mathematical model. However, not withstanding qualitative differences away from the point at which the damper forces are measured, ΔF is a suitable quantity for validating the damper force behavior. A discussion on validation and the validation procedure used for the damper force models in this investigation is presented in Appendix IV. The percentage errors were less than 2 percent for the constant amplitude runs and less than 1 percent for the constant frequency runs, with the exception of Fig. 3.3(b).

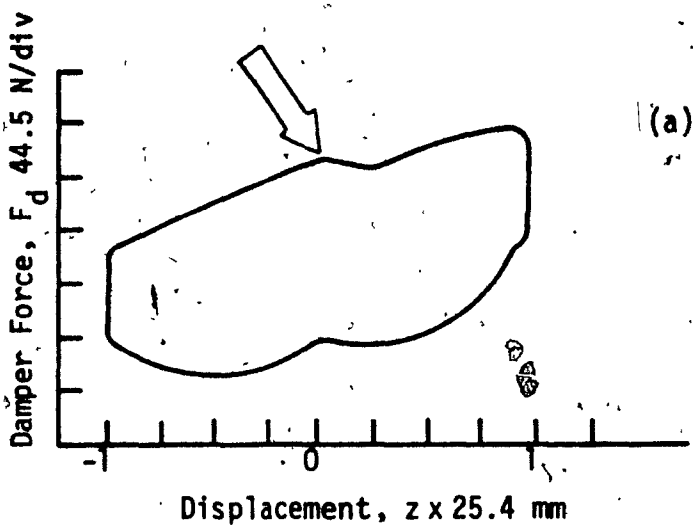

(a) f = 1.0 Hz
Y = 25.4 mm
Arrow indicates the dynamic behavior of the load cell

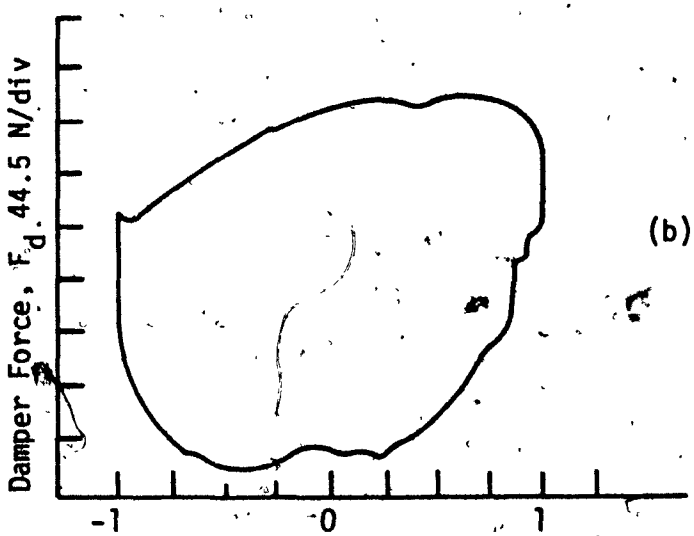

(b) f = 3.0 Hz
Y = 25.4 mm

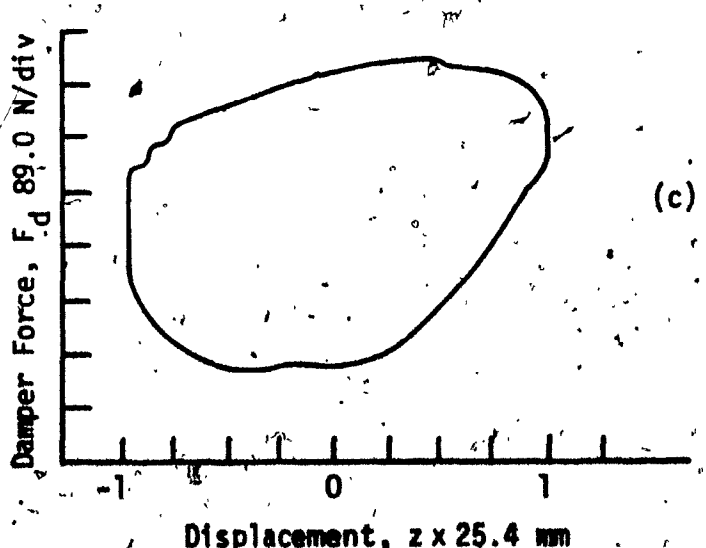

(c) f = 5.0 Hz
Y = 25.4 mm

Fig. 3.9: Front Fork - Experimental Results

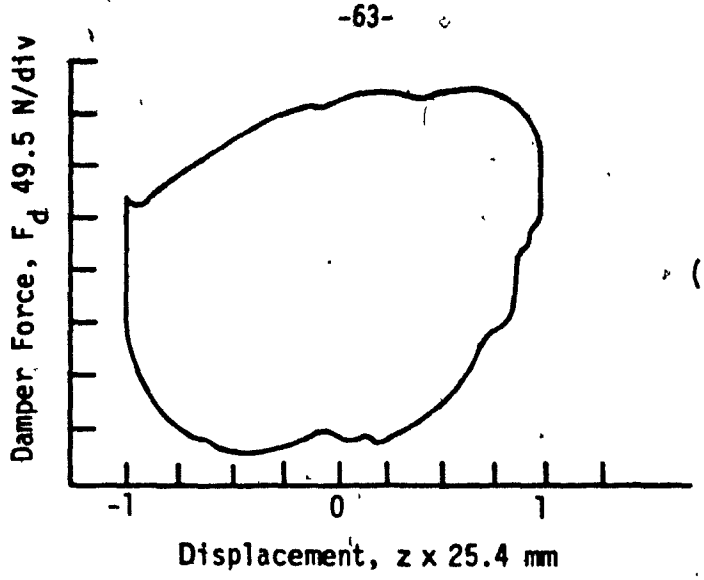

(a) f = 3.0 Hz
Y = 25.4 mm

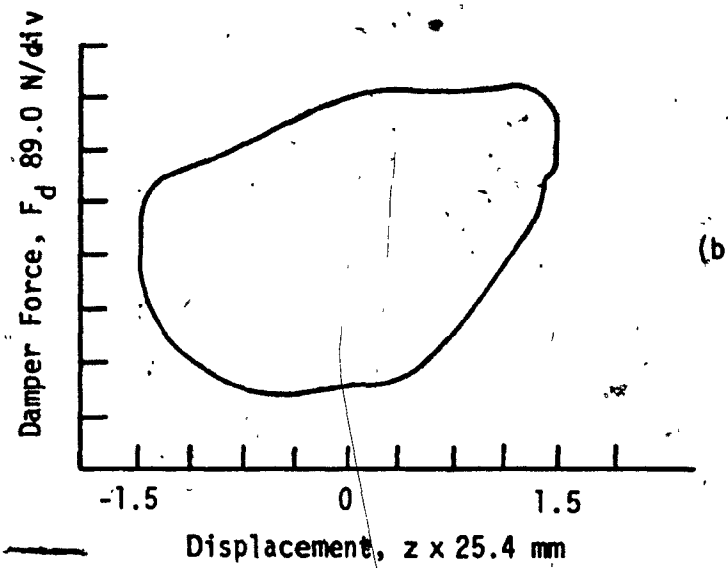

(b) f = 3.0 Hz
Y = 38.1 mm

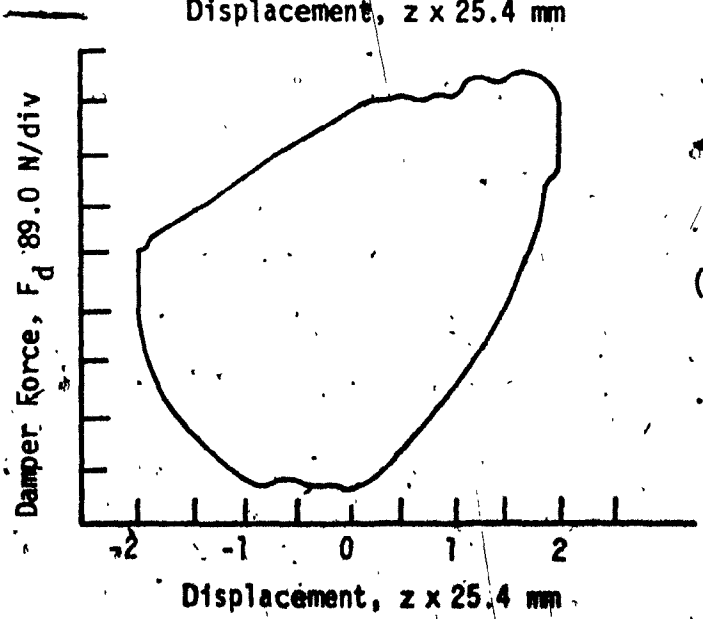

(c) f = 3.0 Hz
Y = 50.8 mm

Fig. 3.10: Front Fork - Experimental Results

3.4.2 Rear Shock Absorber

The experimental results corresponding to the simulated results in Fig. 3.6 and Fig. 3.7 are shown in Fig. 3.11 and Fig. 3.12. Qualitatively, the two sets of data are in good agreement. The skewness due to the gas charged chamber can be noted in both cases. The peak to peak force values are listed in Table 3.2. The percentage error varies from 1.7 to 13.3 percent. The error follows an interesting pattern in that it decreases with stroking frequency. This pattern is due to the omission of a seal stiction term in the model. The decrease in error at the higher frequencies is expected because the damping forces will then be dominant.

Further comparison between the theoretical and experimental plots reveal two more minor discrepancies. Referring to Fig. 3.7(a) and (b), the operation of the relief valves is clearly distinguishable by the dips in the compression (upper) part of the F-D diagrams. Unfortunately, this high frequency phenomenon was filtered out in the recording of the corresponding experimental results (Fig. 3.12(a) and (b)). In addition, the F-D diagrams obtained from experiment contain a dip at the extremities (indicated by an arrow in Fig. 3.11(c)). This was due to compliance of the clevis mounts in the shock absorber test rig and was not accounted for in the computer simulation model.

3.5 Summary

In this chapter, the damper force models described in Chapter 2 were verified using laboratory testing techniques. The theoretical response of the models was obtained by computer simulation. A digital and analog computer were used for the front fork and rear shock absorber, respectively. The results were presented in the form of plots and

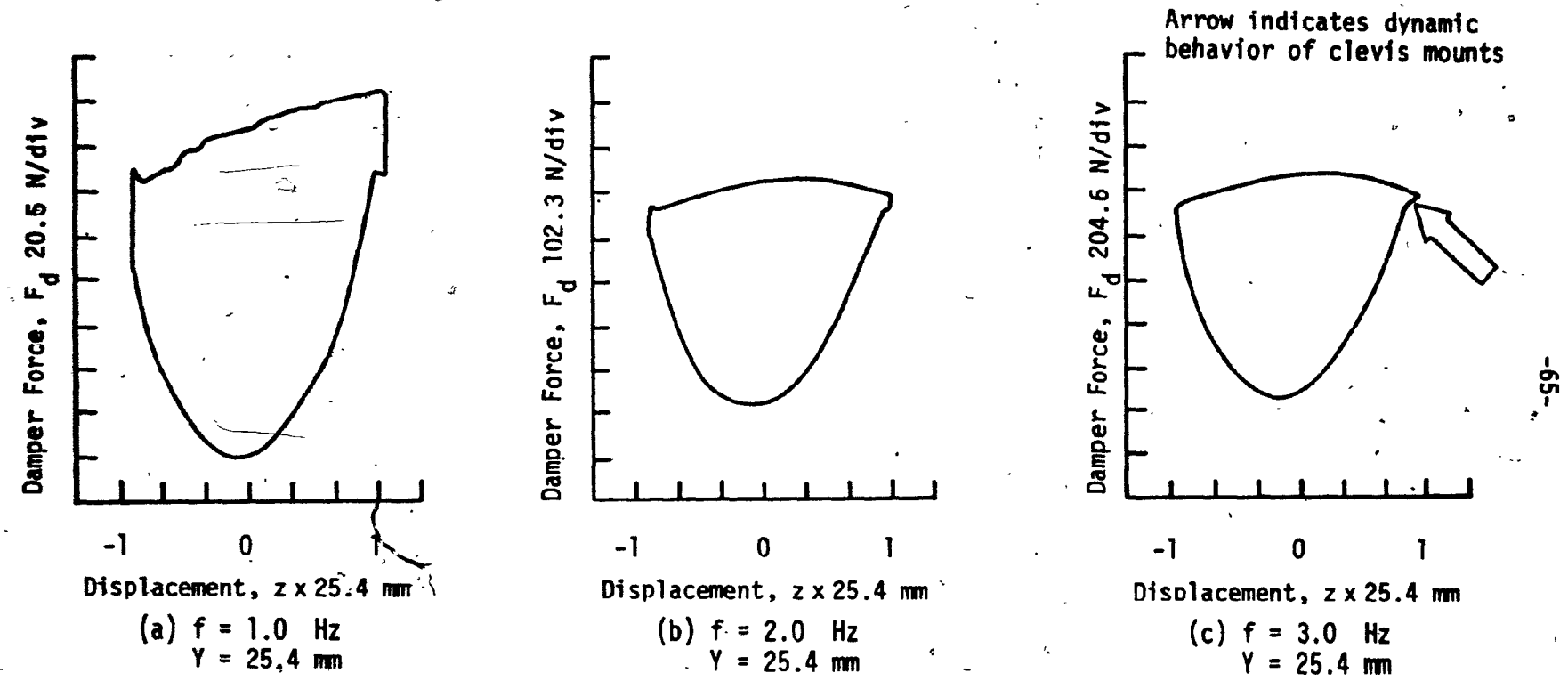

Fig. 3.11: Rear Shock Absorber - Experimental Results

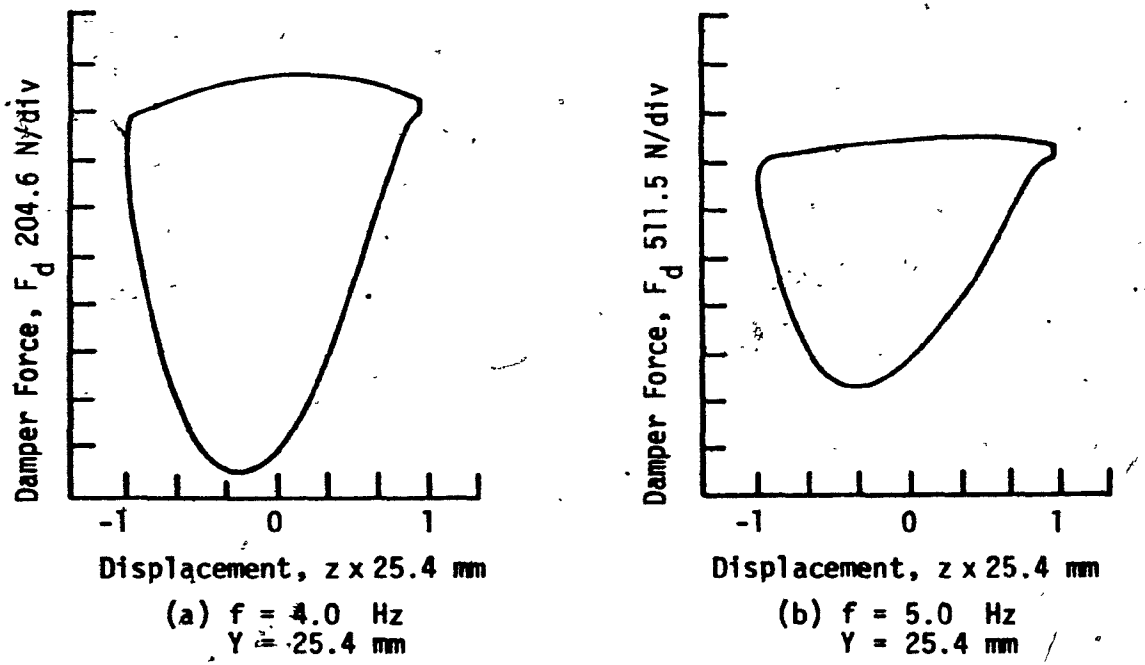

(a) f = 4.0 Hz
Y = 25.4 mm

(b) f = 5.0 Hz
Y = 25.4 mm

Fig. 3.12: Rear Shock Absorber - Experimental Results

tabular data. The experimental techniques were described and the results correlated to those obtained by computer simulation.

CHAPTER 4

COMPUTER SIMULATION AND EXPERIMENTAL VERIFICATION OF THE SUSPENSION SYSTEM MODEL

CHAPTER 4

COMPUTER SIMULATION AND EXPERIMENTAL VERIFICATION OF THE SUSPENSION SYSTEM MODEL

4.1 Introduction

In this chapter, a computer simulation and experimental verification of the suspension system model described in section 2.3 is performed. The experimental verification of the suspension system model is based on innovative new techniques, as opposed to the conventional test methods used in the damper force model verification.

4.2 Computer Simulation

The governing equations of the suspension model; equations (2.48) and (2.50), and coefficient expressions; equations (2.42), (2.47), and (2.49), were programmed on a VAX-11/780 computer in FORTRAN. The results were plotted using a CalComp drum plotter. The response surfaces were plotted with the aid of a hidden-line algorithm [87].

4.2.1 Simulation in the Frequency Domain

In mechanical systems, frequency domain characteristics are often given in terms of the system transmissibility [88]. The transmissibility of a system under sinusoidal excitation at a given frequency is the absolute ratio of response amplitude to excitation amplitude. The variation of the transmissibility with excitation frequency is the transmissibility characteristic of the system. It is independent of excitation amplitude only if the system is linear.

One method of simulating the non-linear suspension model in the frequency domain is to use an equivalent linearization technique [88].

However, it has been shown [89] that large errors are introduced when this technique is applied to systems containing velocity squared and coulomb damping. Since the suspension model contains sizable amounts of velocity squared and coulomb type damping, an alternative method of solution was used.

The system equations are solved as an initial value problem under harmonic excitation. A predictor-corrector integration scheme [90] is used to obtain the system response. When steady-state is reached, the amplitude ratio (in this case velocity ratio) is stored. The routine is restarted at an incremented excitation frequency using the steady-state values as initial conditions, in order to minimize the settling time. In this manner a frequency sweep is performed and the quantities of interest are obtained.

The system transmissibility curve for a specified excitation amplitude is shown in Fig. 4.1. The flat portion of the curve in the low frequency range is due to seal stiction (i.e. equation (2.48)). The curve breaks at a frequency:

$$f = [F_{coul_1}/4\pi^2 mY]^{\frac{1}{2}} \qquad (4.1)$$

where F_{coul_1} is the value of breakaway seal stiction

m is the system mass

Y is the excitation amplitude.

Above this frequency the system behaves as a lightly damped system (equation (2.50)). Since the break frequency can be located on either side of the natural frequency, the excitation amplitude is an influential factor in the performance of the system. The transmissibility

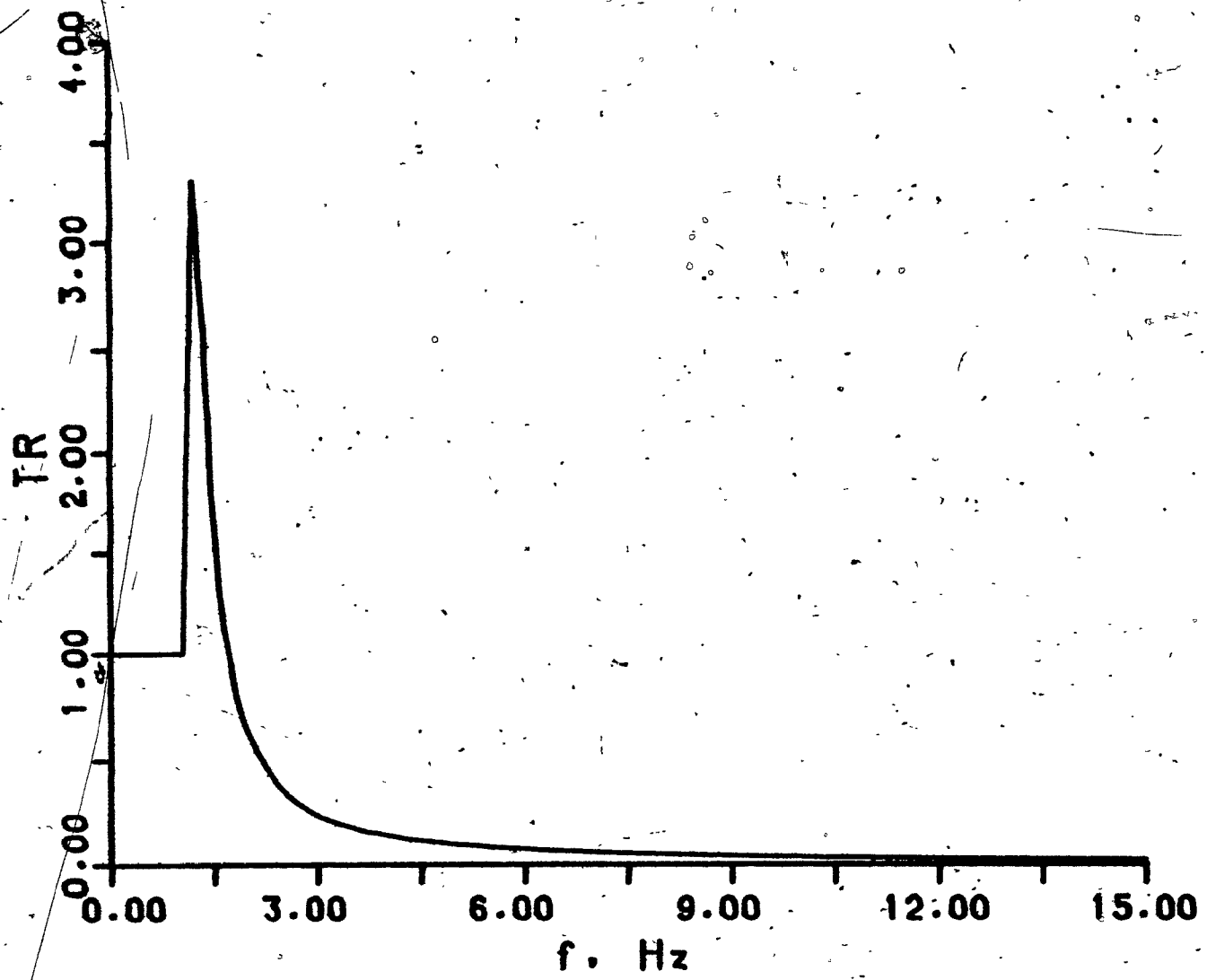

Fig. 4.1: Transmissibility Curve, Y = 12.7 mm

characteristics of the suspension are more fully represented by plotting the TR vs f curve against Y. The resulting response surface is shown in Fig. 4.2. The dependancy of the break frequency upon the excitation amplitude, and its effect on the peak transmissibility can be observed in the figure.

4.2.2 Simulation in the Time Domain

In the time domain, the system response to a displacement or velocity step is a paramount design consideration [91]. As in the case of frequency domain simulation, the system equations are solved using an initial value routine [90]. A step displacement or velocity is used for the initial condition. The response to positive and negative displacement steps is shown in Fig. 4.3. The difference in the compression and extension values is due to the asymmetric nature of the fork. In actual operating conditions the velocity step is a more realistic input. An off-road motorcycle travelling on a typical terrain often encounters repeated jumps of up to two meters without loss of rider control. If both wheels contact the ground simultaneously, velocity steps of up to 6.3 m/s are realized. The response to various velocity steps is shown in Fig. 4.4. The two design quantities of interest during the response are transmitted force and relative displacement. When these quantities are plotted for specified velocity steps, Lissajous diagrams as shown in Fig. 4.5 are obtained. These diagrams can be interpreted physically as follows; referring to Fig. 4.5(a) and Fig. 4.4, the force transmitted along path 0-1-2 occurs during the first quarter period of the response (initial compression). Path 0-1 is determined by the initial velocity and seal stiction. For higher velocity steps, the path 1-2 suddenly

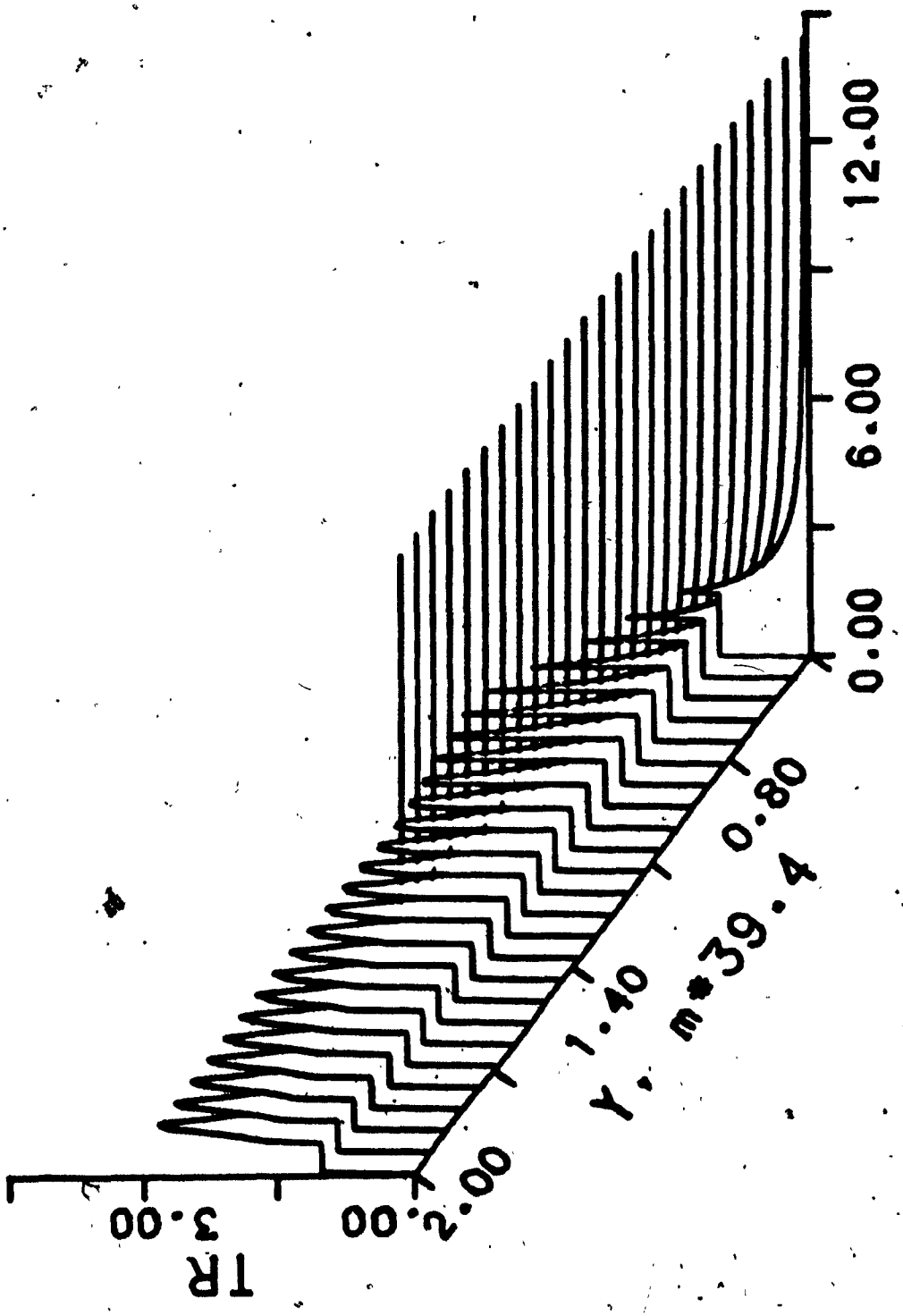

Fig. 4.2: Frequency Response Surface for an Existing Design

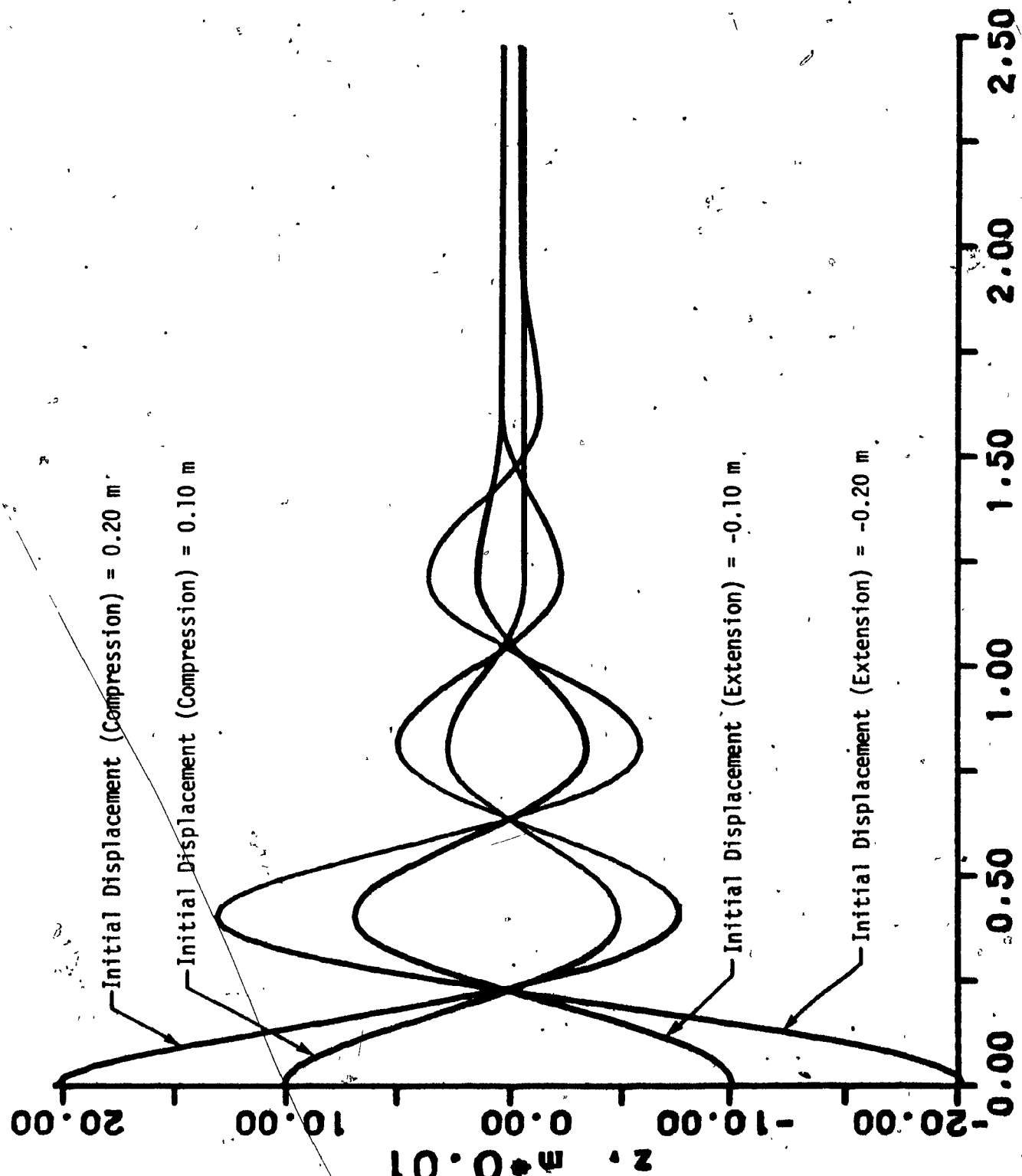

Fig. 4.3: Displacement Step Response

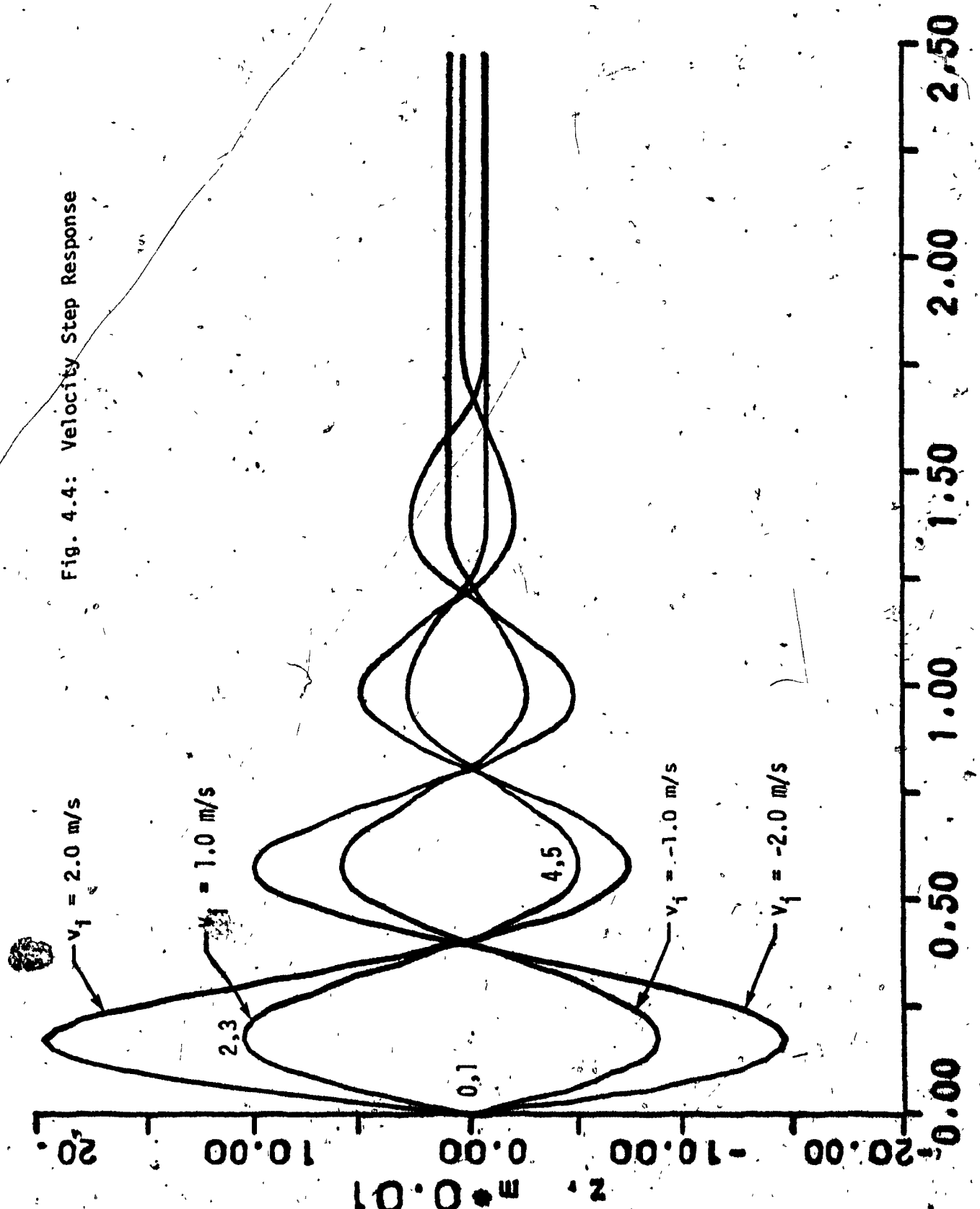

Fig. 4.4: Velocity Step Response

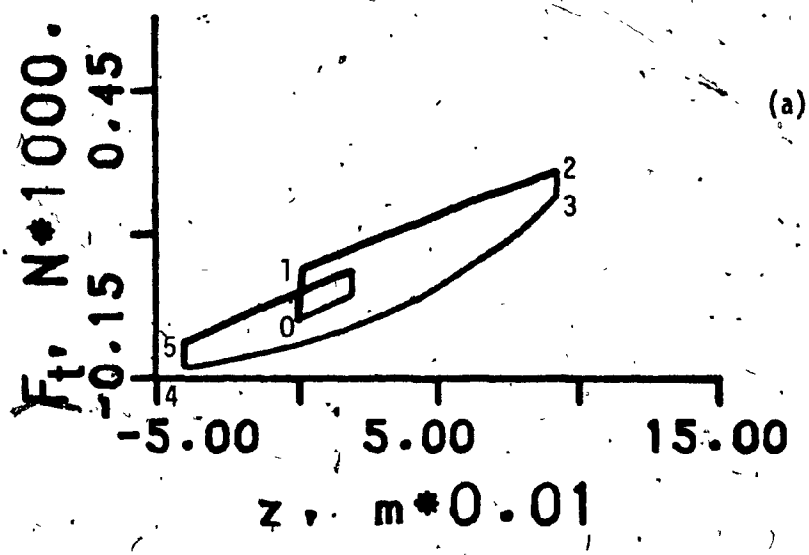

(a) v_i = 1.0 m/s

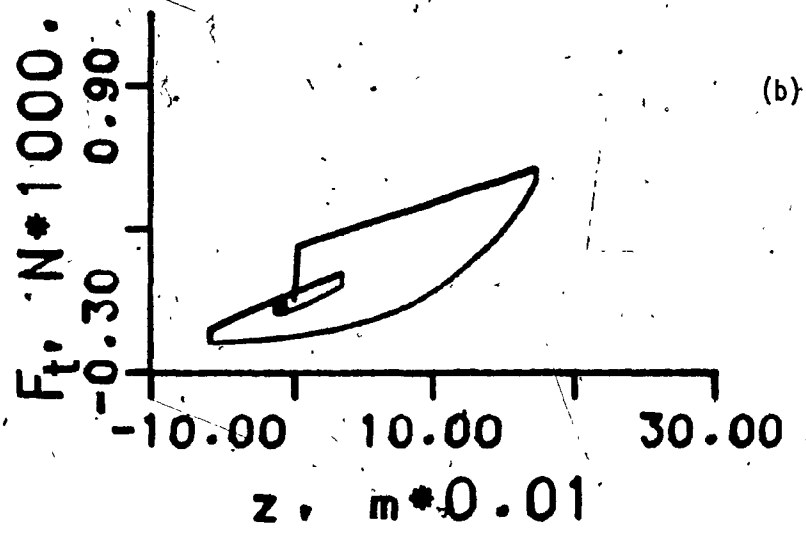

(b) v_i = 2.0 m/s

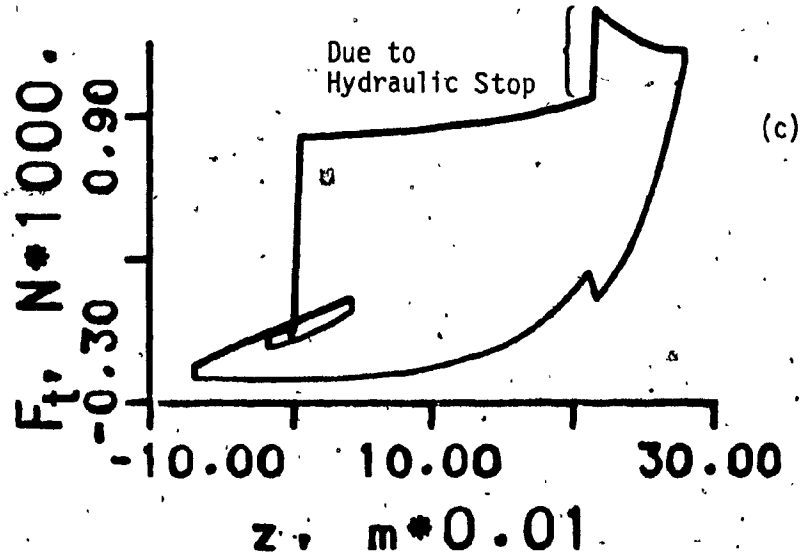

(c) v_i = 4.0 m/s

Fig. 4.5: F_t vs z Lissajous Diagrams for Velocity Step Input

increases when the hydraulic stop is encountered (Fig. 4.5(c)). Paths 2-3 and 4-5 are due to seal stiction and path 3-4 is the system response during rebound (extension). The peak transmitted force lies along path 0-1-2. Since in the time domain the quantities of interest (peak force and maximum relative displacement) are generated during the first quarter period of the response, only path 0-1-2 needs to be plotted to obtain the principal characteristics of the response. In practice, the suspension must respond to a range of inputs. Hence the time domain characteristics are better represented by the response surface shown in Fig. 4.6.

4.3 Experimental Verification

Experimental verification was carried out on the suspension model using a test rig similar to that used to verify the damper force models (Section 3.3). The test rigs differ in that the former rig contained only damper force components whereas the present rig utilizes dampers, springs, and a mass. An additional difference is that a 38 mm Marzocchi fork leg is used instead of the 35 mm Betor fork leg used previously.

A single degree of freedom hardware model was used to verify the results obtained from computer simulation. The test rig consists of a 38 mm fork leg, with internal helical spring and charged air volume, mounted between a mass and an electro-hydraulic shaker. The amount of mass used (28.8 kg) was determined by measuring the static deflection of an off-road motorcycle with an average size rider on board. The instrumentation consists of accelerometers mounted on the base and mass. The signals are displayed on a Philips oscilloscope with storage facilities. A pictorial view of the test configuration is shown in Fig. 4.7. To provide guidance for the mass, a set of linear bearings

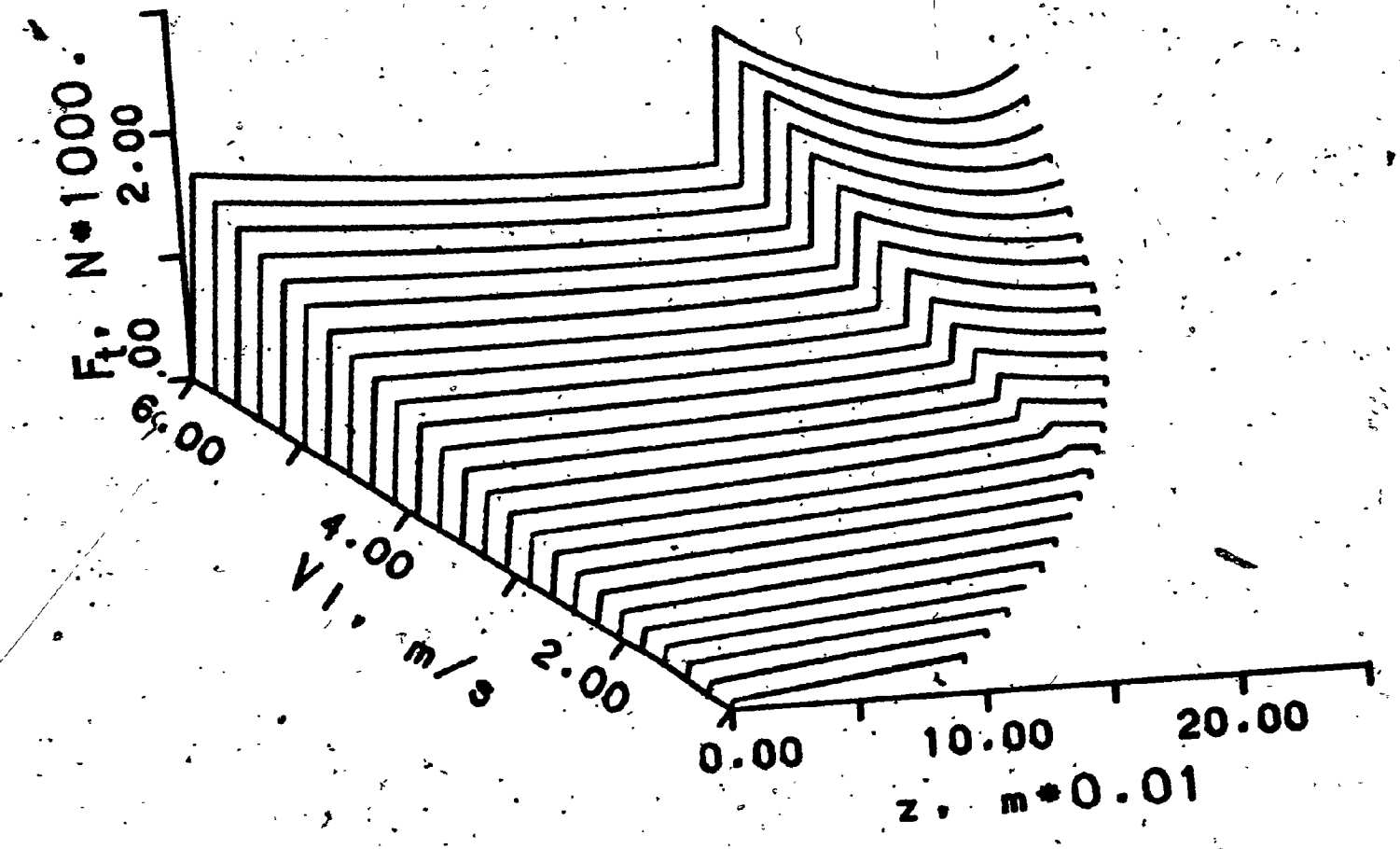

Fig. 4.6: Velocity Step Response Surface for an Existing Design

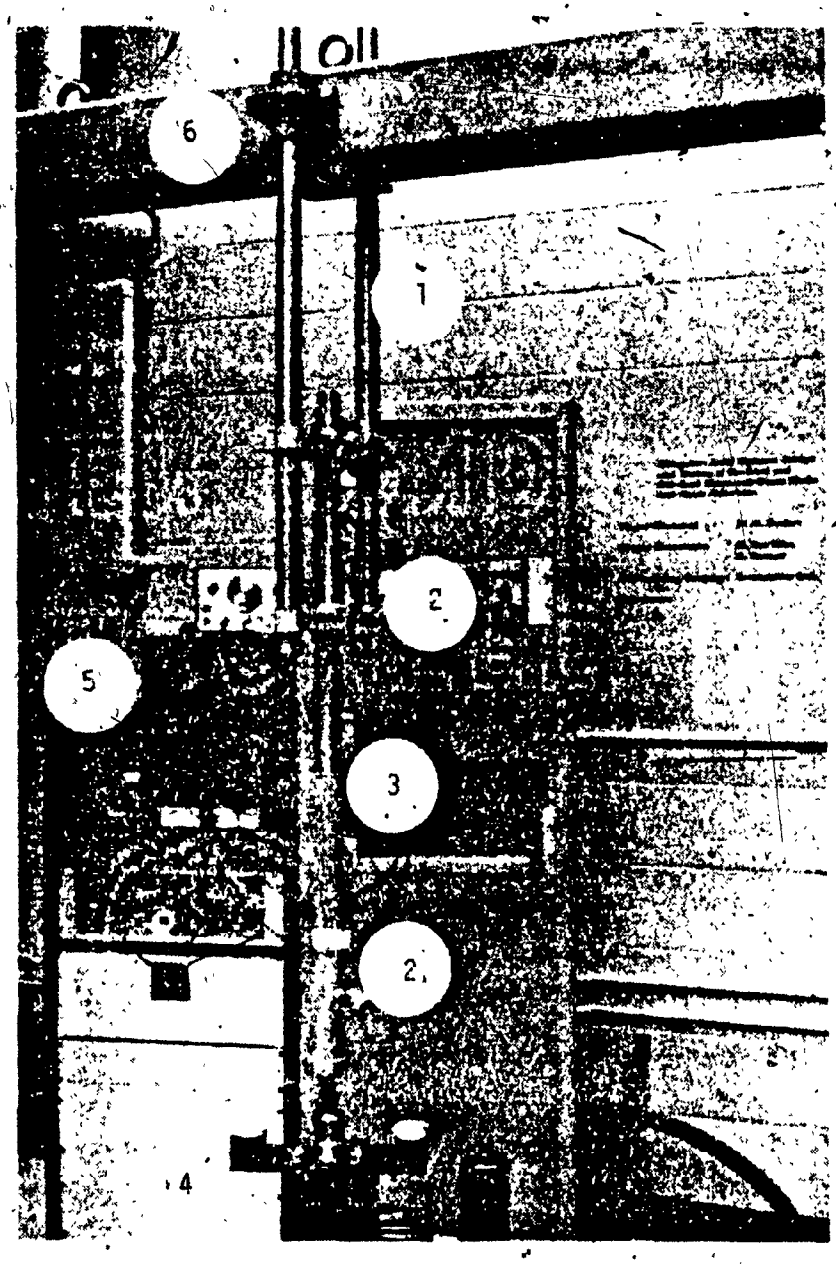

1 - Mass
2 - Accelerometer
3 - 38 mm Fork Leg
4 - Electro-Hydraulic Shaker
5 - Oscilloscope
6 - Guidance Bearing

Fig. 4.7: Pictorial View of Suspension System Testing Configuration

with wiper seals are used. Unfortunately, the seals introduce stiction of the same order of magnitude as those of the fork.

4.4 Correlation of Results

The governing equations presented in section 2.3 model the front suspension of a typical off-road motorcycle. The test rig described in the previous section attempts to do the same except that the rig introduces an additional stiction mechanism in the suspension. In order to obtain good correlation between the computer and experimental results, the mathematical model was modified to incorporate the additional stiction mechanism.

The additional stiction mechanism differs from the seal friction of the fork leg because of its dependency on the sign of the absolute velocity $\dot{x}$, instead of the relative velocity $\dot{z}$. Designating the breakaway forces in the fork seal and guidance bearing seal as F_{coul_1} and F_{coul_2}, respectively, equations (2.48) and (2.50) become

1. $|m\ddot{x}| < F_{coul_1} + F_{coul_2}$

$$\ddot{x} = \ddot{y}$$

$$\dot{x} = \dot{y} \qquad (4.2)$$

$$x = y$$

2. $|m\ddot{x}| > F_{coul_1} + F_{coul_2}$

$$m\ddot{x} + [T_p + T_{or} + T_{hyd}]\,\dot{z}^2\,\mathrm{sgn}(\dot{z}) + F_{seal_1} + F_{seal_2}$$

$$+ kz + \left[\frac{MRT}{V_o - (A_p + A_{tube})z} - p_{at}\right](A_p + A_{tube}) = 0 \qquad (4.3)$$

where $F_{seal_2} = F_{coul_2} \cdot sgn(\dot{x})$ for $|\dot{x}| \geq \epsilon$

$F_{seal_2} = F_{coul_2} \cdot \left(\frac{\dot{x}}{\epsilon}\right)$ for $|\dot{x}| < \epsilon$

4.4.1 Frequency Domain

The computer simulation was re-run incorporating the additional stiction mechanism. In the laboratory, a frequency sweep at various amplitudes was performed. Both sets of results are plotted in Fig. 4.8. The non-linear nature of the suspension is evidenced by the strong dependency on excitation amplitude. There is good agreement between the results obtained through computer simulation and those obtained in the laboratory.

4.4.2 Time Domain

In the time domain, a displacement step was used instead of a velocity step because of the physical limitation of the shaker test facility which cannot produce a suitable range of velocity steps. Since the damping characteristics of the fork are asymmetric, a set of negative (extension) steps was used to produce sizable transients (see Fig. 4.3). The experimental results are plotted with the corresponding computer simulation results in Fig. 4.9. Again there is good agreement between the two sets of results.

4.5 Summary

To summarize, the computer simulation of the suspension system was verified in both frequency and time domains. The mathematical model was modified to include the guidance stiction present in the test rig. The experimental techniques were described and the results compared to those

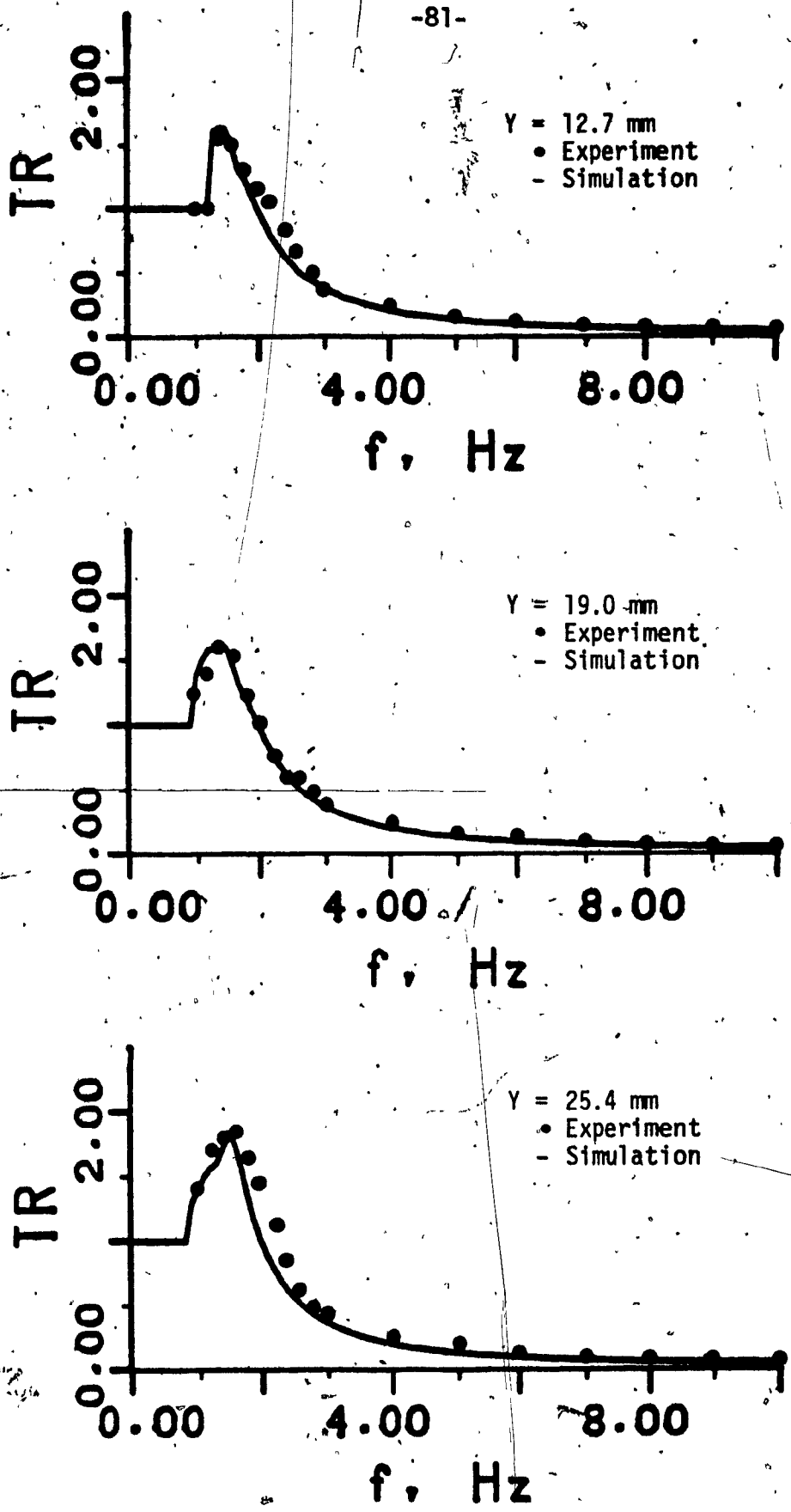

Fig. 4.8: Frequency Domain Results

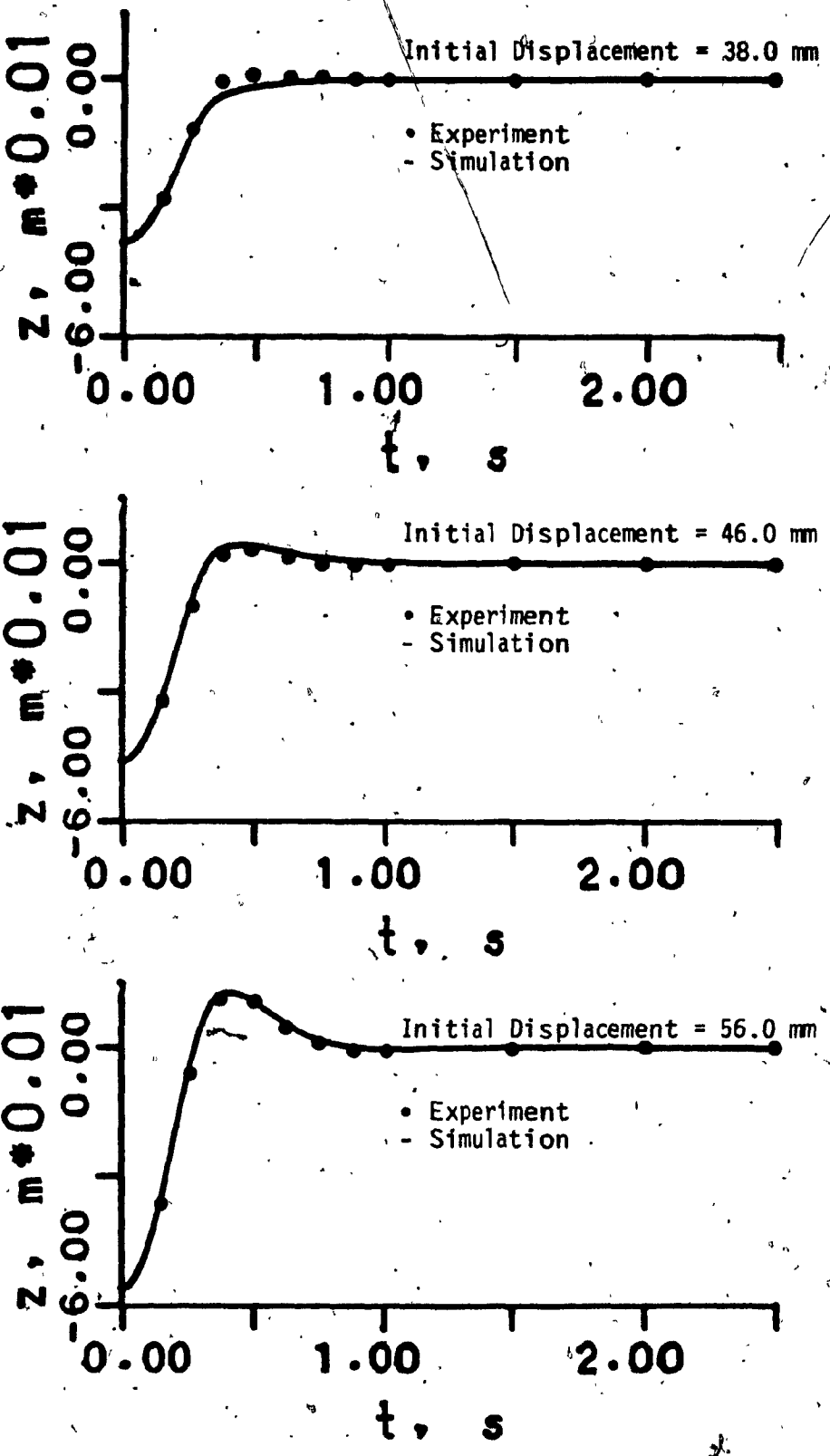

Fig. 4.9: Time Domain Results

obtained through computer simulation. The close agreement between both sets of results in both the frequency and time domains validates the use of the suspension system model in the succeeding chapters. In addition, the good correlation increases the extent of validation (although indirectly) of the damper force model of Chapter 3. A detailed discussion on validation is given in Appendix IV.

CHAPTER 5

SUSPENSION PERFORMANCE CRITERIA

CHAPTER 5

SUSPENSION PERFORMANCE CRITERIA

5.1 Introduction

The choice of performance index is important since it establishes the sense in which the design is best, or optimum. The performance index may be a function of the system response variables or of the suspension component parameters, or of both. The latter situation is represented by a performance index that includes; cost, maintainability, or reliability, which depend on the details of a specific suspension configuration. However, the ability to establish theoretical limits to the performance index without a priori choice of suspension configuration requires that the index be expressed only in terms of the system response quantitites. For this reason only such forms of performance indices are considered in this investigation.

Perhaps the most common form of performance index for mechanical systems is [92]:

$$I = \max |q| \tag{5.1}$$

The quantity q, may be displacement, velocity, acceleration, stress, or some combination of these quantities. When the specific interaction between two response quantities is to be controlled, a suitable performance index may be

$$I = \max |q_1| + D \max |q_2| \tag{5.2}$$

where q's are response variables and D is a weighting factor. For small values of D the performance index favors q_1, while for large values of D the preference is for q_2.

Another form of performance index is the integral of a response variable over a specified time period:

$$I = \int_{t_1}^{t_2} f(q)\, dt \qquad (5.3)$$

where $f(q)$ is a known function, e.g. $f(q) = q^2$. This type of performance index is common in control theory applications [93]. It is related to the forms considered by classical analytical optimization techniques such as the calculus of variations. The relative merits of various performance indices have been discussed by Karnopp and Trikha [94]. They show the performance limitations of a system optimized according to one criterion when considered from the point of view of another criterion. They conclude that the index given by equation (5.2) should be used to establish suspension system performance whereas equation (5.3) should be used as a supplementary performance index when (5.2) does not yield a unique solution (i.e. at large t).

5.2 Performance Criterion for Frequency Domain Analysis

In the frequency domain analysis of a suspension system, it is essential to have high damping at resonance and relatively less damping at high frequencies. A form of equation (5.2) which reflects this performance characteristic has been proposed [95] as:

$$I_f = (TR_p) + D(TR_h) \qquad (5.4)$$

where TR_p = peak transmissibility

TR_h = transmissibility in the higher range (8 f_p in this case)

D = weighting factor.

A decreasing value of I_f indicates an improvement in the suspension performance. Since the suspension model is non-linear, I_f is amplitude dependent (recall Fig. 4.2). The performance index can be plotted over the input amplitude range to yield a performance characteristic of the suspension in the frequency domain. This characteristic, shown in Fig. 5.1, is convenient to use because the system equations need to be solved only twice at each excitation amplitude. The curve shows an increasing trend in I_f with excitation amplitude, which follows logically from the increasing trend in peak transmissibility in Fig. 4.2.

5.3 Performance Criterion for Time Domain Analysis

The performance of shock isolation systems such as aircraft landing gears, railcar draft gears, and gun recoil mechanisms is usually described in the time domain [62-65,96-98]. In aircraft landing gear studies a typical performance index [64] is, for a specified maximum stroke, and descent velocity,

$$I = \max |F_g| \tag{5.5}$$

where F_g is the ground load during landing.

In the area of railcar cushioning gears a typical performance requirement is that during lading and railcar impact the lading accelerates to a specified level and remains constant until the relative velocity is zero, dissipating a maximum amount of energy [96]. The performance index is similar to that of aircraft landing gear except that the ground load (acceleration) and stroke are interchanged. For a specified contact velocity and peak acceleration,

$$I = \max |z| \tag{5.6}$$

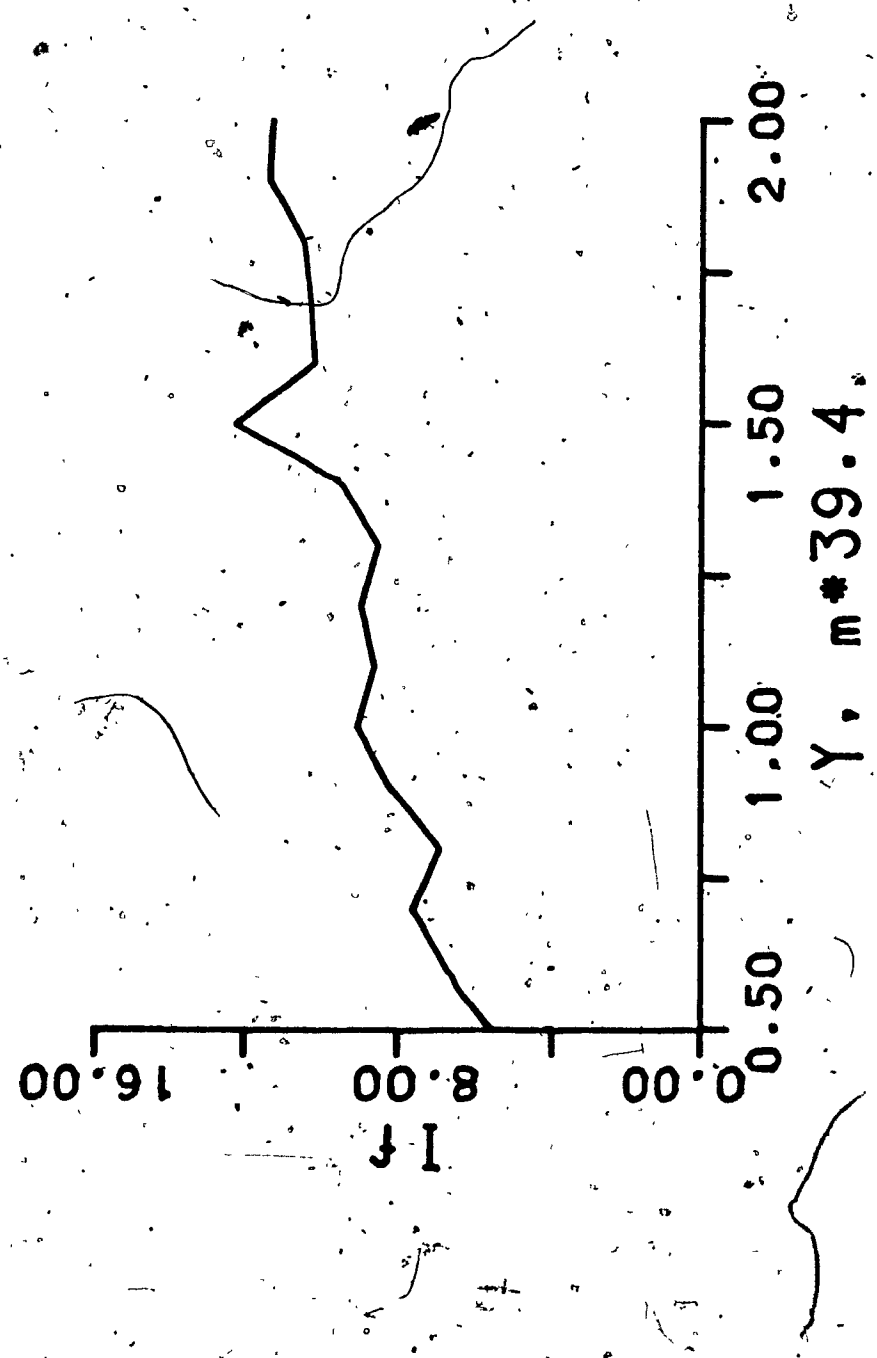

Fig. 5.1: Frequency Domain Performance for an Existing Design

where z is the stroke of the cushioning gear.

Another relavent shock isolation system is the recoil mechanism used in artillery. A typical performance requirement [97] is that the recoil force be reduced according to equation (5.5). In typical artillery, such as the M-102 (a 105 mm howitzer gun), different rounds are used. The firing of different rounds results in a range of breech forces. This situation is analogous to the motorcycle suspension responding to a range of velocity steps. Madiwale et al [98] have optimized the response of the M-102 to various rounds using a form of equation (5.5).

In the off-road motorcycle the allowable fork travel is constrained, whereas the peak transmitted force is the response variable requiring minimization. Referring to Fig. 4.5(a), the area beneath path 0-1-2 is the energy stored and dissipated during the first quarter period of response. This energy is determined by the initial condition. Hence, for a velocity step v_i

$$1/2\ m v_i^2 = \int_0^2 F\ dz \qquad (5.7)$$

An optimal performance requirement is that, for a specified maximum suspension travel z_{max}, the transmitted force is constant. Equation (5.7) then becomes

$$F_{opt} = m v_i^2/(2\ z_{max}) \qquad (5.8)$$

In suspension design, allowable travel z_{max}, and peak transmitted force F_p, are paramount design quantities. In equation (5.8), F_{opt} gives the lower bound on the peak force during initial compression. The value of

F_{opt} is compared to the peak force along path 0-1-2, calculated from the response, yielding a suitable performance index for the time domain. For a specified v_i,

$$I_t = \frac{F_{opt}}{F_p} \times 100\% \qquad (5.9)$$

When I_t is 100%, the suspension performance is ideal, thus the performance decreases with decreasing I_t.

In practice, the suspension must respond to a range of inputs (recall Fig. 4.6). The variation of I_t over the input range gives the performance characteristic of the suspension in the time domain. A plot of I_t vs v_i is shown in Fig. 5.2. I_t increases until v_i is 2.8 m/s. It then takes on a reduced, nearly constant value. This trend can be readily understood with the aid of Fig. 4.6. The response surface becomes flatter with v_i until the hydraulic stop is encountered at v_i = 2.8 m/s. The peak force location then shifts from location 2 (Fig. 4.5(a)) to the hydraulic stop location (Z_c) and remains there for the rest of the excitation range.

5.4 Summary

In this chapter the performance indices for the frequency and time domain analysis of the suspension system were presented. The nature of the indices was discussed and various alternative performance indices that were presented in the literature were discussed. Suitable performance indices for the respective domains were then presented. These indices serve as the basis for evaluating the performance of the suspension system and in the formulation of objective functions for suspension optimization in the next chapter.

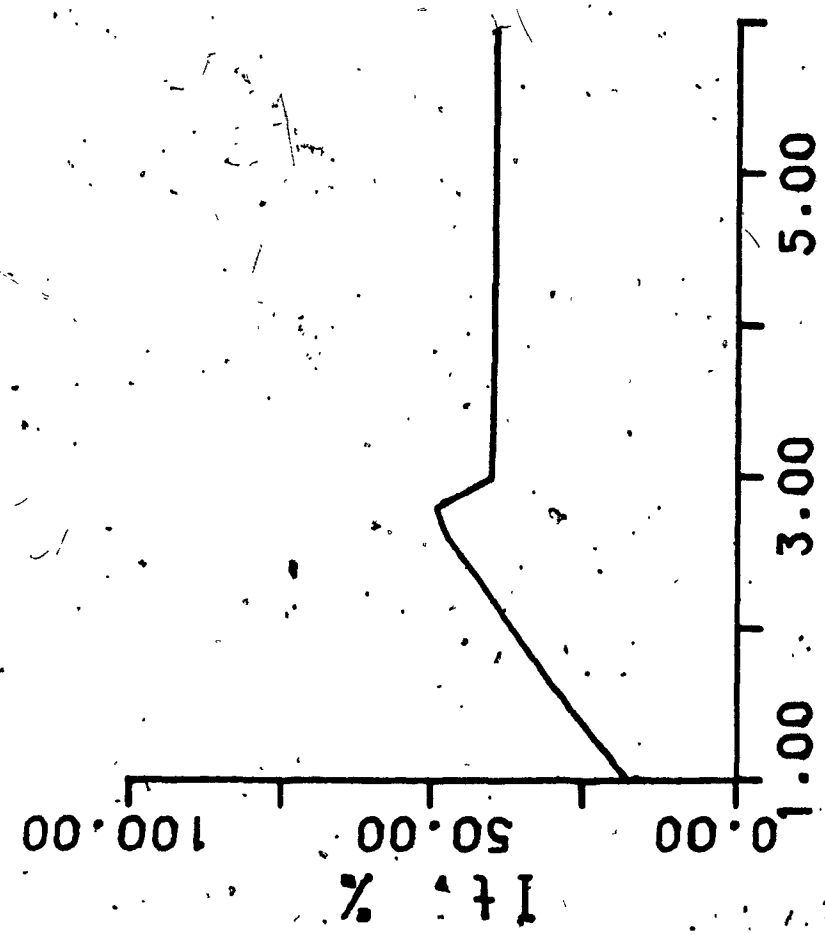

Fig. 5.2: Time Domain Performance for an Existing Design

CHAPTER 6

SUSPENSION OPTIMIZATION

CHAPTER 6

SUSPENSION OPTIMIZATION

6.1 Introduction

In the area of suspension optimization, the objective is to provide a design whose performance is in some sense better than that of the candidate designs with which it is compared. An "optimum design" is seldom optimum in any absolute sense. Rather, it is a tradeoff between several competing dynamic specifications. The available optimization methods for suspension optimization fall into two categories: techniques based on control theory, and computational techniques.

Control theory techniques for suspension optimization were introduced by Bender et al [99]. They minimized a weighted sum of mean squared vehicle acceleration and rattlespace for a two-degree of freedom vehicle model. Karnopp and Trikha [94] were among the first researchers to investigate optimal suspension design, minimizing mean square acceleration and rattlespace using a single degree of freedom model. The most outstanding attribute of the control theory approach is its suitability to synthesis of suspensions utilizing active components [100-104]. However, the nature of the quadratic performance index (equation 5.3) and the inherent difficulties associated with complex suspension models limit the usefulness of this approach to suspension optimization [105].

Due to the popularity of digital computers, computational optimization techniques are in widespread use in mechanical design. Different methods and their relative merits constitute a large body of literature [106-115]. All computational methods progress toward the desired optimum in an iterative fashion. At any stage in the process,

a trial set of design parameters is selected, the equations of motion are solved, and then the response constraints are tested. If the constraints are satisfied, the performance index is evaluated and compared to the minimum value (minimization) obtained previously. The current minimum and associated design parameters are retained and another set of design parameters is selected. If the constraints are not satisfied, then this trial set of design parameters is rejected and another set is selected. The various optimization methods differ principally in their manner of deriving the next set of design parameters and of verifying the constraints.

The performance criteria (objective function) represents a surface in design-parameter space (a hypersurface if more than two design parameters are involved). The constraint functions restrict the admissible region of the space. The optimum design is the minimum altitude (minimization) of the response hypersurface within the admissible region of the design space. The optimization procedure amounts to a search procedure for exploring the topology of the hypersurface, where the description and position of the boundaries of the surface are found by solution of the system dynamics.

6.2 Formulation of the Objective Function

From the formulation of the two performance indices: I_f and I_t (equations (5.4) and (5.9)), it is evident that their values depend on the magnitude of excitation amplitude Y, and initial velocity v_i, respectively. The objective in the optimal design of the suspension is to identify the design parameters of the fork that will minimize I_f or maximize I_t. To account for the dependency of I_f and I_t on the range of input values, the objective function for each domain is formulated through an integral

function of the respective performance index.

6.2.1 Objective Function for Frequency Domain Analysis

The objective function for frequency domain analysis is to minimize the area under the I_f vs Y curve shown in Fig. 5.1. Mathematically it can be expressed as:

$$\text{Min } U_f \tag{6.1}$$

where

$$U_f = \int_{Y^\ell}^{Y^u} I_f \, dY$$

Y^ℓ and Y^u are lower and upper bounds on the excitation amplitude. The constraint set consists of limit constraints on the design parameters and an inequality constraint on the relative displacement. The constraints are

$$\begin{aligned} &k,\ V_o,\ F_{coul_1},\ T_p,\ T_{or},\ T_{hyd} \geq 0 \\ &z \leq z_{max} \end{aligned} \tag{6.2}$$

6.2.2 Objective Function for Time Domain Analysis

The objective function for time domain analysis is to minimize the negative area under the I_t vs v_i curve shown in Fig. 5.2. Mathematically it can be expressed as:

$$\text{Min } U_t \tag{6.3}$$

where

$$U_t = -\int_{v_i^\ell}^{v_i^u} I_t \, dv_i$$

v_i^{ℓ} and v_i^{u} are lower and upper bounds on the initial velocity. The constraint set for time domain analysis is the same as the constraint set for frequency domain analysis:

$$k,\ V_o,\ F_{coul_1},\ T_p,\ T_{or},\ T_{hyd} \geq 0$$

$$z \leq z_{max} \tag{6.2}$$

6.3 Optimization Method

The objective functions formulated in both frequency and time domains represent non-linear constrained optimization problems. The optimization procedure is to modify the constrained problem to an unconstrained optimization problem by introducing an exterior penalty function.

Consider an objective function

$$U(\underset{\sim}{X}) = U(X_1, X_2, \ldots X_n)$$

$$\text{subject to } g_i(\underset{\sim}{X}) \geq 0 \qquad i = 1,2,\ldots m$$

Using an exterior penalty function, the modified objective function becomes [116]

$$U_m(\underset{\sim}{X}) = U(\underset{\sim}{X}) + 10^{2.0} \sum_{i=1}^{m} H \cdot g_i(\underset{\sim}{X}) \tag{6.4}$$

where $H = 1$ for $g_i(\tilde{X}) < 0$

$H = 0$ for $g_i(\tilde{X}) \geq 0$

A direct search method based on the Hooke and Jeeves pattern search technique [117] is then used for solving the unconstrained optimization problem. The method consists of two phases, an "exploratory search"

around the base point and a "pattern search" in a direction selected for minimization. To initiate an exploratory search, the objective function is evaluated at a base point (the base point is the vector of initial guesses of the independent variables for the first cycle). Each variable is then changed in rotation, one at a time, until all the parameters have been changed. The successfully changed variables (i.e. those variables which reduced the objective function) define a vector that represents a successful direction for minimization. A series of accelerating steps, or "pattern searches", is made along this vector as long as the objective function is decreased by each pattern search. The process is repeated until an optimum is located. After an optimum is found, a random search [116] is used to test the global nature of the optimum. The function used in time domain optimization appeared to be convex and the random search showed no improvement, indicating that the results were globally optimum. By contrast, the frequency domain optimization function displayed several local optima and a series of random searches yielded a succession of improvement in $U_m(\underset{\sim}{X})$. The optimal values in both domains were verified using perturbed starting values.

A flowchart of the step-by-step procedure in the optimization process for each domain is shown in Figs. 6.1 and 6.2. The programs used in the optimization procedure are listed in Appendix II.

6.4 Optimization Results and Discussion

The results of optimization in both the frequency and time domain are shown in Table 6.1. Physical insight can be gained from the optimized set of parameters by examining their effect on the functions used to formulate the objective functions (equations (6.1) and (6.3)). Those

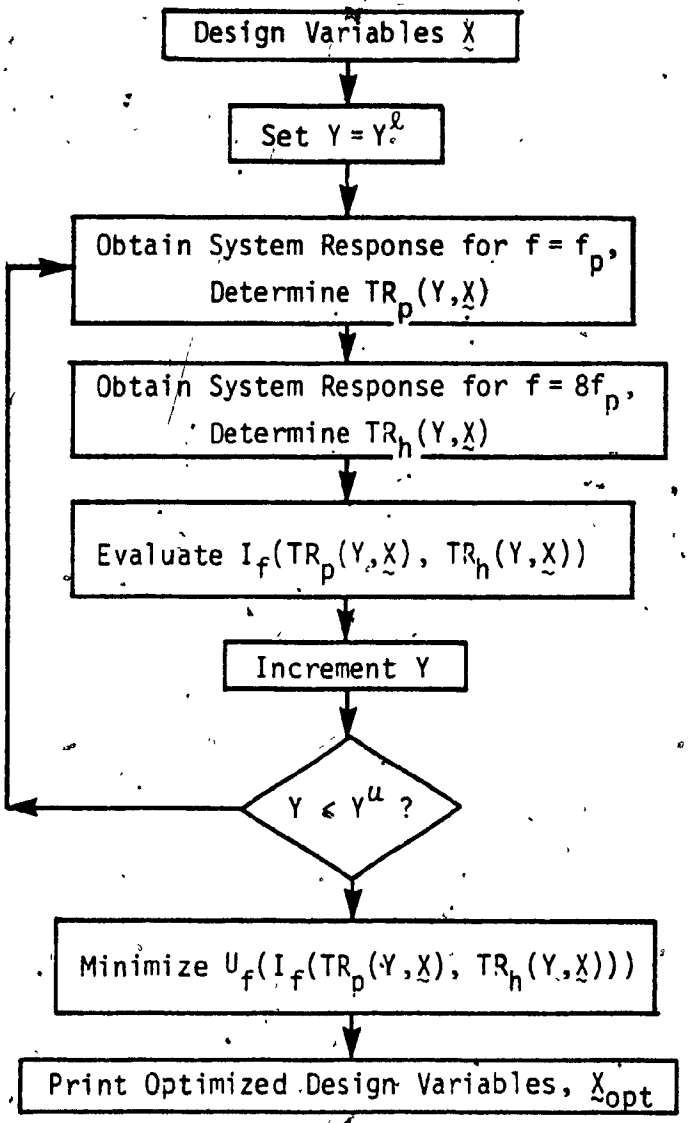

Fig. 6.1: Flowchart of the Optimization Procedure-Frequency Domain

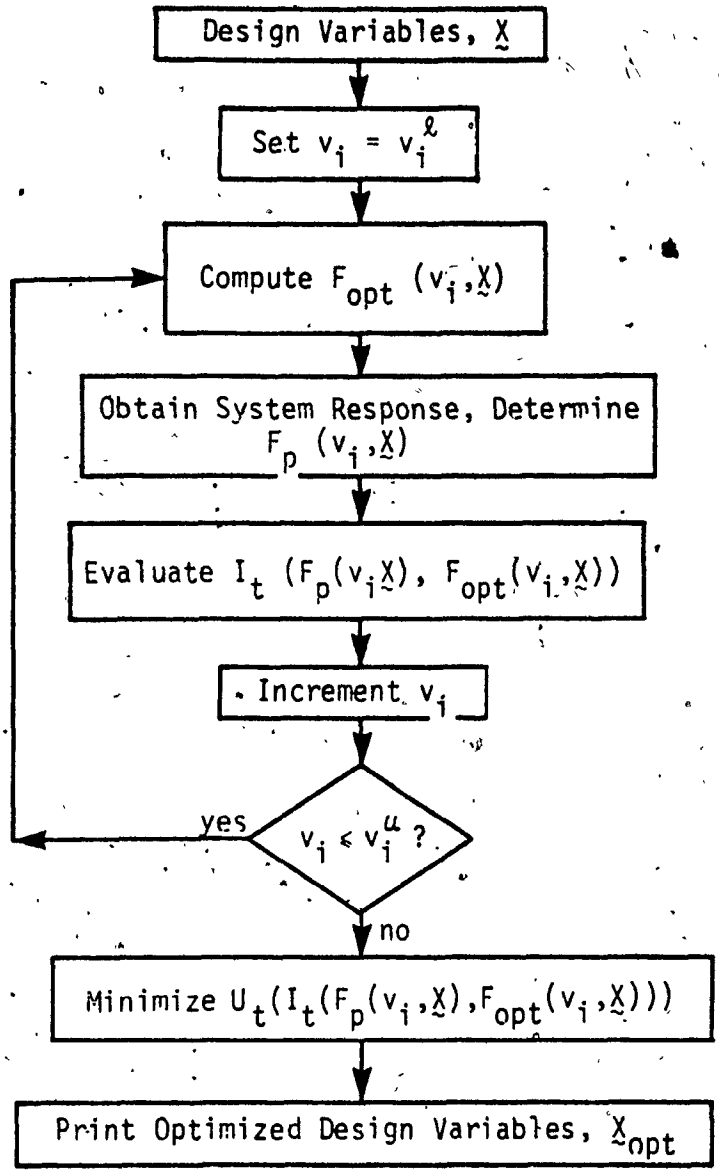

Fig. 6.2: Flowchart of the Optimization Procedure-Time Domain

TABLE 6.1: Five Parameter Optimization Results

Design Parameter	Existing Design Values	Optimal Design Values	
		Frequency Domain	Time Domain
k (N/m)	2.067×10^{3}	8.396×10^{2}	1.947×10^{3}
V_o (m^3)	6.934×10^{-4}	8.321×10^{-4}	6.566×10^{-4}
F_{seal_1} (N)	1.677	1.845	8.749
$T_v + T_{or}$ (kg/m)	40.92	4.346	34.09
T_{hyd} (kg/m)	30.58	30.58	18.38

functions are the response surfaces, Figs. 4.2 and 4.10, and the performance indices over their respective input ranges, Figs. 5.1 and 5.2.

Referring to Table 6.1, the results in the frequency domain can be interpreted physically as follows: the damping is reduced to improve high frequency response whereas the damping coefficient due to the hydraulic stop remains unchanged for the excitation range selected (i.e. z is always less than Z_c in equation (2.47)). The air column and spring stiffnesses are reduced to lower the resonant frequency. This change, combined with increased stiction, retains the system in the sticking mode at resonance over a larger part of the input range. The improvement due to these changes can be observed by comparing the frequency response surface of the original suspension, Fig. 4.2, with the response surface of the optimized suspension, Fig. 6.3. The improved performance is reflected in the I_f vs Y curves shown in Fig. 6.4.

In the time domain, the optimized parameter set exhibits a different trend. Recalling section 5.3, the requirement for optimal performance in the time domain is that the response surface in Fig. 4.10 remain flat with respect to z. Hence, the parameters which affect non-flatness, such as damping and stiffness, are reduced. Since a high value of seal stiction produces a constant F_p, its value is increased considerably. The response surface for the time domain optimized suspension is shown in Fig. 6.5 (compare with Fig. 4.10). The improved time domain performance is reflected in the I_t vs v_i curves in Fig. 6.6. The performance of the optimized suspension is slightly decreased compared to the existing suspension for initial velocities less than 2.3 m/s. This is because the higher seal stiction imposes a DC type bias at small v_i (recall Figs. 4.5 and 4.6), however at larger v_i the combined effects of curve flatness and

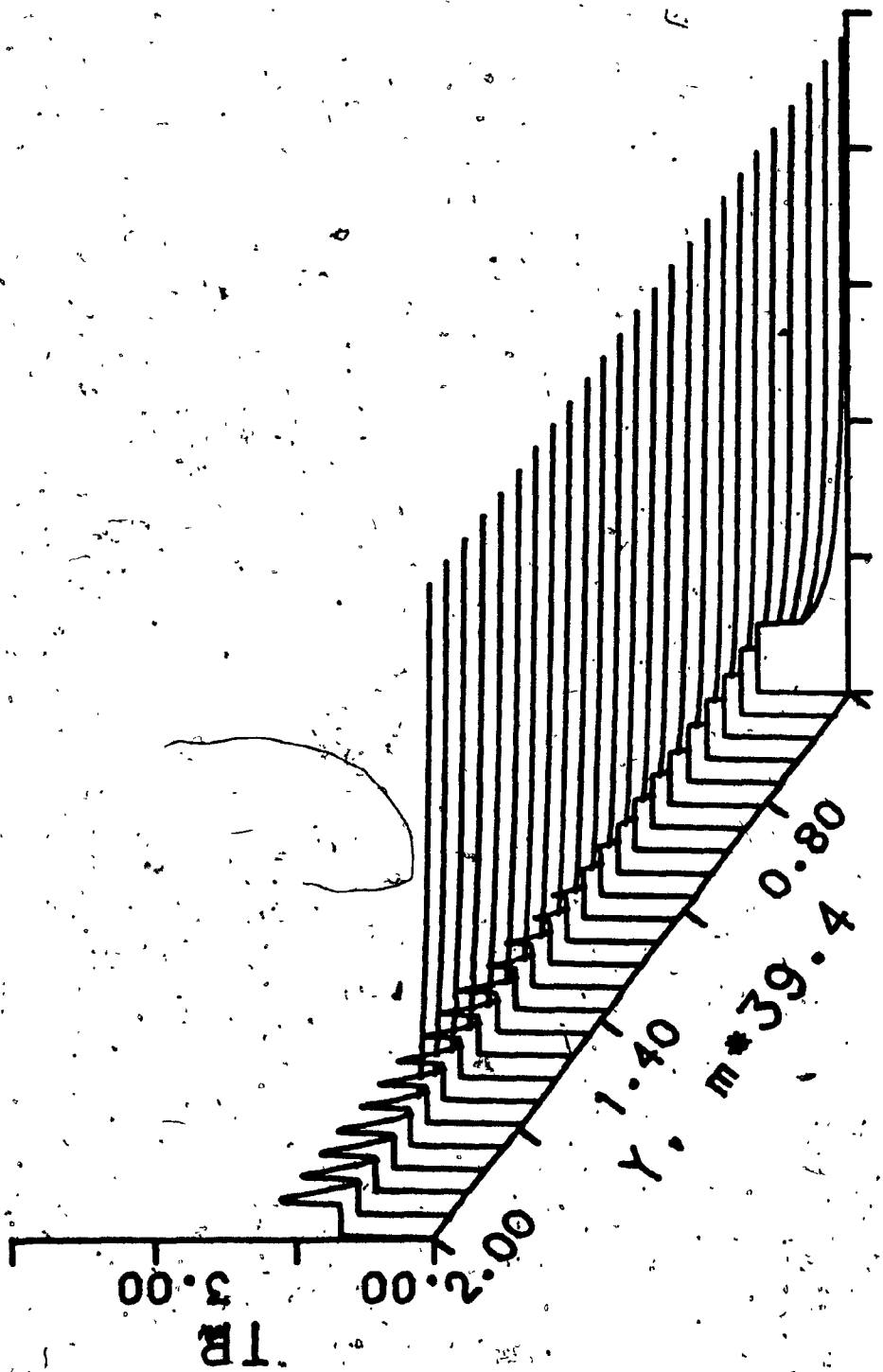

Fig. 6.3: Frequency Response Surface for an Optimal Design

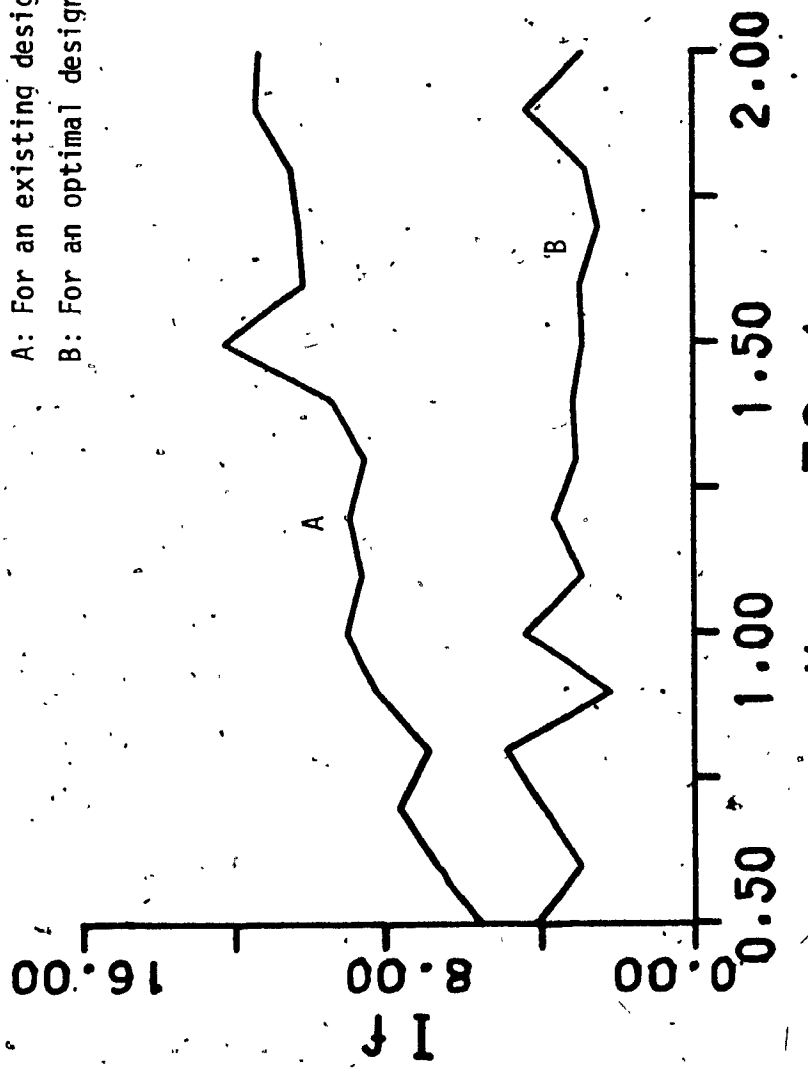

Fig. 6.4: Frequency Domain Performance

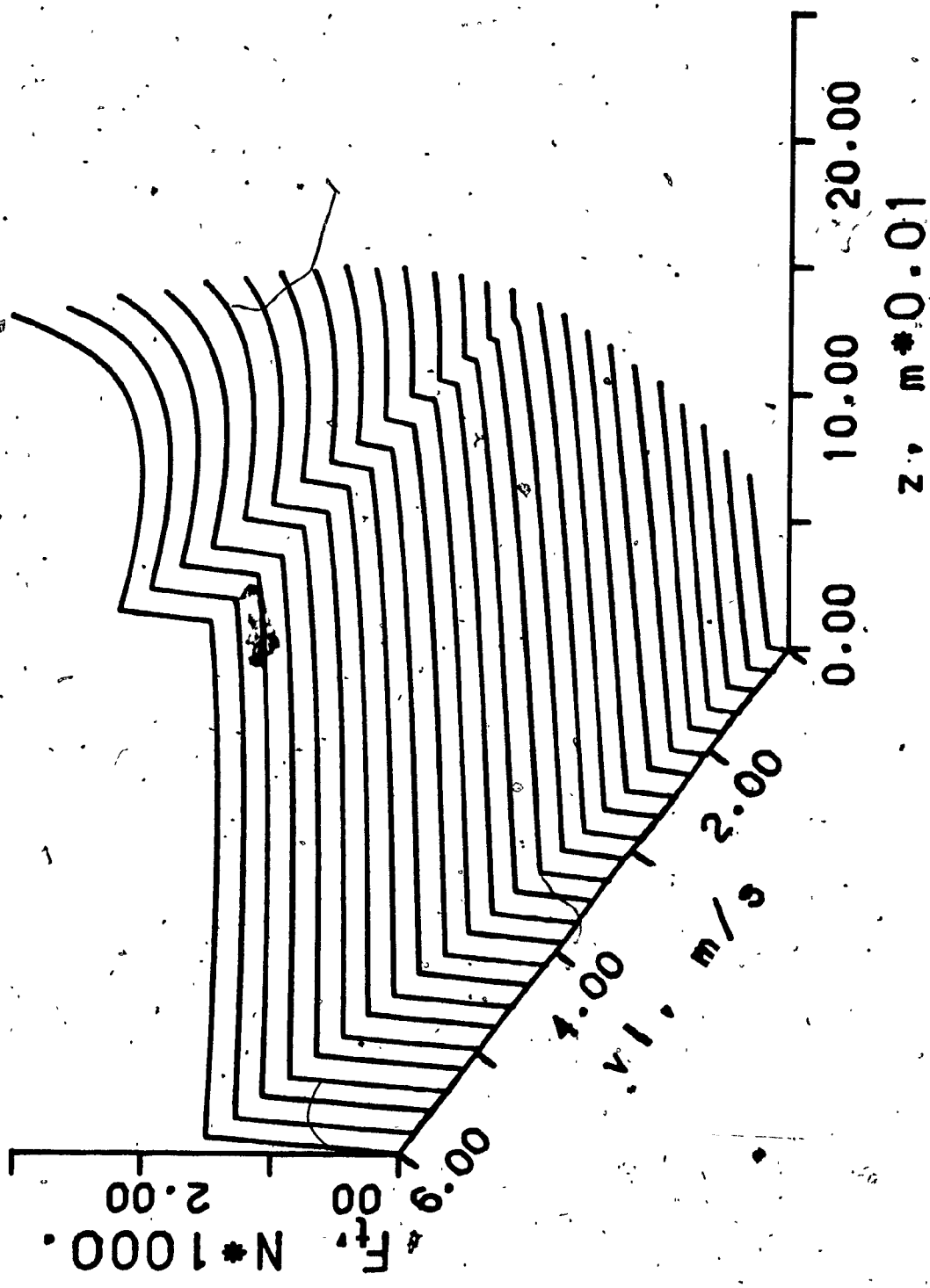

Fig. 6.5: Velocity Step Response Surface for an Optimal Design

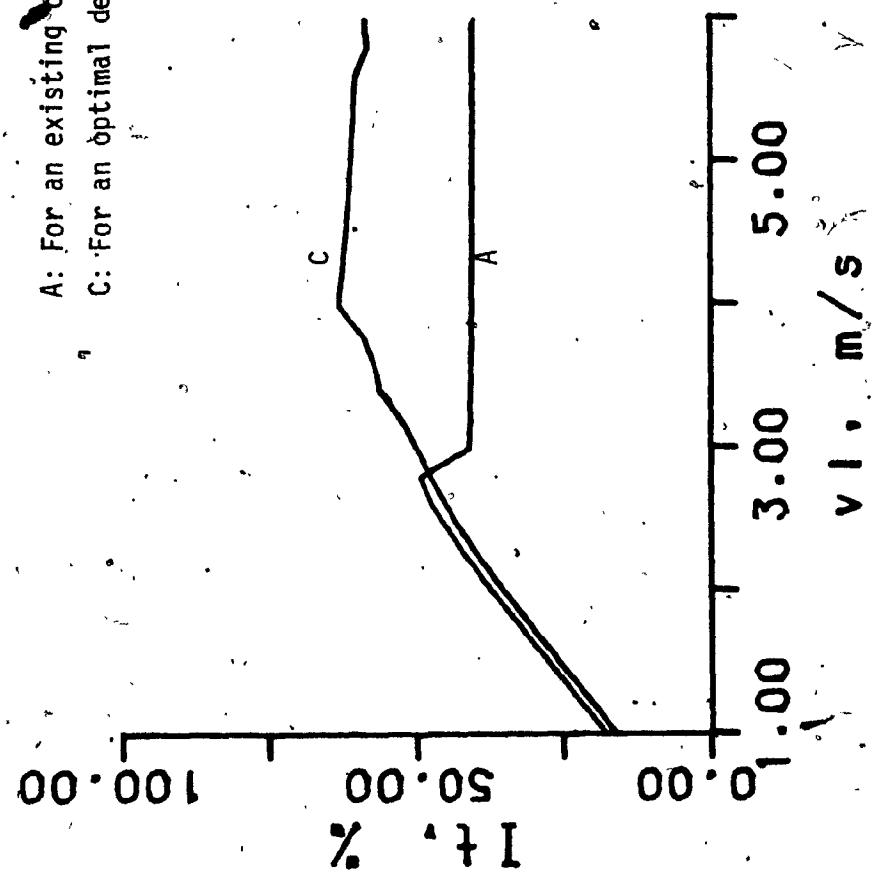

Fig. 6.6: Time Domain Performance

bias yield a significant performance increase.

In practice, the suspension can be analyzed in the frequency and/or time domains. A point of interest is to know how the suspension optimized in the frequency domain behaves in the time domain and vice-versa. Such a comparison is shown in Figs. 6.7 and 6.8. The suspension optimized in the time domain performs poorly in the frequency domain at low excitation levels because the high value of stiction degrades the frequency domain performance. In the time domain, the performance of the suspension optimized in the frequency domain is better than the suspension optimized in the time domain, and the original suspension, for initial velocities less than 3.3 m/s. At higher initial velocities the suspension optimized in the time domain performs better than the one optimized in the frequency domain, which in turn continues to out perform the original design.

6.5 Experimental Verification of an Optimally Designed Suspension

To test the validity of the optimal results, the test rig described in section 3.3 was used. The design parameters such as spring stiffness and seal stiction are difficult to modify, so only the remaining three parameters were considered in the design modification. For this purpose a three parameter optimization was carried out with the frequency domain objective function. The optimal values of the parameters are listed in Table 6.2. Based on the optimized design parameters, a typical fork was modified and tested. The transmissibility values at low and high frequencies (for a given excitation amplitude) were measured and are listed in Table 6.3.

Using the optimized design parameters, computer simulation in the frequency domain was carried out to obtain the transmissibility values at

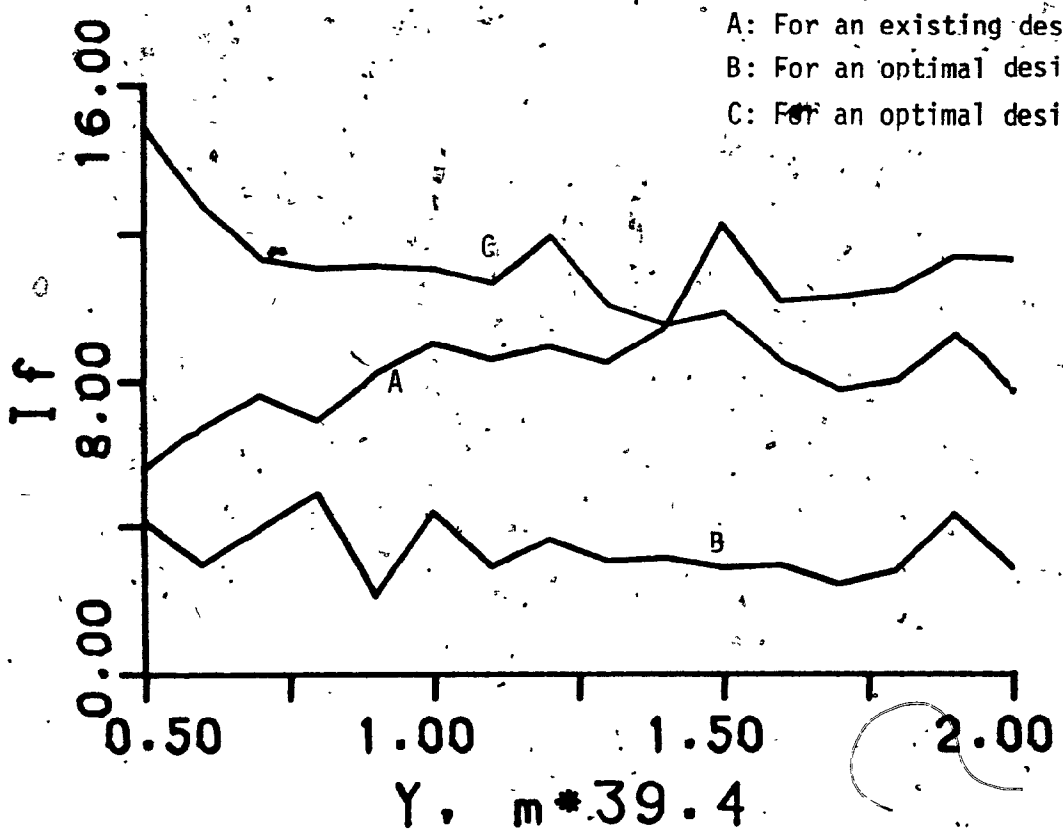

Fig. 6.7: Frequency Domain Performance

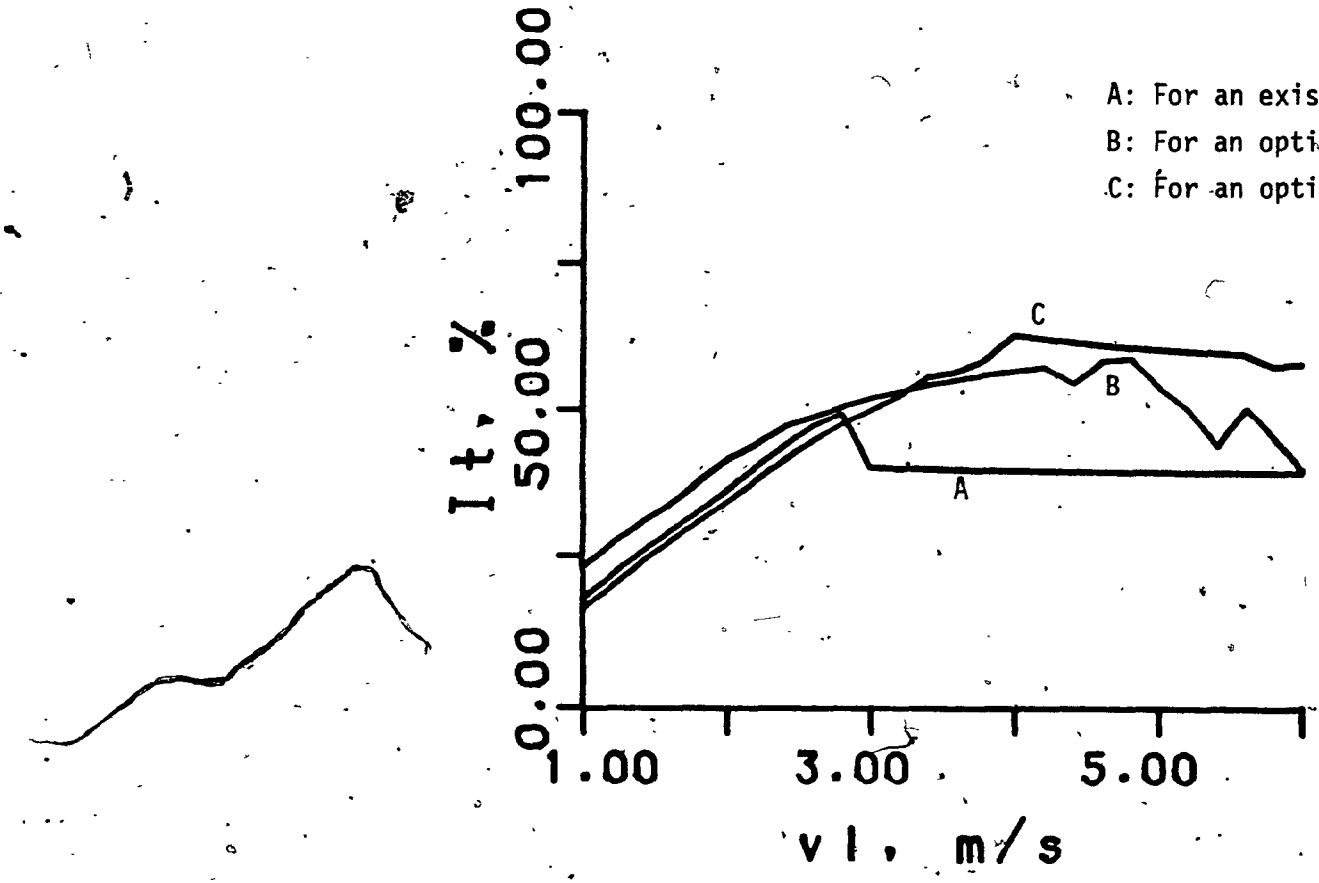

Fig. 6.8: Time Domain Performance

TABLE 6.2: Three Parameter Optimization Results

Parameter	Existing Design Value	Optimal Design Value
$T_p + T_{or}$ (kg/m)	40.92	41.74
T_{hyd} (kg/m)	30.58	36.51
V_o (m^3)	6.934×10^{-4}	2.923×10^{-4}

TABLE 6.3: Experimental Verification of Optimal Performance

Excitation Amplitude (mm)	Experimental Results		Numerical Results		Absolute Error	
	TR_p^e	TR_h^e	TR_p^n	TR_h^n	$\lvert TR_p^e - TR_p^n \rvert$	$\lvert TR_h^e - TR_h^n \rvert$
6.35	1.000	0.374	1.000	0.330	0.000	0.044
12.7	1.625	0.234	1.886	0.293	0.261	0.059
19.0	1.667	0.208	1.618	0.307	0.049	0.099
2.54	1.571	0.276	1.670	0.323	0.099	0.047

low and high frequencies. Since in the test rig an additional friction (due to guidance stiction) is introduced, the mathematical model was modified with the addition of this guidance stiction before the frequency domain computer simulation with the optimized design parameters was carried out. The results of this computer simulation are listed in Table 6.3. The average error in absolute transmissibility is 0.102 and 0.062 in the low and high ranges, respectively. Hence, the experimental results substantiate the optimal results obtained through computer simulation.

6.6 Summary

In this chapter, the motorcycle suspension was optimized using computational techniques. The performance indices of the previous chapter were used to formulate objective functions in the frequency and time domains. The optimization procedure for each domain was outlined along with the optimization method. The optimal design parameters were presented and an experimental verification performed.

CHAPTER 7

STOCHASTIC RESPONSE OF THE SUSPENSION SYSTEM

CHAPTER 7

STOCHASTIC RESPONSE OF THE SUSPENSION SYSTEM

7.1 Introduction

In the previous chapters, the response of the motorcycle suspension was treated using a deterministic approach. The deterministic approach yields the response characteristics only for an input process specified in space and time. The environments in which off-road motorcycles are operated, except those purposely constructed otherwise, are random in nature. Likewise, the response is also random in character [45]. Hence, for a complete investigation, the input excitation should be described stochastically and the response described by a random process. The stochastic approach can be considered as the general solution to the overall problem whereas the approach using deterministic analysis is suitable for investigating certain special cases.

The terminology is introduced in the next section. Then the experimentally measured input excitation is described in statistical terms in section 7.3. The available techniques for solving nonlinear systems subjected to stochastic excitation are reviewed in section 7.4. New methods of equivalent linearization for stochastically excited mechanical systems are presented in section 7.5. The various schemes are compared and the most suitable technique for the present investigation is selected. The technique is then applied together with suitable optimization schemes to obtain an optimal design based on the stochastic response.

7.2 General Notes on the Stochastic Response

Most time varying signals require two measures for adequate

description of the signal. These measures typically relate to amplitude and frequency. With a deterministic signal, quantification at one point in time will determine its future behavior. With a random signal, only the likelihood of an expected behavior can be found.

In random vibration, the amplitude probability density is used to determine the expected probability of finding a given level of a dynamic quantity such as acceleration, velocity and displacement. The cumulative probability function relates to the probability of having a level of the particular dynamic quantity of interest below a specified peak value.

The frequency content of a random signal can be given in terms of its power spectrum (PS). The term "power" is synonymous with the "mean square" of the varying quantity under consideration. The change in power with change in frequency, or power spectral density (PSD) is also used to describe random signals. The PSD of a signal is theoretically obtained from its auto-correlation function [118]. The auto-correlation function is the average value of the product of two values of the signal separated by a predetermined time interval. This average value is therefore a function of the time interval. For studies in vehicle dynamics, Virchis and Robson [119] have shown that the terrain signal can be assumed to be a stationary random process. Stationarity implies that only the time interval, not the starting time, affects the auto-correlation function. Converting from the time domain to the frequency domain via the fourier transform yields the PSD of the signal. Practically, converting a series of time or distance sampled data into a sampled frequency spectrum is a tedious and difficult task [120]. Therefore, routine evaluations of power spectra require a digital processing capability.

For this reason, the application of the power spectra was not popular until the late 1950's [48]. The first investigation using discrete fourier transform methods was conducted by Walls et al [66]. The use of power spectra was later applied to guideways and other surfaces [121]. Since then, power spectra have been used extensively in automotive [43,122,123], aircraft [69-71] and railway [49,124,125] studies.

The choice of using power spectrum or power spectral density is a matter of convenience. In analytical works [47,48,118], the PSD is obtained directly and hence is commonly used. In works utilizing experimental data [44,79,101] the PS is obtained one step earlier than the PSD during the analysis and hence is a more convenient form of data description. In this investigation, the experimental data is described in terms of its power spectrum.

7.3 Statistical Description of Field Data

In order to obtain the stochastic response of the motorcycle suspension, the characteristics of the input had to be acquired. The excitation induced by a typical off-road environment was measured by an instrumentation package developed in-house [126]. It consists of an accelerometer, amplification and frequency modulation circuit, and a portable cassette recorder. The package is very compact and lightweight. A Can-Am 250 MX-6 motorcycle was fitted with the instrumentation package as shown in Fig. 7.1. The cassette recorder was mounted in a foam lined knapsack mounted on the riders' back as shown in Fig. 7.2. An experienced rider than drove the motorcycle around various race tracks in the Greater Montreal area at speeds normally encountered during competition. Typical input acceleration time histories, recorded in the field, are shown in Fig. 7.3.

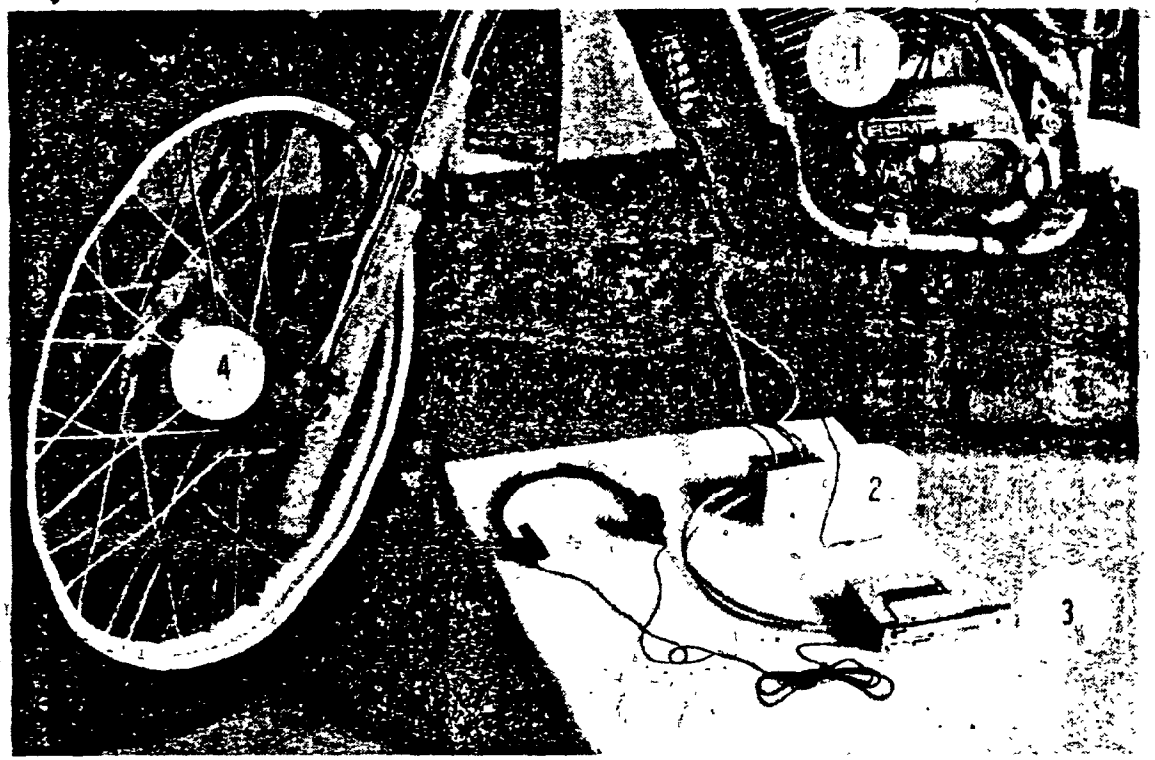

1 - Test Motorcycle
2 - Frequency Modulator
3 - Cassette Recorder
4 - Accelerometer

Fig. 7.1: Pictorial View of the Field Instrumentation Package

1 - Power Supply
2 - Cables and Connectors
3 - Off-Road Motorcycle
4 - Padded Instrument Housing

Fig. 7.2: Field Instrumentation Package, Installed

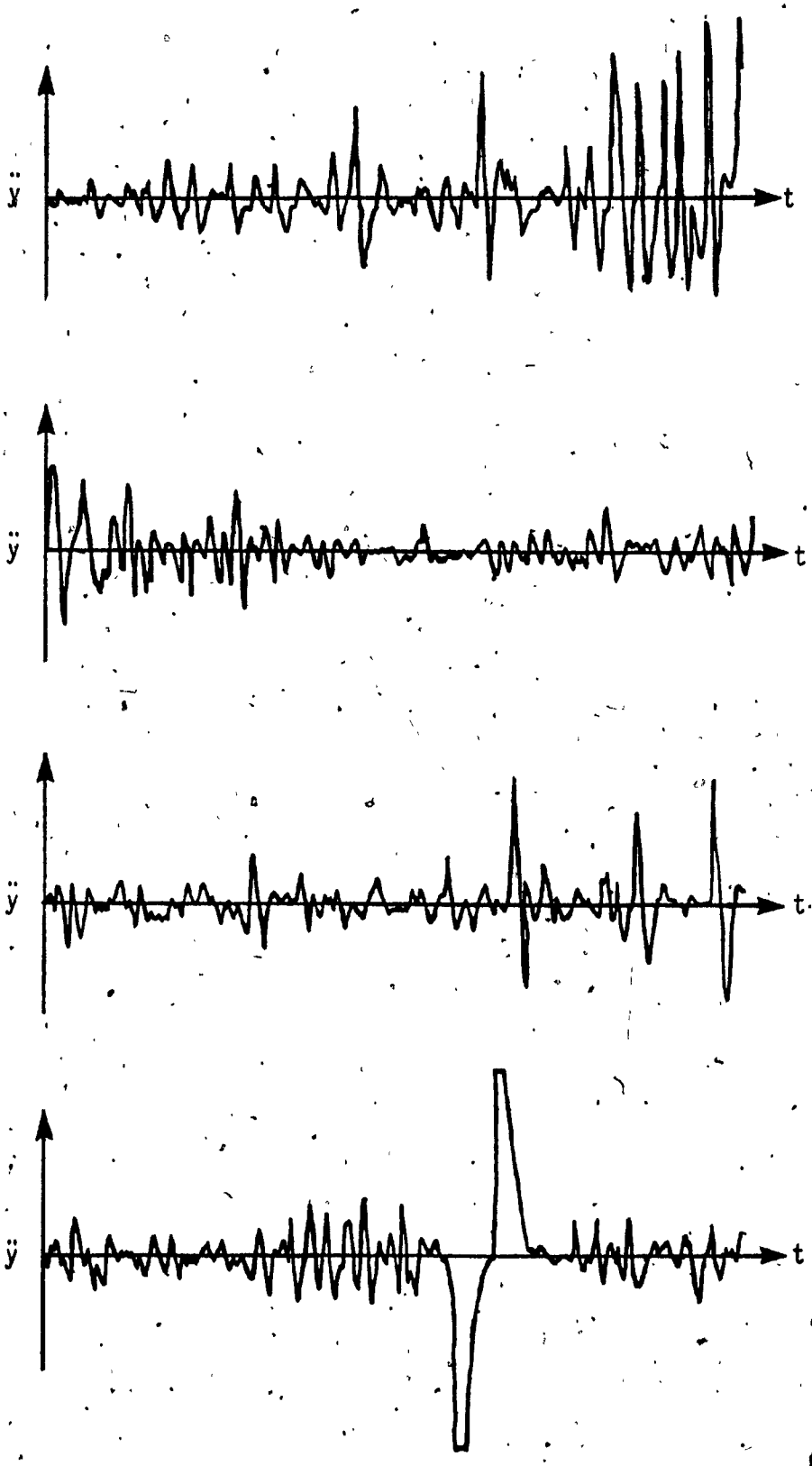

Fig. 7.3: Typical Acceleration vs Time Records

The recordings were demodulated and fed into a Nicolet 660 a FFT spectral analyzer, shown in Fig. 7.4. The guidelines set down by Healey [46], with respect to record length and sampling frequency, were followed. Peak averaging was utilized at maximum sample redundancy to obtain the "worst case" field data characteristics. The power spectra of the field data are shown in Fig. 7.5. The ensemble constitutes the input power spectrum used as the input excitation for suspension analysis. That spectrum is shown in Fig. 7.6.

7.4 Analytical Techniques

There are presently four approaches relevant to the study of stochastically excited, single degree of freedom, nonlinear systems. They are:

i) Markov methods, based on the Fokker-Planck equation.

ii) Perturbation methods.

iii) Equivalent linearization methods.

iv) Simulation methods.

The major advantages and limitations of these techniques are reviewed in this section. The objective is to select a technique suitable for the solution of the stochastic response of the motorcycle suspension.

7.4.1 Markov Methods

Markov methods, based on the Fokker-Planck equation [127], have the advantage of yielding an exact solution in terms of response prediction. This powerful advantage over the other techniques is compromised by the fact that solutions have been found only for a certain restricted class

1 - Power Package
2 - Test Motorcycle
3 - Accelerometer
4 - Recording Instrumentation
5 - Spectral Analyzer

Fig. 7.4: Pictorial View of the Field Instrumentation Package and Spectral Analyzer

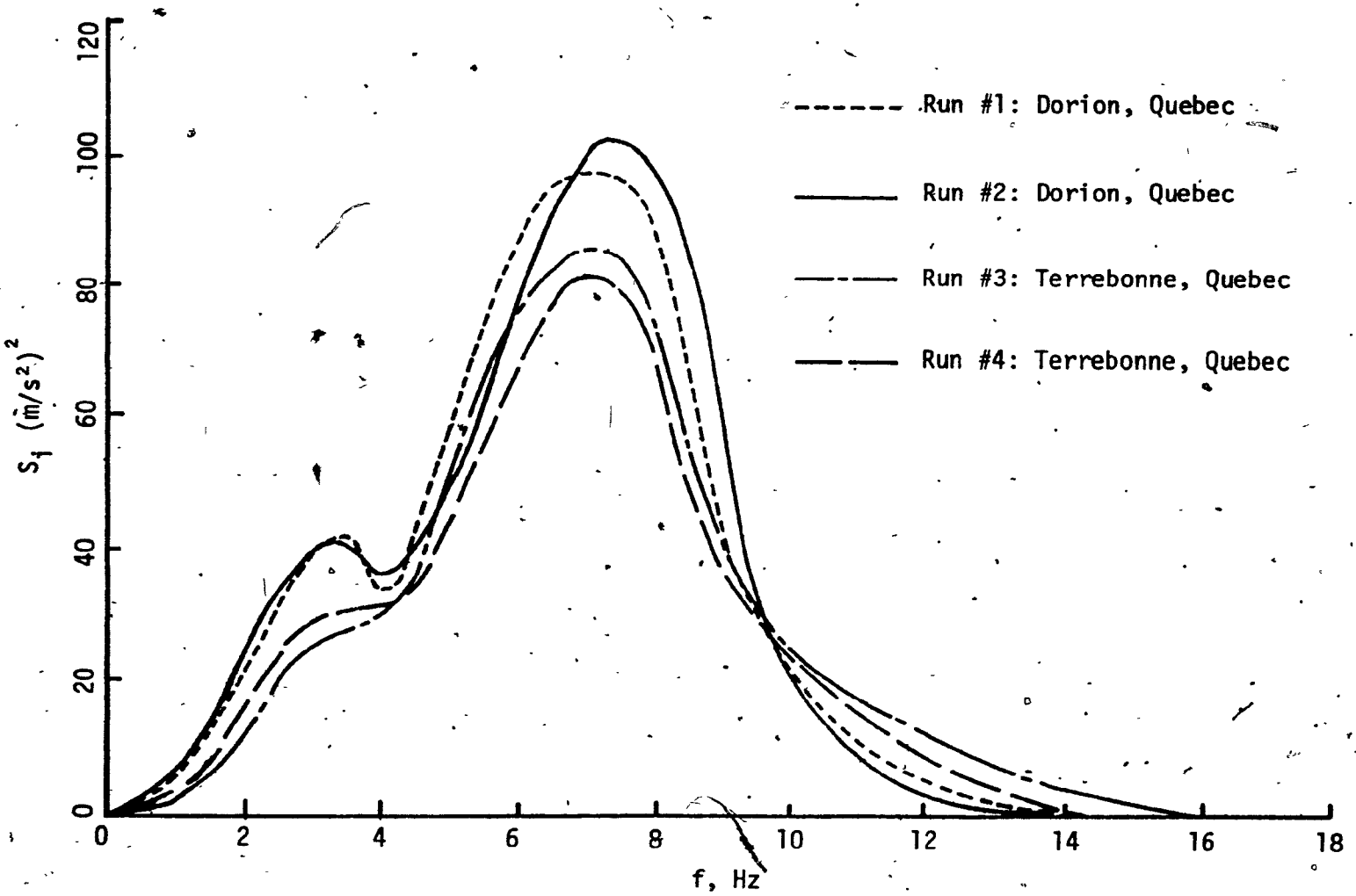

Fig. 7.5: Power Spectra of Measured Field Data

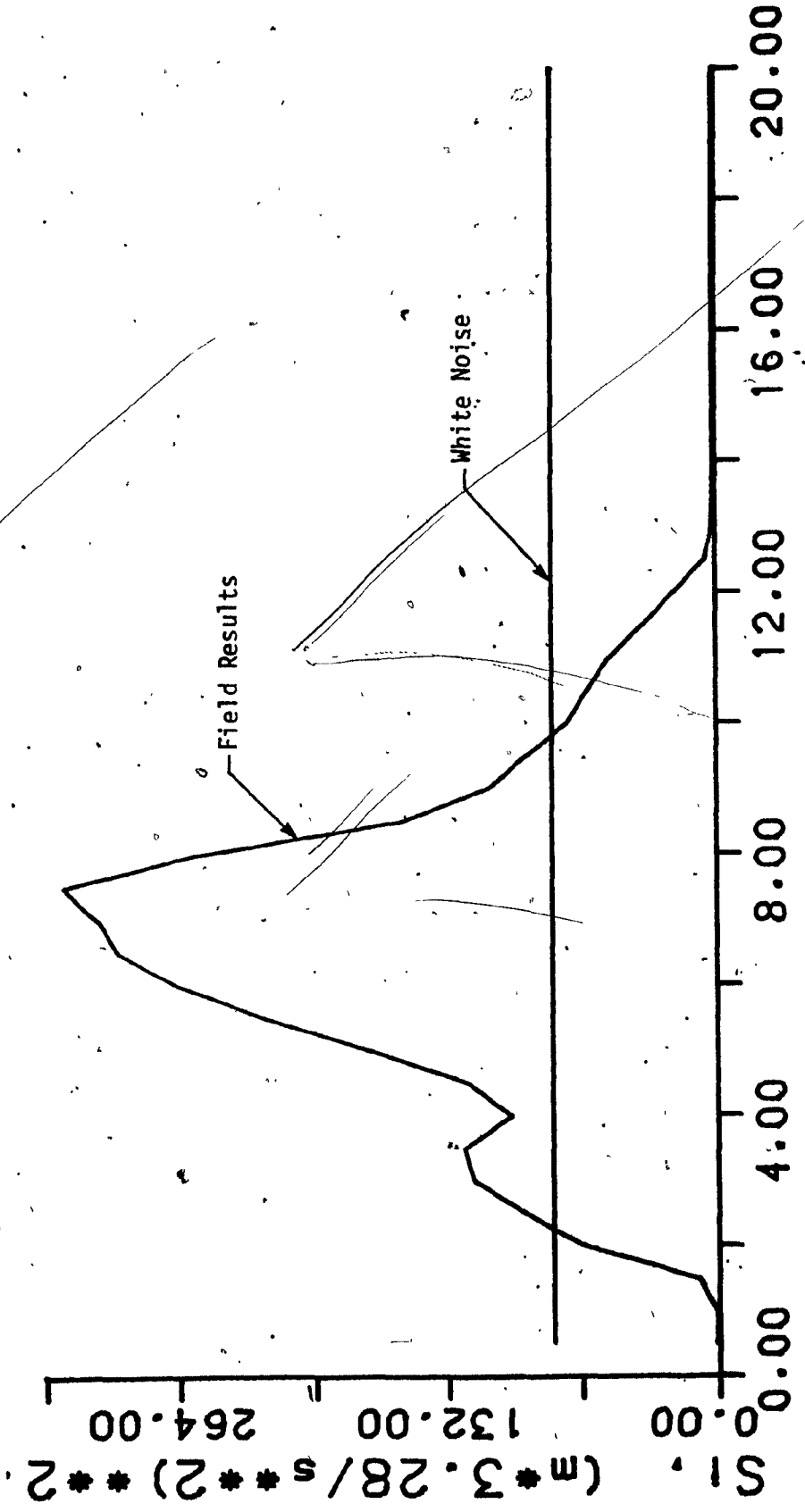

Fig. 7.6: Excitation Spectra Used in the Analysis

of problems [128]. The Fokker-Planck approach was developed to study the phenomenon of Brownian motion and is closely related to the theory of random walk [129]. A historical survey of Markov methods, based on the Fokker-Planck equation, has been published by Fuller [130].

For a system subjected to white noise excitation, the transitional probability density of the response process is governed by the Fokker-Planck equation [127]. This transitional probability density can completely define the statistics of the response process. Unfortunately, the complete nonstationary Fokker-Planck equation remains to be solved. Even the solution of the stationary Fokker-Planck equation is available only for a few limited cases.

In the case of a linear second order system excited by white noise, an exact solution to the Fokker-Planck equation has been found [131]. Caughey [132] and Arjaratnam [41] have provided solutions for a second order nonlinear system, which bears resemblence to the motorcycle suspension model. They have shown that the first probability density of the Markovian response process can be obtained provided the damping terms are linear and the excitation is Gaussian white noise.

Unfortunately, the present problem does not satisfy the aforementioned conditions. The motorcycle suspension model (equations 2.48 and 2.50) contains quadratic and coulomb damping. An alternative would be to combine the techniques presented by Kirk [133] and Lutes [134], for quadratic and coulomb damping, and obtain an equivalent linear system. The Fokker-Planck equation could then be solved for coulomb and quadratic damping under white noise excitation. However, it is the white noise restriction that eliminates the use of a Markov method in the present

investigation. Recalling Fig. 7.5 it is clear that the input excitation spectra bears little resemblence to noise generated from a "white" source. Hence, Markov methods are unsuited for this application.

7.4.2 Perturbation Methods

If the nonlinearities of a system are sufficiently small, the perturbation method of solution can be used. In this technique, the response is assumed as an expansion in powers of a perturbation parameter corresponding to the magnitude of the nonlinearity. Substituting the power series solution into the original equations of motion and equating the coefficients of like powers of the nonlinearity parameter, α, a set of linear differential equations is obtained for the terms in the expansion of the solution. This leads to a first order approximation which is obtained from the solution of the two sets of linear differential equations. The first set of differential equations is solved, assuming all nonlinearities equal to zero. The second set of differential equations is solved, assuming an excitation which is a function of the solution of the first set of equations. In this manner the statistics of the linear solution and first order perturbation are found. The calculations are usually lengthy and become progressively tedious as the order of α increases. In practice, results are usually obtained only to the first order of α.

The application of this method to stochastic processes was pioneered by Crandall [135]. The method has been applied to systems possessing weakly nonlinear damping [136], yielding the statistics of the response. In addition, the response spectrum of various weakly nonlinear systems has also been studied using this technique [137-139].

The major limitations of this approach are that the system under study should possess only weak nonlinearities and the system must contain some finite amount of linear, viscous damping. The motorcycle suspension model (equations 2.48 and 2.50) contains strong nonlinearities and there are no linear, viscous damping terms. Hence, if a perturbation method were applied, the statistics of the response would tend to infinity and simply indicate an instability in the solutions obtained.

7.4.3 Equivalent Linearization Methods

Equivalent linearization methods overcome many of the limitations and difficulties encountered in the methods discussed thus far. The technique is based on the concept of replacing the nonlinear system by a related linear system in such a way that the difference in behavior is minimized in some appropriate sense. The first development of a suitable equivalent linearization procedure for randomly excited nonlinear systems is usually attributed to Booton [140] and Caughey [141]. Various minimization criteria have been presented by Iwan and Patula [142]. Under certain conditions, such as Gaussian distributed white noise excitation, closed form solutions for highly nonlinear systems have been obtained [143-147]. Of particular relevance is the facility with which the technique handles systems containing sizable coulomb friction [148-150]. These attributes, independent of the sense in which the difference between the linear and nonlinear system is minimized, rank equivalent linearization methods as the most suitable methods for the present investigation.

7.4.4 Simulation Methods

In the simulation approach, sample functions of the excitation

process are generated. Corresponding sample functions of the response processes are computed. Statistical processing of the output process then yields the information of interest. Lengthy processing is needed to reduce the statistical uncertainty of the results to acceptable limits. The method is simplified in the case of stationary, ergodic processes because only one input (and output) realization of sufficient duration need be generated.

Although most of the studies are performed on a digital computer, some simulation work has been done using a random signal generator, filters, and an analog computer [150]. Digital simulation is facilitated if the excitation can be modelled as white noise because appropriate sample functions can be generated directly from a sequence of independent random numbers [151]. For non-white excitation, a digital filter can be constructed to obtain the desired spectrum [152]. Various other simulation methods have been demonstrated by Shinozuka and Jan [153], Hudspeth and Borgman [154], and Smith [146].

Simulation methods have an advantage over the other methods in their flexibility. They also provide more statistical information about the response than is available with some of the other methods. However, considerable computation time is required if the probability of exceeding high amplitude levels is to be reliably estimated. For this reason, the chief role of simulation methods is to provide a means of assessing the validity of approximate theoretical methods [42].

7.5 Application of Equivalent Linearization Methods

In any equivalent linearization method, the nature of the desired quantities is of paramount importance. Some approaches [144,148,150]

assume a Gaussian distribution for the relevant dynamic quantities in which case the expressions for the equivalent linear coefficients are available in terms of the mean square response of the system. An advantage of this approach is that the mean square response statistics are obtained early in the iterative solution. In this investigation, the quantities of interest are the mean square (or "power") spectra of the absolute acceleration and relative displacement response of the suspension system. These spectra are used later in this chapter to evaluate the performance of the suspension to a stochastically described input excitation.

In the linearization methods discussed in this section, the input spectrum is synthesized in terms of its dominant harmonics, thus yielding a deterministic description. The nonlinear system is then replaced by an equivalent linear system such that a deterministically described error is minimized in some sense. The equivalent linear system can then be used in the expressions [155]

$$S_a(\omega) = |H_a(j\omega)|^2 \, S_i(\omega) \tag{7.1}$$

$$S_z(\omega) = \left|\frac{H_r(j\omega)}{\omega^2}\right|^2 S_i(\omega) \tag{7.2}$$

where

$H_a(j\omega)$ is the absolute transmissibility of the suspension system

$H_r(j\omega)$ is the relative transmissibility of the suspension system

$S_i(\omega)$ is the input acceleration power spectrum

$S_a(\omega)$ is the absolute acceleration response spectrum

$S_z(\omega)$ is the relative displacement response spectrum

To summarize, the stochastically described input is used in a suitable deterministic linearization process, yielding a stochastic description of the response quantities of interest.

7.5.1 Energy Methods (EM)

Energy methods minimize the difference in energy, dissipated and stored per quarter cycle, between the nonlinear and equivalent linear system. Three approaches are introduced in this section. The first two approaches each yield one set of linear coefficients for a given input spectrum. The third approach supplies a set of linear coefficients at each discrete excitation frequency of the input spectrum.

a) Statistical Linearization (SL)

The statistically linearized energy method (SLEM) minimizes throughout the input frequency range the expected value of the difference between the total energy dissipated and stored during four quarter periods of response. The total energy dissipated and stored over the four quarter periods is considered because of the asymmetric nature of the suspension elements. Since the input spectrum is discretized and treated in a deterministic sense, the usual procedure [148,150] of assuming Gaussian distributed dynamic quantities is forgone in favor of minimizing the mean square error using a numerical procedure. The response spectra are then obtained directly. A flowchart of the linearization procedure is shown in Fig. 7.7. The computer program is listed in Appendix III.

b) Harmonic Linearization (HL)

In the harmonically linearized energy method (HLEM), the total energy dissipated and stored during four sequential quarter periods of response is equated to that of an equivalent linear system, at a specified

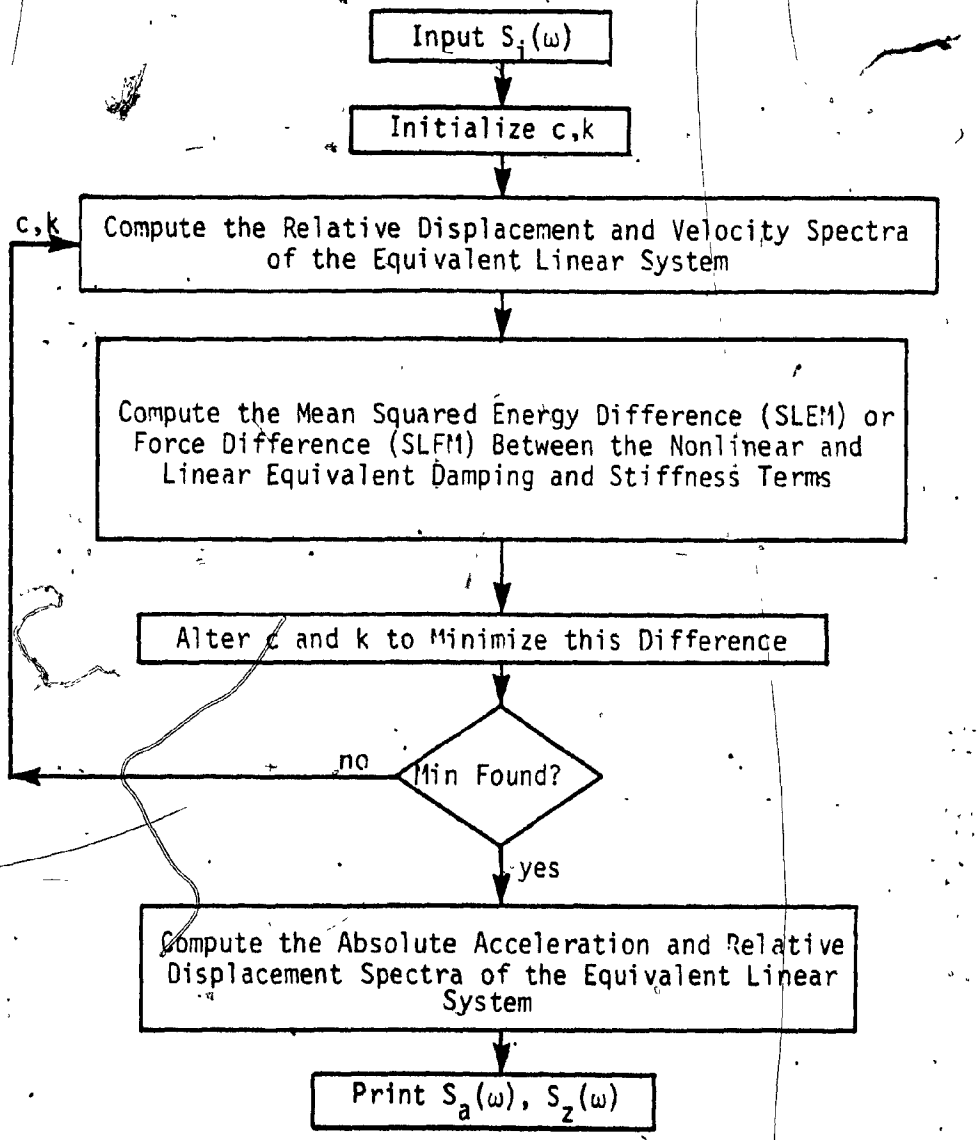

Fig. 7.7: Flowchart for the Statistical Linearization (SL) Method

excitation frequency. In the case of white noise excitation, the natural frequency (f_n) is the most suitable frequency for linearization. For excitation spectra such as those obtained from field measurements (Fig. 7.5), the frequency at which the peak excitation takes place is used for linearization. A flowchart of the linearization procedure is shown in Fig. 7.8 and the computer program is listed in Appendix III.

c) Discrete Harmonic Linearization (DHL)

The discrete harmonically linearized energy method (DHLEM) is identical to the HLEM except that the linear coefficients are obtained at each discrete excitation frequency. The technique is powerful in that it supplies a set of equivalent linear coefficients at each frequency, hence the error (based on energy difference) is reduced to zero. Once the array of linear coefficients has been obtained, the discrete response characteristics are obtained directly using equations (7.1) and (7.2). The flowchart is shown in Fig. 7.9 and the computer program is listed in Appendix III.

7.5.2 Force Methods (FM)

Force methods minimize the difference in the transmitted force between the nonlinear and equivalent linear suspension systems. The three approaches described for the energy method are used in this sub-section with suitable changes such that the transmitted force differences are minimized.

a) Statistical Linearization (SL)

The statistically linearized force method (SLFM) minimizes over the input frequency range the expected value of the difference between the

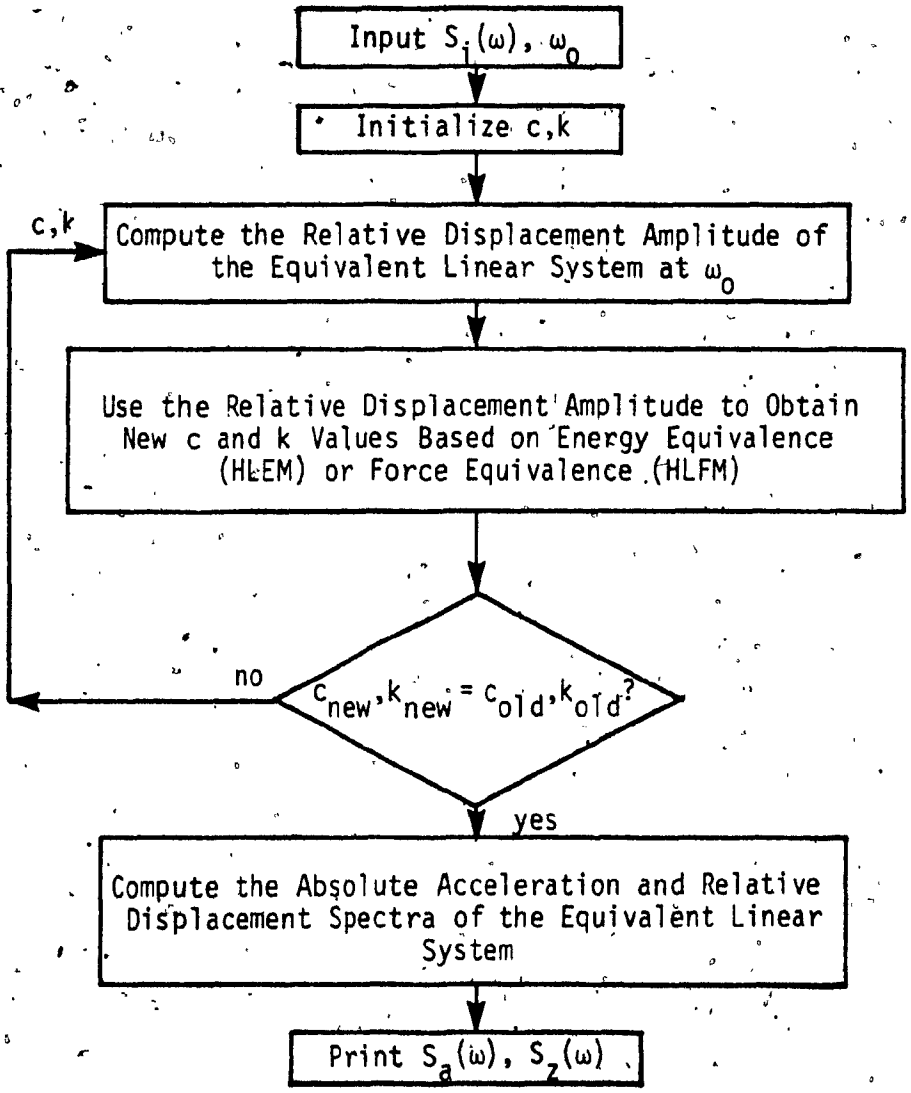

Fig. 7.8: Flowchart for the Harmonic Linearization (HL) Method

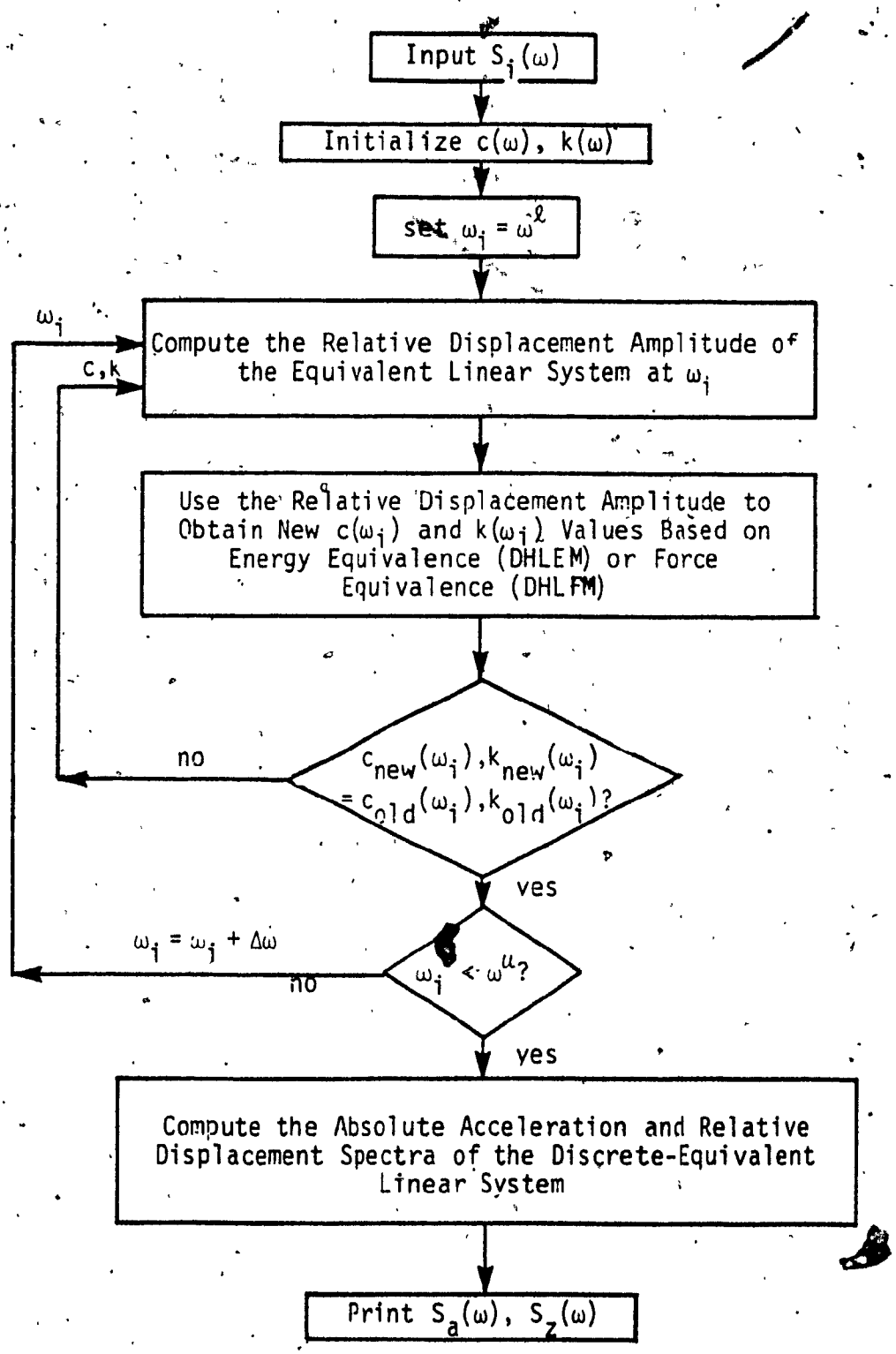

Fig. 7.9: Flowchart for the Discrete-Harmonic Linearization (DHL) Method

average transmitted force per cycle of the nonlinear and linear suspension systems. This equivalent linearization method is in widespread use [143-150], however, it will be shown in section 7.5.3 that it is not the most suitable method for the motorcycle suspension system. As in the corresponding energy method, minimization of the error is performed numerically so that the response spectra are obtained directly. The flowchart and computer program listing are shown in Fig. 7.7 and Appendix III, respectively.

b) Harmonic Linearization (HL)

In the harmonically linearized force method (HLFM), an appropriate frequency of the input spectrum is selected (recall section 7.5.1(b)). The average force transmitted, per cycle, by the nonlinear suspension system is then equated to that transmitted by an equivalent linear suspension system (linear stiffness and damping), at the pre-selected excitation level. The flowchart and computer program are shown in Fig. 7.8 and Appendix III, respectively.

c) Discrete Harmonic Linearization (DHL)

The discrete harmonically linearized force method (DHLFM) is identical to the HLFM except that the linearization procedure is repeated at each discrete input frequency. As with the DHLEM, this method is very accurate compared to the other linearization techniques, and requires less computational effort. The flowchart is shown in Fig. 7.9 and the computer program listing is given in Appendix III.

7.5.3 Comparison of the Methods

At the present time there is no literature available comparing

various equivalent linearization methods. There are, however, works which compare the results obtained by one equivalent linearization method to a "true" solution. The "true" solution is either obtained using a Markov method or computer simulation.

The exact solution (Markov method) of a second order system, containing a cubic stiffness element, has been compared to the solution obtained using the equivalent linearization method, (SLFM) in section 7.5.2(b), by Atalik and Utku [143]. A similar comparison has been presented by Iwan and Yang [155]. For systems containing nonlinear damping, Roberts [156] has applied an approximate Markov method and compared the results to those obtained by an equivalent linearization method (SLFM). All three investigations indicated errors less than ten percent.

Computer simulation has been used successfully as a comparative solution by several authors [149,150,156,157], with good agreement. Unfortunately, the comparisons using simulation as well as exact methods are not comprehensive nor conclusive, since typically only one of the linearization techniques described in section 7.5 is used.

The various equivalent linearization methods described in the subsections 7.5.1 and 7.5.2 were applied to the suspension model (equations 2.48 and 2.50). Two excitation spectra were used; white noise and field results, as shown in Fig. 7.6. The white noise excitation has little bearing on realistic behavior, however, it serves to indicate the dependency of the results on the nature of the excitation spectrum. The "true" results for both excitation spectra are obtained by representing the stochastically described input by a discrete series of harmonic records. An initial value solving routine [90] is used at each frequency

and excitation level. The program is listed in Appendix III. The steady-state response (absolute acceleration and relative displacement) of the non-linear suspension system to any one given harmonic can, under certain conditions [158], be considered harmonic and represents one point in the response spectra. In this manner, the excitation spectrum is swept, yielding a "true" set of response spectra.

The suspension model contains two damping nonlinearities which are due to friction and quadratic damping, and a stiffness nonlinearity which is due to the air column. The nonlinearities were introduced one at a time into the model, with the remaining non-linearities set to zero. In this manner the deviation of the response from the true solution due to coulomb damping only, quadratic damping only, coulomb and quadratic damping, and finally coulomb and quadratic damping and air column stiffness, can be observed. Table 7.1 contains the results for white noise excitation. For each type of non-linearity the absolute mean square (ms) acceleration error and absolute mean relative displacement error is listed. The quantities are relevent only in their respective columns, hence the choice of using mean square or mean values is arbitrary. Mean square acceleration and mean displacement are used because they are readily available in the program. From the table, it is clear that the DHLEM is the most accurate method when coulomb damping and quadratic damping are both present or when only quadratic damping is present. The DHLFM yields the most accurate results when only coulomb damping is used, or when all the non-linearities are present. It should be noted that when all the non-linearities are present, both the DHLEM and DHLFM yield relatively accurate results.

TABLE 7.1: Comparison of Linearization Methods - White Spectra

Linearization Method	Type of Nonlinearity Present							
	Coulomb Damping		Quadratic Damping		Coulomb and Quadratic Damping		Coulomb and Quadratic Damping Air Column Stiffness	
	$\lvert\bar{x}^2_{sim} - \bar{x}^2_{lin}\rvert$	$\lvert\bar{z}_{sim} - \bar{z}_{lin}\rvert$	$\lvert\bar{x}^2_{sim} - \bar{x}^2_{lin}\rvert$	$\lvert\bar{z}_{sim} - \bar{z}_{lin}\rvert$	$\lvert\bar{x}^2_{sim} - \bar{x}^2_{lin}\rvert$	$\lvert\bar{z}_{sim} - \bar{z}_{lin}\rvert$	$\lvert\bar{x}^2_{sim} - \bar{x}^2_{lin}\rvert$	$\lvert\bar{z}_{sim} - \bar{z}_{lin}\rvert$
SLEM	47.17	3.87×10^{-2}	16.79	4.04×10^{-2}	15.30	4.42×10^{-2}	34.18	4.36×10^{-2}
HLEM	5.22	0.236	1.14	0.232	3.86	0.231	24.19	0.245
DHLEM	2.75	8.82×10^{-3}	0.865	1.04×10^{-2}	2.178	9.91×10^{-3}	21.65	1.807×10^{-2}
SLFM	8.46	4.28×10^{-2}	12.86	4.34×10^{-2}	12.61	4.70×10^{-2}	32.95	4.82×10^{-2}
HLFM	4.79	0.231	3.49	0.233	5.92	0.232	24.17	0.245
DHLFM	1.83	8.70×10^{-3}	3.93	1.15×10^{-2}	3.39	1.05×10^{-2}	21.14	1.806×10^{-2}

sim is the subscript used to denote the "true" value, obtained by simulation.
lin is the subscript used to denote the approximate solution, obtained by linearization.

The comparative procedure was repeated for the excitation spectra obtained from field measurements. The results are listed in Table 7.2. In this case the DHLFM produces the least error, independent of the nature of the non-linearity, however, the error produced by the DHLEM is very close in each comparison. The acceleration and relative displacement response spectra calculated for the field excitation spectra for both the energy and force methods are shown in Figs. 7.10 to 7.13. Two distinct regions of the frequency range can be distinguished for comparison purposes; 0 to 4 Hz, and 4 to 20 Hz.

For energy methods in the low frequency range (0 to 4 Hz) the statistically linearized method, SL, gives the most accurate ms acceleration response (Fig. 7.10) while giving the most deviant rms displacement response (Fig. 7.11). In this range, both the harmonically linearized, HL, and discrete-harmonically linearized, DHL, methods deviate significantly from the "true" solution in both the ms acceleration and rms displacement response spectra. For energy methods in the high frequency range (4 to 20 Hz), the accuracy of the DHL method clearly surpasses that of the other methods. The DHL method follows the "true" solution closely in the ms acceleration spectrum, accurately predicting the change at 12.5 Hz. In the rms displacement spectrum, the DHL method is nearly indistinguishable from the "true" response. In this range, it can be noted that the DHL and HL results are identical at 7.5 Hz. This is expected because the HL methods are linearized at the frequency at which the excitation spectrum has its peak value, namely 7.5 Hz (recall Fig. 7.6).

In the low frequency range, the force methods follow a different trend than the energy methods because not one of the methods approximates the "true" solution better than any other method in both the ms

TABLE 7.2: Comparison of Linearization Methods - Field Spectra

Linear-ization Method	Type of Nonlinearity Present							
	Coulomb Damping		Quadratic Damping		Coulomb and Quadratic Damping		Coulomb and Quadratic Damping Air Column Stiffness	
	$\lvert\bar{\ddot{x}}^2_{sim} - \bar{\ddot{x}}^2_{lin}\rvert$	$\lvert\bar{z}_{sim} - \bar{z}_{lin}\rvert$	$\lvert\bar{\ddot{x}}^2_{sim} - \bar{\ddot{x}}^2_{lin}\rvert$	$\lvert\bar{z}_{sim} - \bar{z}_{lin}\rvert$	$\lvert\bar{\ddot{x}}^2_{sim} - \bar{\ddot{x}}^2_{lin}\rvert$	$\lvert\bar{z}_{sim} - \bar{z}_{lin}\rvert$	$\lvert\bar{\ddot{x}}^2_{sim} - \bar{\ddot{x}}^2_{lin}\rvert$	$\lvert\bar{z}_{sim} - \bar{z}_{lin}\rvert$
SLEM	3.12	3.22	0.406	2.74×10^{-2}	2.89	3.05×10^{-2}	2.87	3.04×10^{-2}
HLEM	2.24	7.11×10^{-3}	0.351	1.07×10^{-2}	2.22	7.06×10^{-3}	2.96	7.0×10^{-3}
DHLEM	1.10	4.24×10^{-3}	0.351	5.76×10^{-3}	1.09	4.32×10^{-3}	2.05	5.21×10^{-3}
SLFM	2.79	3.00×10^{-2}	0.385	2.76×10^{-2}	2.66	2.93×10^{-2}	3.60	3.0×10^{-2}
HLFM	2.32	7.00×10^{-3}	0.352	1.00×10^{-2}	2.29	7.00×10^{-3}	3.10	6.90×10^{-3}
DHLFM	0.970	4.14×10^{-3}	0.348	5.75×10^{-3}	0.965	4.11×10^{-3}	1.87	5.06×10^{-3}

sim is the subscript used to denote the "true" value, obtained by simulation.
lin is the subscript used to denote the approximate solution, obtained by linearization.

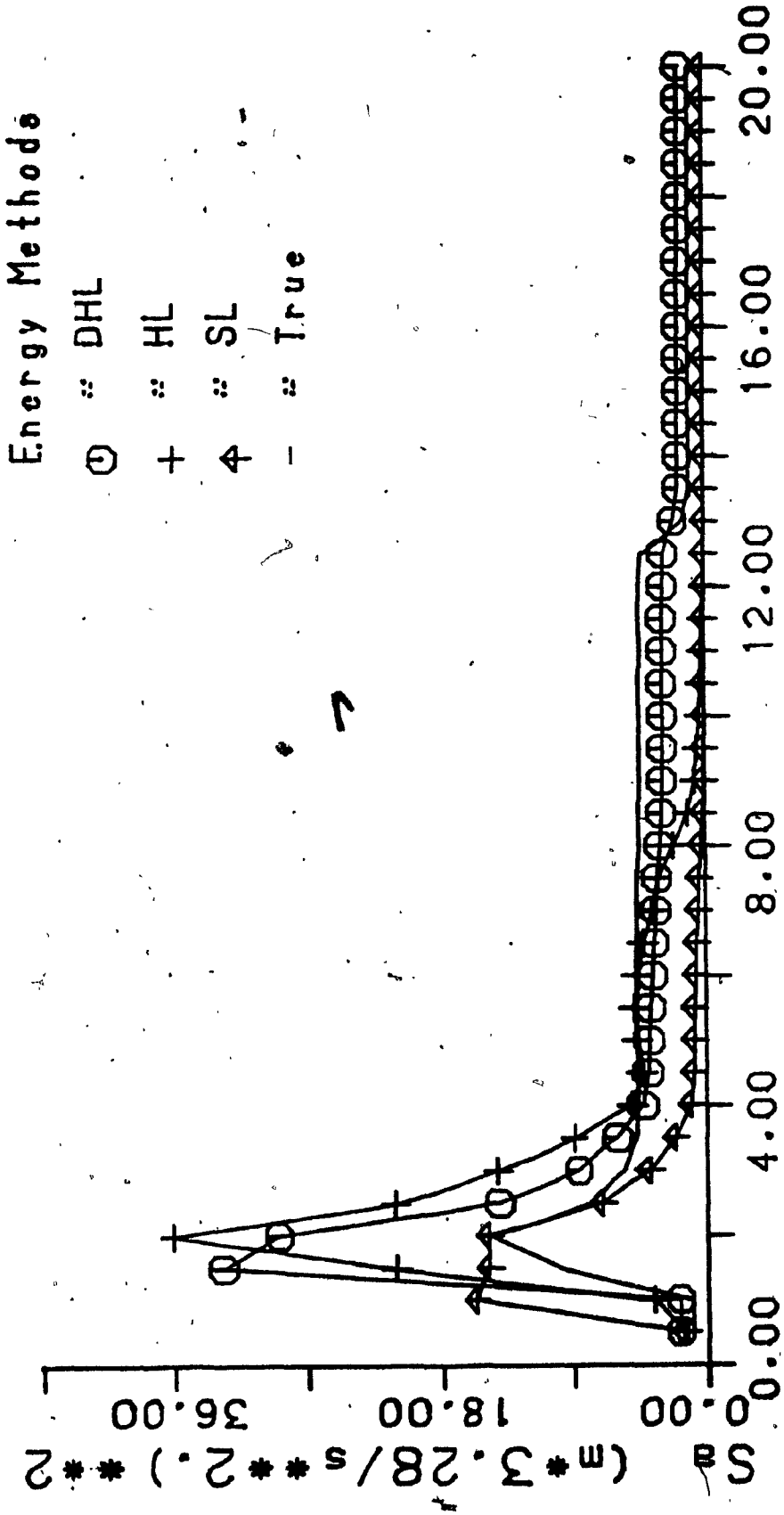

Fig. 7.10: Acceleration Spectra for Energy Methods

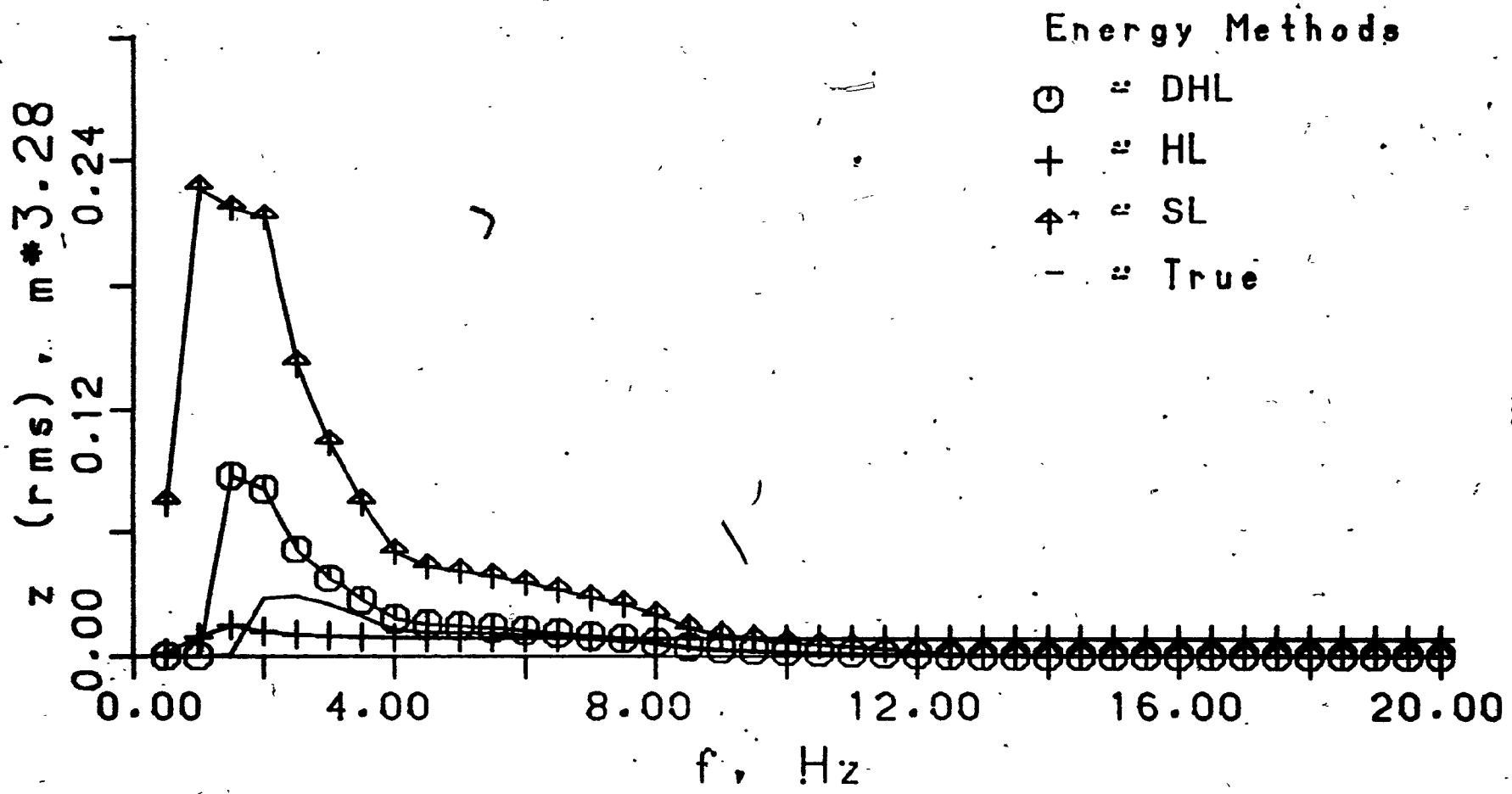

Fig. 7.11: Displacement Spectra for Energy Methods

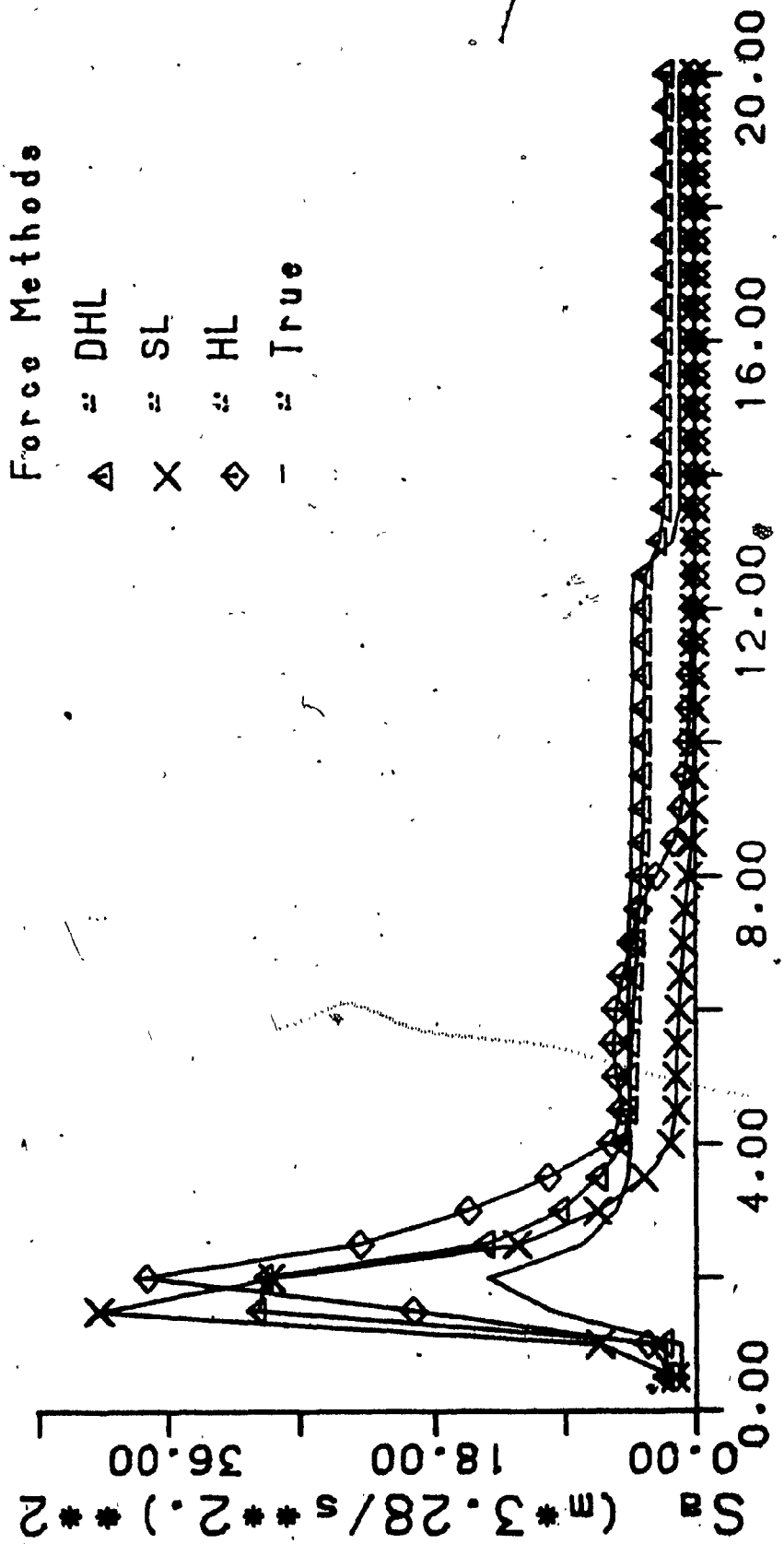

Fig. 7.12: Acceleration Spectra for Force Methods

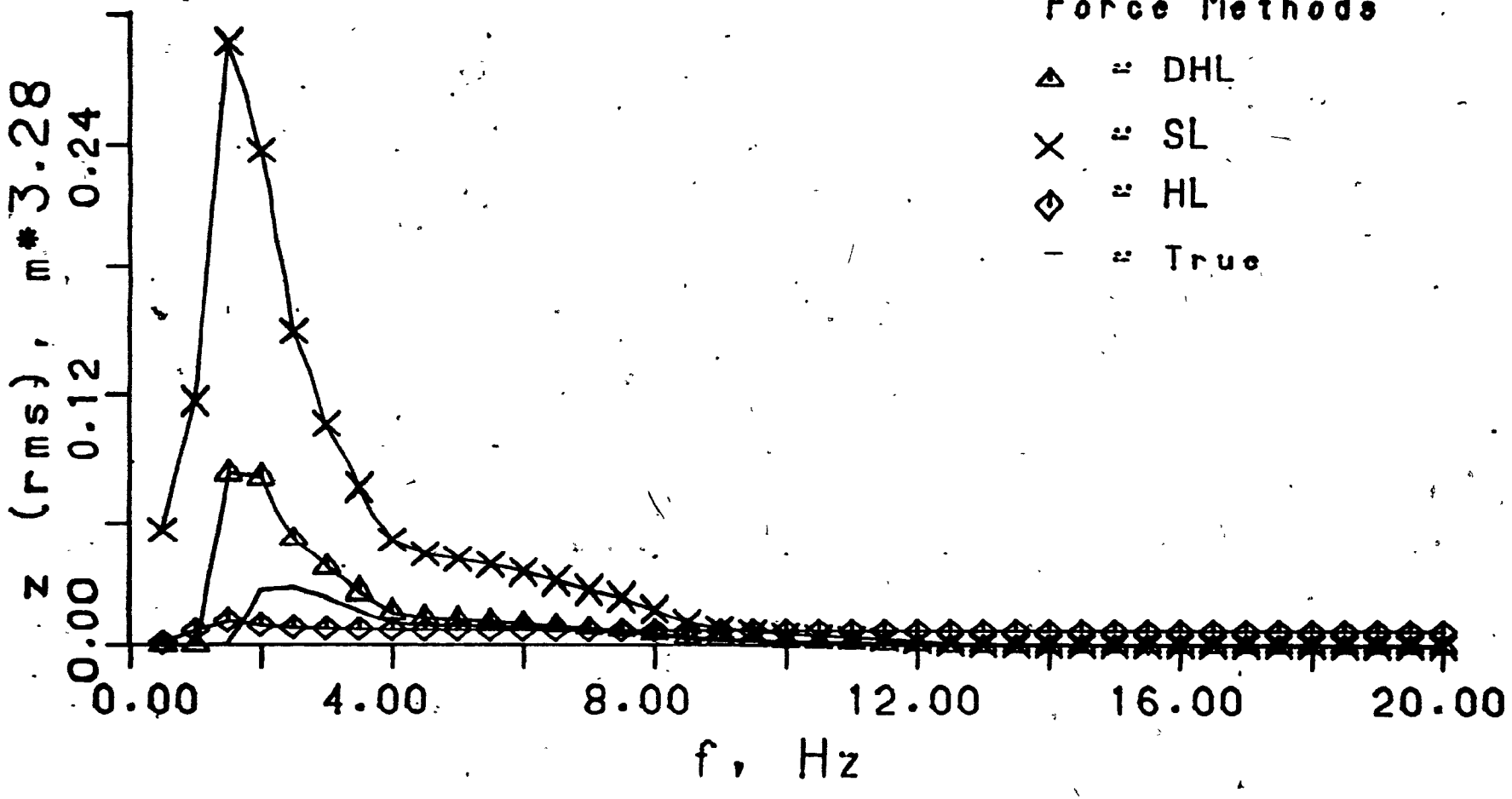

Fig. 7.13: Displacement Spectra for Force Methods

acceleration and rms displacement response spectra (Figs. 7.12 and 7.13). It is clear, however, that the HL method gives the most inaccurate results. In the high frequency range, the DHL force method clearly yields the most accurate results in both response spectra. As in the DHL energy method, the DHL force method accurately predicts the change in the ms acceleration response at 12.5 Hz. Similarly, the HL and DHL responses are congruent at 7.5 Hz.

7.6 Stochastic Response of the Suspension System

Using the Discrete-Harmonically Linearized Force Method (DHLFM), the stochastic response of the suspension system is evaluated. A suitable performance criterion is established to obtain sets of optimal design parameters. The stochastic responses of the stock (original design) and the two parameter optimized suspension are verified by laboratory experiment. Then the complete suspension system is optimized (five parameter optimization) for stochastic excitation and the results are presented and discussed.

7.6.1 Application of the Discrete-Harmonically Linearized Force Method (DHLFM)

The superior performance of the DHLFM has been illustrated in section 7.5. The DHLFM was applied to the laboratory suspension model which included the guidance stiction (equations 4.2 and 4.3) and the ms acceleration plot was recorded. The field excitation spectrum shown in Fig. 7.6 was utilized as the input for this model. The response was verified in the laboratory using the set-up shown in Fig. 4.7. The excitation spectrum of the field data (Fig. 7.6) was generated by a Brüel and Kjaer Type 1026 narrowband random signal generator and fed into an

electro-hydraulic shaker. The response acceleration signal was recorded by a Brüel and Kjaer 7003 series FM recorder. After the testing was completed, the taped record was analyzed using a Nicolet 660 A spectral analyzer. The ms acceleration spectra obtained by the DHLFM and laboratory testing are shown in Fig. 7.14. They both display the same trend, with good correlation at the peak values. In the 3 to 10 Hz range, the dominant damping characteristic is due to coulomb friction. In the laboratory, the slip-stick mechanism is not truely coulombic, which accounts for the deviation between the two curves in this range.

7.6.2 Suspension Optimization

To carry out suspension optimization in the case of stochastically described input excitation, probabilistic performance indices analgous to the deterministic forms (in Chapter 5) are utilized. As in the deterministic case, only performance indices which are functions of the system response parameters are appropriate for this investigation. Karnopp and Trikha [94] analyzed a performance index I_r, which is commonly used [55, 92,101,159-161] to evaluate the performance of systems subject to random excitation. It has the form:

$$I_r = E[\ddot{X}^2] + D\,E[z^2] \tag{7.3}$$

where $E[\ddot{X}^2]$ and $E[z^2]$ are the expected ms responses of the absolute acceleration and relative displacement, respectively. The value of the weighting factor D, depends on the relative importance of the two dynamic quantities.

a) Two Parameter Optimization

The motorcycle suspension contains two parameters which can be

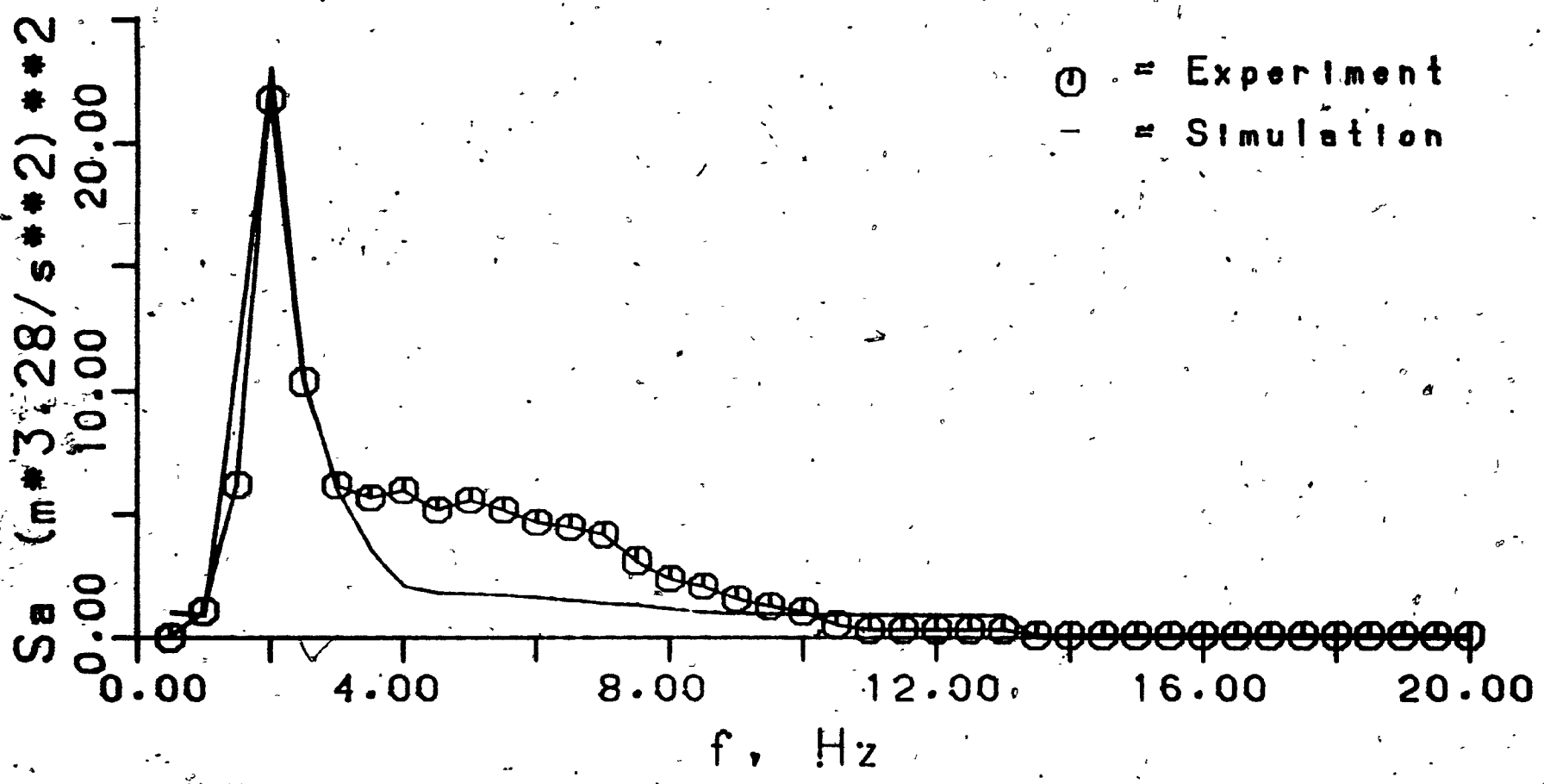

Fig. 7.14: Acceleration Spectra for an Existing Design

readily modified in the laboratory; orifice area and air column volume. The remaining potential optimization parameters; helical spring stiffness, initial air pressure (which dictates the static ride height), and seal stiction, require more extensive modification effort. Hence, in this sub-section, a two parameter optimization is presented and the results are verified by laboratory experiment.

The optimization problem was formulated using the suspension model without the guidance stiction in a manner very similar to the one described in section 6.5 with the exception that the input excitation is the field spectra of Fig. 7.6. The DHLFM was used to obtain the response, and the performance index for random input (equation 7.3) was evaluated. The available instrumentation in the laboratory is not suitable for the measurement of ms relative displacement. Subsequently, the weighing factor D, was assigned a value of zero so that the sense in which the suspension was optimized could be observed in the laboratory. The optimization method described in section 6.3 was then applied. The optimal design values are listed in Table 7.3. From the table, it is apparent that the optimization procedure yielded a very lightly damped system. This result is expected since, with the weighing parameter in equation 7.3 set to zero, only the ms absolute acceleration is minimized.

The optimal design values were used to modify the hardware model. Because of the guidance stiction, the mathematical model of the suspension system was modified to include this additional coulomb friction (the procedure is similar to that in section 4.4) and the stochastic response was calculated with the optimal parameters. Both sets of results are plotted in Fig. 7.15. The results obtained by simulation and laboratory testing are in excellent agreement, both indicating a fifty percent

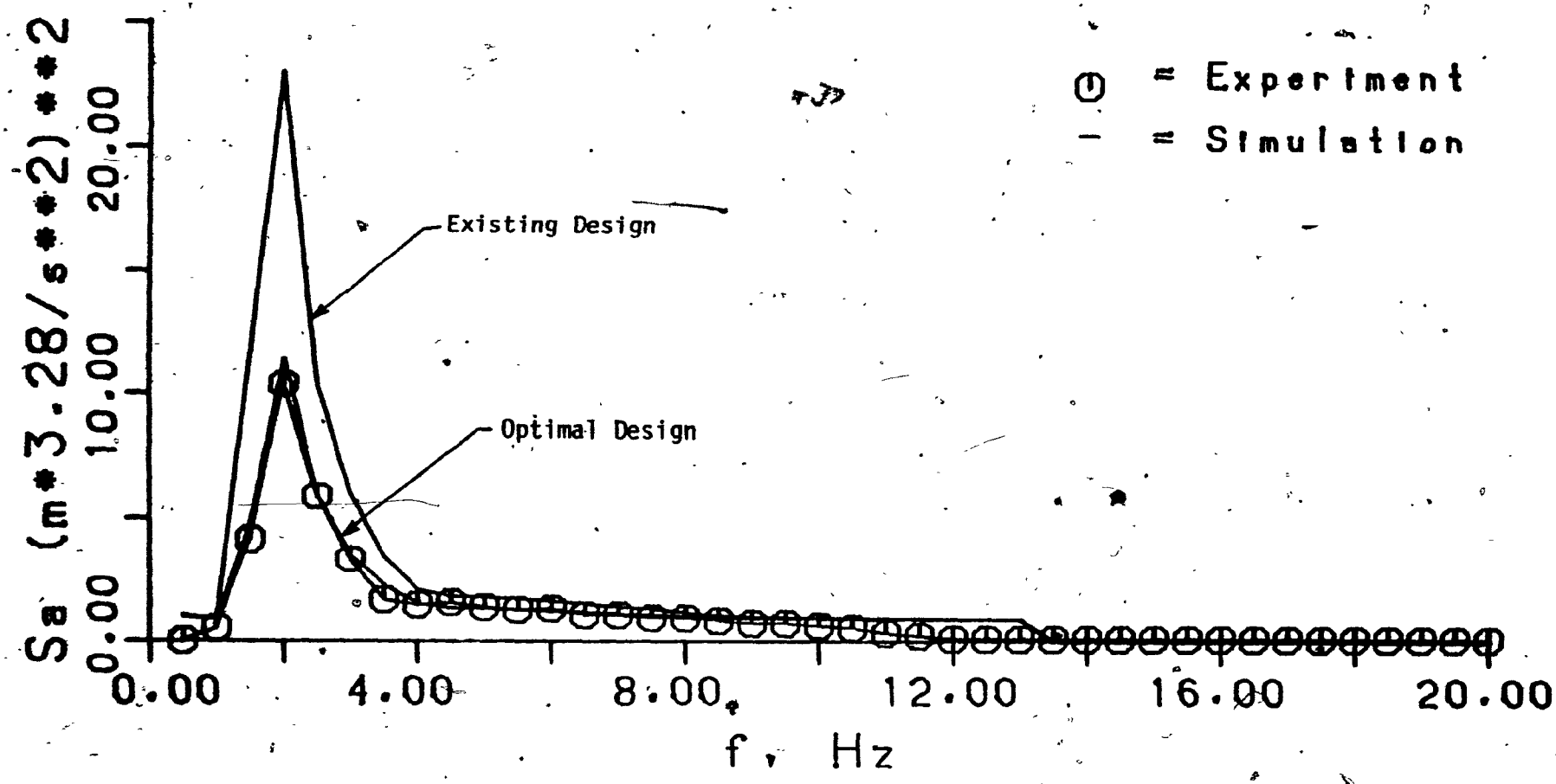

Fig. 7.15: Acceleration Spectra for Optimal and Existing Designs (2 Parameter Optimization)

reduction in the peak ms acceleration response.

b) Five Parameter Optimization

A five parameter optimization was conducted following the procedure used in the two parameter optimization, with a few alterations. The principal difference was that the performance of the actual suspension, rather than the performance of the laboratory model, was the objective function. Hence, the performance index (equation 7.3) was used with a weighing factor set to unity. The five parameters are: helical spring stiffness, k, initial air volume, V_o, seal stiction, F_{coul_1}, quadratic damping, $T_p + T_{or}$, and initial air pressure, p_o. The optimization method described in section 6.3 was applied, and the optimized parameter values obtained. These values are listed in Table 7.4. The stock and optimized ms acceleration response spectra are shown in Fig. 7.16, and the stock and optimized rms displacement spectra are shown in Fig. 7.17. Both figures show a significant performance increase over the stock response.

The optimized parameter values for the stochastic response in Table 7.4 can be compared to the optimization results for the frequency and time domain in Table 6.1. The stochastic response values for helical spring stiffness, k, and quadratic damping coefficients, $T_p + T_{or}$, follow the same trend as those for the frequency domain optimization. Similarly, the trend for the initial air volume, V_o, is the same for the stochastic response and time domain optimization, although not to the same extent. The optimal value of seal stiction is reduced for optimal stochastic response, whereas it is increased for the frequency and time domain optimizations. This characteristic is due to the emphasis on the response in the 4 to 10 Hz range (recall Fig. 7.6). If this range is weighed in the

TABLE 7.3: Two Parameter Optimization Results

Design Parameter	Existing Design Value	Optimal Design Value
$T_p + T_{or}$ (kg/m)	40.92	1.724×10^{-2}
V_o (m^3)	6.934×10^{-4}	5.461×10^{-2}

TABLE 7.4: Five Parameter Optimization Results

Design Parameter	Existing Design Value	Optimal Design Value
k (N/m)	2.067×10^3	7.811×10^2
V_o (m^3)	6.934×10^4	1.484×10^5
F_{seal_1} (N)	1.677	0.3363
$T_p + T_{or}$ (kg/m)	40.92	8.184
P_o(kPa)	84.55	846.4

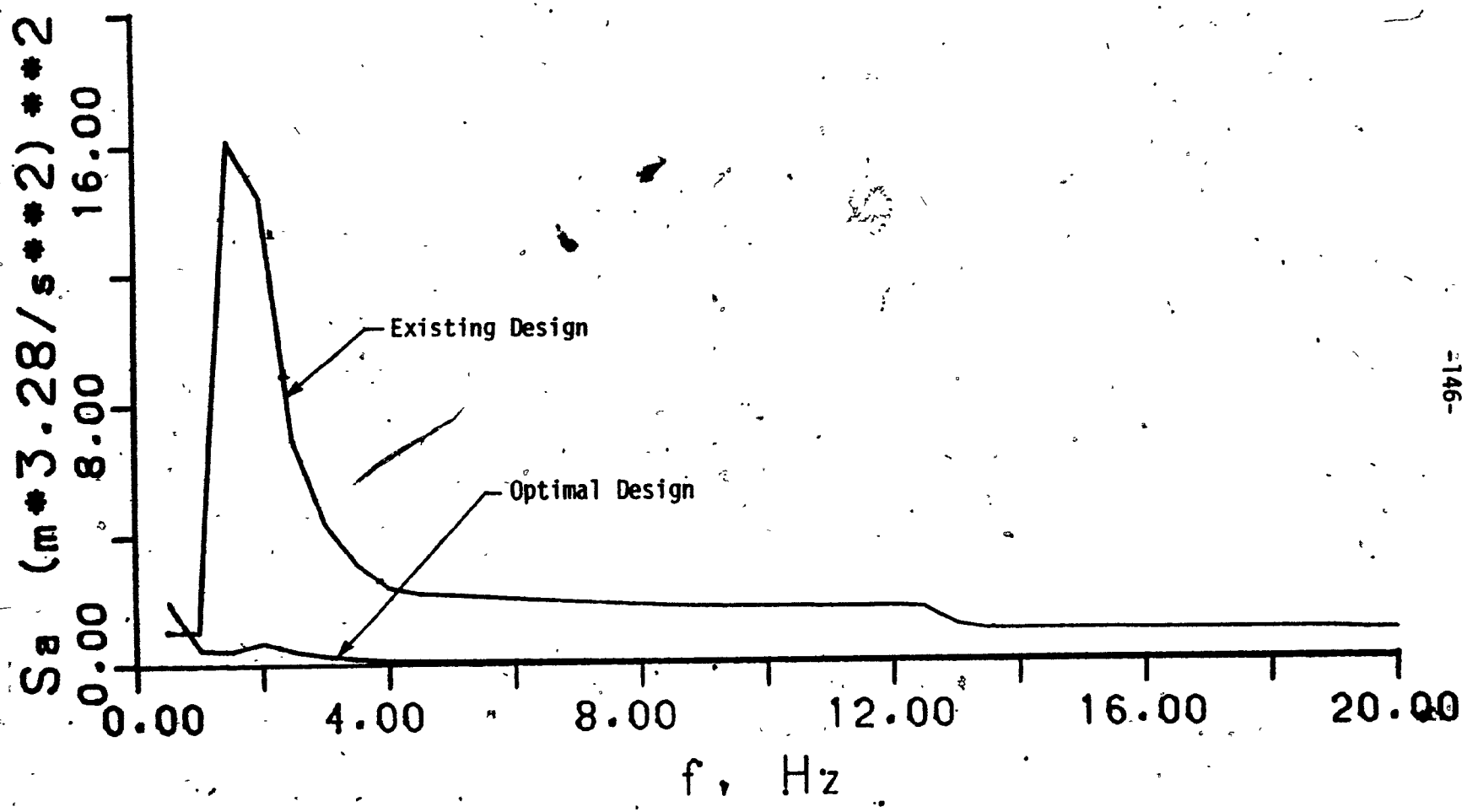

Fig. 7.16: Acceleration Spectra for Optimal and Existing Designs (5 Parameter Optimization)

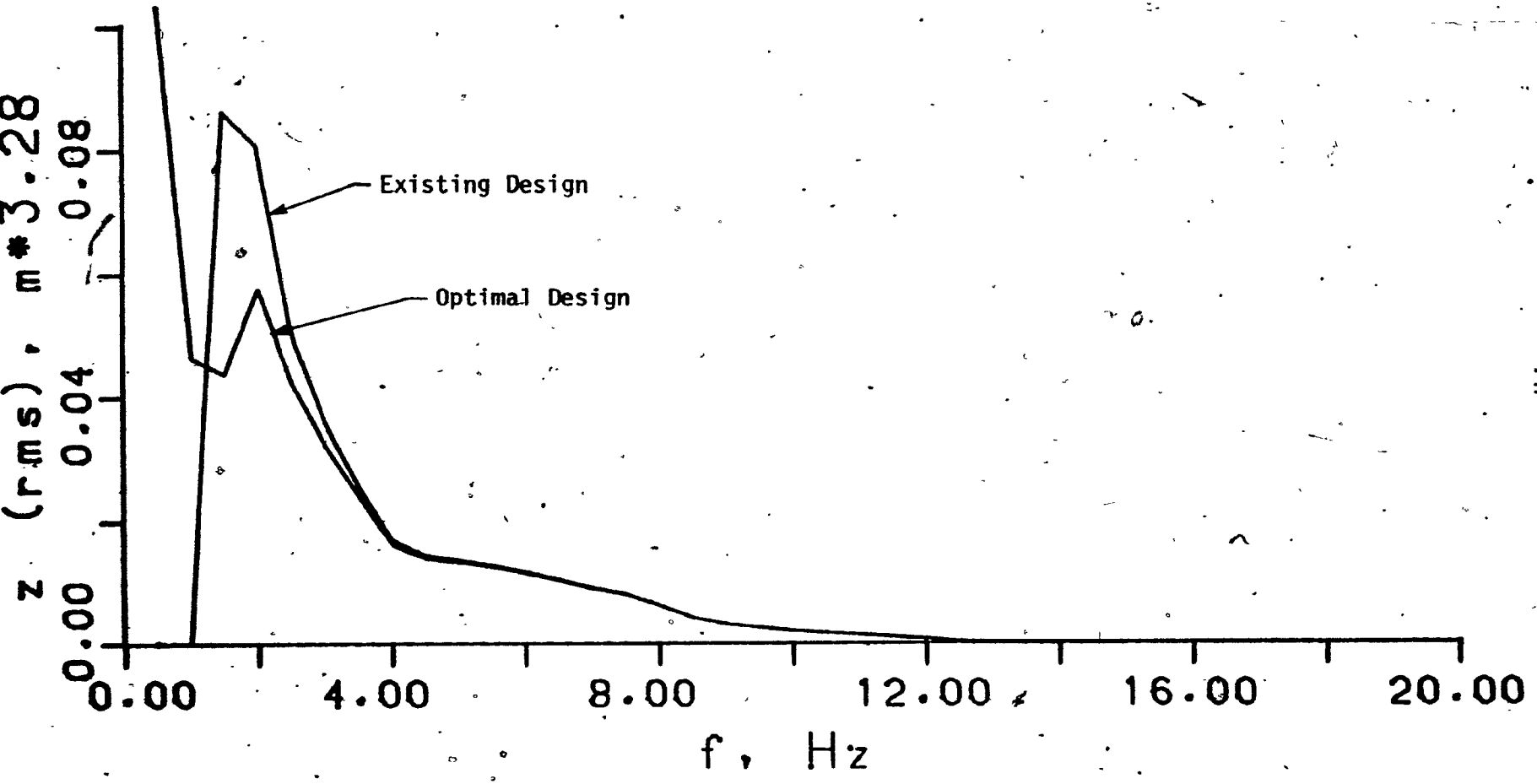

Fig. 7.17: Displacement Spectra for Optimal and Existing Designs (5 Parameter Optimization)

frequency domain optimization, a similar trend in the seal stiction alteration is expected. To summarize, the trend in the optimal design values obtained from the stochastic response optimization follows those of either the frequency or time domain optimization. This trend is expected since the terrain induced excitation consists of components which are best described in either the frequency or time domain.

7.7 Summary

In this chapter, methods for obtaining the stochastic response of the nonlinear suspension system were presented and suitable linearization techniques were applied. The input ms acceleration spectrum was obtained from field measurements. Once the nature of the excitation and system model was known, the analytical techniques for obtaining the stochastic response were reviewed with respect to suitability for the present problem. Once a suitable technique was selected (equivalent linearization), the performance of various innovative approaches was compared. The discrete-harmonically linearized force method (DHLFM) exhibited the least error. Hence it was used as the method for obtaining the stochastic response in the optimization procedures. The linearization technique was used in computational optimization techniques for two and five variable optimization. Whenever possible, the response spectra were verified in the laboratory.

CHAPTER 8

CONCLUSIONS AND RECOMMENDATIONS FOR FUTURE WORK

CHAPTER 8

CONCLUSIONS AND RECOMMENDATIONS FOR FUTURE WORK

8.1 Conclusions

In this investigation, a computer aided analysis and design methodology is presented. The presented material illustrates that the performance of a given motorcycle suspension can be evaluated using appropriate modeling and simulation techniques. This approach yields significant time and cost savings when compared to the traditional method of full scale hardware testing. The extension of the methodology to optimal design synthesis (Chapters 5-7) is even more significant because not only can several hundred combinations of the design parameter values be critically evaluated in a few seconds, but the global nature of the optimal design set can also be readily observed (see section 6.4).

The methodology utilizes mathematical models which are developed from basic principles. This approach yields intricate, non-linear suspension component models. Analog and digital computer simulation techniques are applied to the damper elements and the results are compared to those obtained by experiment, showing good agreement. Having verified the damper element characteristics, computer simulation techniques are then applied to a suspension system model. The model utilizes non-linear damper and air spring elements together with idealized mass and stiffness elements. Results are obtained in both the frequency and time domains, and are supported by results obtained in the laboratory. The validation procedure is discussed in Appendix IV. Suspension performance criteria are introduced for each domain. The criteria are used to formulate a set of objective functions. A numerical optimization technique based on the Penalty function approach is then applied and the

results are obtained. An existing suspension system is modified using the set of optimal design parameters. The predicted optimal performance is verified in the laboratory using the modified suspension.

The investigation is extended to include the stochastic response of the motorcycle suspension. For this purpose, the power spectra of the terrain induced excitation obtained from realistic field measurement are utilized. Various techniques for obtaining the nonlinear system response under stochastic excitation are discussed. The most suitable technique is determined and the accuracy of several variations is critically evaluated. The most accurate version is then used to obtain the stochastic response of the nonlinear suspension system. A performance criteria is formulated and numerical techniques are applied to obtain a set of optimal design parameters, based on the stochastic response. The methodology is verified by comparing the predicted response of the optimized suspension with the response of a hardware model modified in accordance with the optimal design parameter set.

8.2 Highlights of the Investigation

The original contributions of the investigation presented in this thesis can be summarized in terms of the following set of statements:

1) Detailed, effective mathematical models of motorcycle suspension dampers are derived from the basic fluid flow and ideal gas relationships. Although motorcycle dampers are used in this investigation, the approach is readily generalized to any viscous damper. This aspect of the investigation has been presented and published [162].

2) The mathematical model of the suspension system is a simple, yet accurate single degree of freedom model. The nonlinear elements are due

to the dampers and air spring. The linear elements, mass and stiffness, are idealized, however, they represent realistic behavior. The mass is considered to have a constant value. In practice, the pitch motion of the motorcycle alters the effective mass on the front suspension, however a perfect suspension will completely isolate the mass. Hence, the ideal mass representation becomes increasingly realistic during the optimal design procedure. The linear representation of the helical spring is realistic because only a small part of its possible range is used (i.e. relatively small deflections are experienced). To summarize, the mathematical model of the motorcycle suspension utilizes linear element representation wherever possible, while retaining highly discontinuous, non-linear elements so that the non-linearities can be fully exploited in the analysis and optimal design procedure.

3) Performance indices are developed for the frequency and time domain analysis. Traditionally, only the damper characteristics are considered as a quantifiable performance index. In this investigation, the frequency domain performance index presented is precise because it uses an initial value solving routine (retaining the systems' non-linearities), while remaining economical because only two frequencies are used to characterize the transmissibility. The frequency domain performance index concept can conveniently be extended to hardware testing since only two excitation frequencies are required.

The time domain analysis provides a unique performance index which utilizes the dynamic quantities of interest and the theoretically optimal force level. The performance index is useful not only for comparing the performance of two suspension systems, but also for evaluating the

performance of a single suspension system as compared to the theoretically optimal performance. Although in this thesis the index is used in the suspension simulation, it can easily be used in the laboratory testing of suspension systems if suitable system excitation and data storage facilities are available.

Both frequency and time domain performance indices are plotted over the respective range of input values, yielding a performance characteristic for each domain. These aspects of the investigation have been presented and published [163].

4) An optimal design procedure is presented which can be used by the motorcycle suspension designer to maximize the performance of a given suspension system. The performance characteristics are used to formulate a set of objective functions. Conventional numerical optimization methods are then applied to yield sets of optimally designed suspension parameters. This optimal design procedure constitutes several published works [164,165].

5) A summary of various equivalent linearization methods for stochastically excited systems is presented. The accuracy of these methods is evaluated by comparing the stochastic response obtained using a given linearization method with a "true" response obtained through simulation. The comparison is carried out for various excitation spectra and severity of system non-linearity. The benefits are two-fold; the choice of linearization scheme for the type of problem is determined, and secondly, an original method for evaluating the accuracy of various linearization schemes is presented.

6) A design procedure which optimizes the stochastic response of the motorcycle is presented using an accurate linearization method. A suitable

performance index is formulated and a numerical optimization method is applied, yielding an optimal design procedure based on the stochastic response.

8.3 Recommendations for Future Work

Recommendations for future work fall into two categories: recommendations which apply to various phases of the methodology presented in this thesis, and recommendations for work beyond the scope of this investigation. Future work which falls into the first category may be summarized in the following statements:

1) The mathematical model could include a more detailed relationship for the entrapped air column. Such a relationship would include a heat transfer model which utilizes time histories to predict the contribution of the air column and viscosity change of the damping fluid.

2) An improved model for the slip-stick mechanism of the seal stiction should be developed.

3) The effective mass per fork leg is not a constant. The simplicity of the single degree of freedom model could be retained if the statistics of the effective mass variation is estimated. The time history of the mass variation could be generated and the present methodology could be utilized.

4) The effect of entrained gas in the damping fluid and its degrading effect on the damper performance could be modeled. As with the heat transfer model (statement (1)), the entrained gas model could utilize time histories of the dynamics of the gas-fluid interface to estimate the change in the effective bulk modulus of the fluid.

5) The linearization methods presented in Chapter 7 could be applied to the frequency domain performance index in section 5.2 to reduce computational effort.

Recommended future work which extends beyond the methodology presented in this thesis can be summarized by the following set of statements:

1) The optimal design procedures for the frequency and time domains could be combined with the procedure for the stochastic response. The resulting package could be used as part of a global CAD/CAM package for motorcycle suspension design.

2) The lateral stiffness of the fork could be considered in the design process. The effects of braking torque and oblique terrain loads on the stiction mechanism could then be investigated.

3) Different valving mechanisms could be studied. The valving configurations could include: blow-off, friction, or displacement-dependent types. They could use passive, semi-active, or active control schemes.

4) In order to perform a complete analysis and optimization of the motorcycle suspension, the front and rear suspension models should be incorporated into a model of the motorcycle which considers the pitch and bounce of the motorcycle frame. A thesis on this topic has been published [166], however it doesn't include an optimization of the suspension parameters as presented in this investigation. The motorcycle model could be more fully developed to include the tire influence, wheel lift-off, terrain compliance, and the effect of non-linear linkages (rear suspension).

REFERENCES

REFERENCES

1. Baker, A., "The World of Motorcycles", Vol. 5, Columbia House, New York, 1979, pp. 589-594.

2. Irving, F., "Motorcycle Engineering", Clymer Publications, Los Angeles, 1962, pp. 17-87.

3. Baker, A., "The World of Motorcycles", Vol. 15, Columbia House, New York, 1979, pp. 1741-1786.

4. Cameron, K., "Dampers", Cycle, December 1981, pp. 73-76, 116, 121, 122.

5. Jennings, G., "Suspensions: An Overview", Cycle, May 1975, pp. 54-56, 69, 71, 72.

6. Karr, J., "The Single-Shock Suspension Revolution", Motorcyclist, October 1980, pp. 46-49.

7. Girdler, A., "How Pro-Link Works", Cycle World, March 1981, pp. 34-35.

8. Holeman, D., "Shocks: The Last Technical Frontier", Cycle, February 1977, pp. 89-96.

9. Jordan, M., "Suspension Buyer's Guide", Cycle Guide, January 1980, pp. 73-76.

10. Dean, P., "The Rise of Single Shocking", Cycle Guide, February 1981, pp. 80-81.

11. Fabre, B., "Fabre on Forks", Dirt Rider, February 1976, pp. 17-18.

12. Cline, R., "Shock Absorbers: An Integral Part of Recreational Vehicle Developments", SAE Paper No. 740678, 1974.

13. Nutting, J., "Spring Fever", Cycle World, February 1980, pp. 111-114.

14. Sieman, R., "Works Performance Shocks", Modern Cycle, February 1976, pp. 64-68.

15. Zimmerman, B., "Suspension: Part 1", Popular Cycling, February 1975, pp. 16-21, 64,65.

16. Vucci, L., "Tuning Forks", Cycle World, November 1977, pp. 67-70.

17. Jennings, G., "A Study of Motorcycle Damping Characteristics", SAE Paper No. 740628, 1974.

18. Van Voorhis, G., "How Harley-Davidson's Evolution V^2 Evolved", Cycle News East, Vol. 17, No. 33, August 1983, pp. 24-25.

19. Burgess, G., "An Investigation Into Motorcycle Rear Suspension Geometry", Bombardier Ltd., Internal Engineering Report, December 4, 1980.

20. Morey, C., "Simple and Single", Dirt Rider, May 1983, pp. 71-73.

21. Obata, H., "Development of Analysis Method to Ensure Performance Quality for End-User", Paper TS-C1-12, presented at the International Conference on Quality Control, Tokyo, October 17-20, 1978.

22. Kane, T., "The Effect of Frame Flexibility on High Speed Weave of Motorcycles", SAE Paper No. 780306 (SP-428), 1978.

23. Weir, D. and Zellner, J., "Lateral-Directional Motorcycle Dynamics and Rider Control", SAE Paper No. 780304 (SP-428), 1978.

24. Snowdon, J., "Vibration and Shock in Damped Mechanical Systems", John Wiley and Sons, New York, 1968, pp. 95-130.

25. Weir, D. and Zellner, J., "Experimental Investigation of the Transient Behavior of Motorcycles", SAE Paper No. 790266, 1979.

26. Roe, G., Pickering, W. and Zinober, A., "The Oscillations of a Flexible Caster and the Effect of Front Fork Flexibility on the Stability of Motorcycles", SAE Paper No. 780307 (SP-428), 1978.

27. Campbell, L., "Beyond Teledraulics", Cycle World, April 1979, pp. 73-79.

28. Weisel, J., "Thorks: Thorwaldson Leading Links", Motocross Action, October 1979, pp. 60-67.

29. Black, S. and Taylor, D., "Simulation of Off-Road Motorcycle Ride Dynamics", SAE Paper No. 790261, 1979.

30. Mulvenna, A., "The Shock Absorber Story", Gabriel of Canada Product Engineering Report, October 23, 1968.

31. Csere, C. and Sherman, D., "Shock Treatment", Car and Driver, September 1981, pp. 61-67.

32. Simanaitis, D., "Shock Absorbers", Automotive Engineering, November 1976, pp. 34-39.

33. Sano, S., "Evaluation of Motor Vehicle Handling", International Journal of Vehicle Design, Vol. 3, No. 2, 1982, pp. 171-189.

34. Robson, J., "Road Surface Description and Vehicle Response", International Journal of Vehicle Design, Vol. 1, No. 1, 1979, pp. 25-35.

35. Wong, J., "Theory of Ground Vehicles", John Wiley & Sons, New York, 1978, pp. 210-240.

36. Lang, H., "A Study of the Characteristics of Automotive Hydraulic Dampers at High Stroking Frequencies", Ph.D. Thesis, University of Michigan, 1977.

37. Stephens, D., "Comparative Vibration Environments of Transportation Vehicles", Proceedings from the ASME Design Engineering Conference, AMD-Vol. 24, September 26-28, 1977, pp. 59-72.

38. Dinca, F. and Teodosiu, C., "Studiul Oscilatiilor Libere Ale Sistemelor Cu Disipare Patratica Asimetrica", Academia Republicii Populare Romine. Institutl de Mecania Aplicata. Studi Si Cercetari de Mecanica Aplicata, Vol. 17, 1964, pp. 1173-1186.

39. Dinca, F. and Teodosiu, C., "Calculul Amortizoarelor Hidraulice Telescopice", Academia Republicii Populare Romine. Institutl de Mecania Aplicata. Studi Si Cercetari de Mecanica Aplicata, Vol. 17, 1964, pp. 879-899.

40. Dinca, F. and Teodosiu, C., "Nonlinear and Random Vibrations", Academic Press, Inc., New York, 1973, pp. 105-399.

41. Ariaratnam, S., "Random Vibrations of Non-Linear Suspensions", Journal of Mechanical Engineering Science, Vol. 2, No. 3, 1960, pp. 195-201.

42. Roberts, J., "Response of Non-linear Mechanical Systems to Random Excitation Part 2: Equivalent Linearization and Other Methods", Shock and Vibration Digest, Vol. 13, No. 5, May 1981, pp. 15-29.

43. Smith, C., "Literature Review-Automobile Ride Quality", Shock and Vibration Digest, Vol. 12, No. 4, 1980, pp. 15-20.

44. Stikeleather, L., Hall, G. and Radke, A., "A Study of Vehicle Vibration Spectra as Related to Seating Dynamics", Trans. SAE, Vol. 81, Paper No. 720001, 1972.

45. Butkunas, A., "Power Spectral Density and Ride Evaluation", Trans. SAE, Vol. 75, Paper No. 660138, 1966.

46. Healey, A., "Digital Processing of Measured Vibration Data for Automobile Ride Evaluation, "Proceedings from the ASME Design Engineering Conference, AMD-Vol. 24, September 26-28, 1977, pp. 1-18.

47. Healey, A., Nathman, E. and Smith C., "An Analytical and Experimental Study of Automobile Dynamics with Random Roadway Inputs", Trans. ASME, Journal of Dynamic Systems, Measurement, and Control, December 1977, pp. 284-292.

48. Corbin, J. and Kaufman, W., "Classifying Track by Power Spectral Density", Proceedings from the ASME Winter Annual Meeting, AMD-Vol. 15, November 30-December 5, 1975, pp. 1-20.

49. Law, E. and Cooperrider, N., "A Survey of Railway Vehicle Dynamics Research", Trans. ASME, Journal of Dynamic Systems, Measurement, and Control, June 1974, pp. 132-146.

50. Cryer, B., Nawrocki, P. and Lund, R., "A Road Simulation System for Heavy Duty Vehicles", SAE Paper No. 760361, 1976.

51. Dodds, C., "The Laboratory Simulation of Vehicle Service Stress", Trans. ASME, Journal of Engineering for Industry, May 1974, pp. 391-398.

52. Thompson, A., "Optimum Damping in a Randomly Excited Non-Linear Suspension", Proceedings of the Institution of Mechanical Engineers, Vol. 184, No. 8, 1969-1970, pp. 169-183.

53. Dahlberg, T., "Parametric Optimization of a 1-DOF Vehicle Travelling on a Randomly Profiled Road", Journal of Sound and Vibration, Vol. 55, No. 2, 1977, pp. 245-253.

54. Dahlberg, T., "Comparison of Ride Comfort Criteria for Computer Optimization of Vehicles Travelling on Randomly Profiled Roads", Vehicle System Dynamics, Vol. 9, 1980, pp. 291-307.

55. Bender, E., "Optimum Linear Preview Control with Application to Vehicle Suspension", Trans. ASME, Journal of Basic Engineering, June 1968, pp. 213-221.

56. Karnopp, D., "Are Active Suspensions Really Necessary?", ASME Paper No. 78-WA-12, Presented at the ASME Winter Annual Meeting, San Francisco, Calif., December 10-15, 1978.

57. Bender, E., "Some Fundamental Limitations of Active and Passive Vehicle-Suspension Systems", Trans. SAE, Vol. 77, No. 680750, 1968.

58. Sutton, H., "The Potential for Active Suspension Systems", Automotive Engineer, April/May, 1979.

59. Hedrick, J. and Wormley, D., "Active Suspensions for Ground Transport Vehicles-A State of the Art Review", Proceedings from the ASME Winter Annual Meeting, AMD Vol. 15, November 30-December 5, 1975, pp. 21-39.

60. Hadekal, R., "Shock Absorber Calculations", Aircraft Engineer, Vol. 19, No. 7, 1940, pp. 29-32.

61. Wahi, M., "Oil Compressibility and Polytropic Air Compression Analysis for Oleopneumatic Shock Struts", Journal of Aircraft, Vol. 13, No. 7, July 1976, pp. 527-530.

62. Wahi, M., "Oleopneumatic Shock Strut Dynamic Analysis and Its Real-Time Simulation", Journal of Aircraft, Vol. 13, No. 4, 1976, pp. 303-308.

63. Venkatesan, C. and Krishnan, R., "Dual-Phase Damping in a Landing Gear at Touch-Down", Journal of Aircraft, Vol. 12, No. 10, October 1975, pp. 847-849.

64. Venkatesan, C., "Comparison of Linear and Nonlinear Dampers for Landing Gears", Journal of Aircraft, Vol. 15, No. 10, October 1978, pp. 696-698.

65. Venkatesan, C. and Nagaraj, V., "Optimization of Aircraft Undercarriages", ASME Paper No. 79-DET-89, Presented at the ASME Design Engineering Technical Conference, St. Louis, MO., September 10-12, 1979.

66. Walls, J., Houbolt, J. and Press, H., "Some Measurements and Power Spectra of Runway Roughness", NACA TN 3305, 1954.

67. Thompson, W., "Measurements and Power Spectra of Runway Roughness at Airports in Countries of the North Atlantic Treaty Organization", NACA TN 4303, 1958.

68. Houbolt, J., "Runway Roughness in the Aeronautical Field", Journal of Air Transport, Division of ASCE, Vol. 87, 1961, pp. 11-31.

69. Silby, N., "An Analytical Study of Some Airplane and Landing Gear Factors on the Response to Runway Roughness with Application to Supersonic Transports", NASA TN D-1492, 1962.

70. Tung, C., Pinzun, J. and Horonjeff, R., "The Effect of Runway Uneveness on the Dynamic Response of Supersonic Transports", NACA CR-119, 1964.

71. Geraldi, T. and Lohwasser, A., "A Digital Computer Program for Aircraft Runway Roughness Studies", Shock and Vibration Bulletin, Vol. 43, No. 2, June 1973, pp. 55-63.

72. Anderson, S., "Suspension", Cycle World, Vol. 22, No. 7, July 1983, pp. 46-50, 54, 95.

73. Hunter, S., "Single-Shock Systems", Cycle, Vol. 32, No. 9, September 1981, pp. 41-43, 100.

74. Morey, C., "Twin Shocks vs. Single Shock", Dirt Rider, February 1983, pp. 71-73.

75. Wooten, R., "Passenger Car and Light Truck Shock Absorber Inspection Equipment", National Highway Traffic Safety Administration, April 1975.

76. Streeter, V., "Fluid Mechanics", McGraw-Hill, New York, 1975, pp. 239-332.

77. Faires, V., "Thermodynamics", MacMillan, New York, 1970, pp. 67-81.

78. Ray, A., "Dynamic Modelling and Simulation of a Relief Valve", Simulation, November 1978, pp. 167-172.

79. Levy, S. and Wilkinson, J., "The Component Element Method in Dynamics", McGraw-Hill, New York, 1976, pp. 180-215.

80. Ogata, K., "System Dynamics", Prentice-Hall, Englewood Cliffs, 1978, pp. 8-97.

81. Cooperrider, N., Cox, J. and Hedrick, J., "Lateral Dynamics Optimization of a Conventional Railcar", Trans. ASME, Journal of Dynamic Systems, Measurement and Control, September 1975, pp. 293-299.

82. Cooperrider, N., "Railway Truck Response to Random Rail Irregularities", Trans. ASME, Journal of Engineering for Industry, August 1975, pp. 957-964.

83. Mansour, W. and Teixeira Filho, D., "Impact Dampers with Coulomb Friction", Journal of Sound and Vibration, Vol. 33, No. 3, 1974, pp. 247-265.

84. Young, R., "A Comparative Study of Shock Isolation Systems Having Linear and Non-Linear Damping", Masters Thesis, Concordia University, 1979.

85. Eberan-Eberhorst, R. and Willrich, J., "Beitrag zür Theorie des Schwingungsdämpfers, Untersuchung eines Hydro pneumatischen Stossdämpfers", Automobiltechnische Zeitschrift, Jahrg. 64, Heft 3, März 1962, Seite 81-90.

86. Bennett, A., "Introduction to Computer Simulation", West Publishing Co., St. Paul, 1974, pp. 34-62.

87. Williamson, H., "Hidden-Line Plotting Program", Comm. ACM 15, February 1972, pp. 100-103.

88. Thomson, W., "Theory of Vibrations with Applications", Prentice-Hall, Englewood Cliffs, 1972, 45-78.

89. Bandstra, J., "Comparison of Equivalent Viscous Damping and Non-Linear Damping in Discrete and Continuous Vibrating Systems", ASME Paper No. 81-DET-89, Presented at the 8th ASME Design Engineering Conference, Hartford, Conn., September 20-23, 1981.

90. Hindmarsh, A. and Byrne, "EPISODE: an effective package for the integration of systems of ordinary differential equations", UCID-30112, Rev. 1, Lawrence Livermore Laboratory, University of California, Livermore.

91. Black, S., "A Computer Simulation of the Ride Dynamics of an Off-Road Motorcycle", Masters Thesis, Cornell University, 1978.

92. Sevin, E. and Pilkey, W., "Optimum Shock and Vibration Isolation", Shock and Vibration Information Center, United States Department of Defense, No. SVM-6, 1971, pp. 5-10.

93. Dorf, R., "Modern Control Systems", Addison-Wesley, Reading, Mass., 1974, pp. 111-117.

94. Karnopp, D. and Trikha, A., "Comparative Study of Optimization Techniques for Shock and Vibration Isolation", Trans. ASME, Journal of Engineering for Industry, Vol. 91, No. 4, November 1969, pp. 1128-1132.

95. Zeidler, D. and Frohrib, D., "Optimization of a Combined Ruzicka and Snowdon Vibration Isolation System", Shock and Vibration Bulletin, No. 42, Part 4, January 1972, pp. 77-83.

96. Hassenauer, R. and Novak, G., "The Design of Cushioning Gears for Rail-Car Applications", ASME: Anthology of Rail Vehicle Dynamics, Vol. 1, 1971, pp. 78-84.

97. Townsend, P., Radkiewicz, R. and Gartner, R., "Force Optimized Recoil Control System", Shock and Vibration Bulletin, Vol. 52, No. 4, May 1982, pp. 55-71.

98. Madiwale, A., Kasten, R., Wu, S. and Radkiewicz R., "Optimal Adaptive Control of Active Recoil Mechanisms", Paper Presented at the AMSE Winter Annual Meeting, San Francisco, Calif., December 10-15, 1978.

99. Bender, E., Karnopp, D. and Paul, I., "On the Optimization of Vehicle Suspensions Using Random Process Theory", ASME Paper No. 67-Tran-12, 1967.

100. Hullender, D., Wormley, D. and Richardson, H., "Active Control of Vehicle Air Cushion Suspensions", Trans. ASME, Journal of Dynamic, Systems, Measurement, and Control, Vol. 94, No. 1, March 1972, pp. 41-49.

101. Young, J. and Wormley, D., "Optimization of Linear Vehicle Suspensions Subjected to Simultaneous Guideway and External Force Disturbances", Trans. ASME, Journal of Dynamic Systems, Measurement, and Control, Vol. 95, No. 2, June 1973, pp. 213-219.

102. Thompson, A., "Design of Active Suspensions", Proceedings of the Institute of Mechanical Engineers, Vol. 185, No. 36, 1970-1971, pp. 553-563.

103. Thompson, A., "Quadratic Performance Indices and Optimum Suspension Design", Proceedings of the Institute of Mechanical Engineers, Vol. 187, No. 9, 1973, pp. 129-139.

104. Hrovat, D. and Hubbard, M., "Optimum Vehicle Suspensions Minimizing RMS Rattlespace, Sprung-Mass Acceleration and Jerk", Trans. ASME, Journal of Dynamic Systems, Measurement and Control, Vol. 103, September 1981, pp. 228-236.

105. Sevin, E. and Pilkey, W., "Optimum Shock and Vibration Isolation", Shock and Vibration Information Center, United States Department of Defense, No. SVM-6, 1971, pp. 73-103.

106. Mayne, R. and Ragsdell, K., "Progress in Engineering Optimization", Collection of Papers Presented at the ASME Design Engineering Technical Conferences, Hartford, Conn., September 20-23, 1981.

107. Fox, R., "Optimization Methods for Engineering Design", Addison-Wesley, Reading, Mass., 1971.

108. Sankar, S. and Hargreaves, D., "Hybrid Computer Optimization of a Class of Impact Absorbers", Simulation, July 1979, pp. 11-18.

109. Dahlberg, T., "Optimization Criteria for Vehicles Travelling on a Randomly Profiled Road-a Survey", Vehicle System Dynamics, Vol. 8, 1979, pp. 239-252.

110. Haug, E., Arora, J. and Feng, T., "Sensitivity Analysis and Optimization of Structures for Dynamic Response", Trans. ASME, Journal of Mechanical Design, Vol. 100, April 1978, pp. 311-317.

111. Hedrick, J., Billington, G. and Dreesbach, D., "Analysis, Design and Optimization of High Speed Vehicle Suspensions Using State Variable Techniques", Trans. ASME, Journal of Dynamic Systems, Measurement, and Control, June 1974, pp. 193-203.

112: Pitts, G., "Techniques in Engineering Design", John Wiley and Sons, New York, 1973, pp. 101-141.

113. Middendorf, W., "Engineering Design", Allyn and Bacon, Boston, 1971, pp. 184-215.

114. Avriel, M., Rijckaert, M. and Wilde, D., "Optimization and Design", Prentice-Hall, Englewood Cliffs, 1973, pp. 119-143.

115. Mischke, C., "An Introduction to Computer-Aided Design", Prentice-Hall, Englewood Cliffs, 1968, pp. 55-160.

116. Siddall, J., "OPTISEP Designers Optimization Subroutines", McMaster University, 1971.

117. Himmelblau, D., "Applied Nonlinear Programming", McGraw-Hill, New York, 1972, pp. 142-145.

118. Crandall, S. and Mark, W., "Random Vibration in Mechanical Systems", Academic Press, New York, 1973, pp. 1-54.

119. Virchis, V. and Robson, J., "The Response of an Accelerating Vehicle to Random Road Undulation", Journal of Sound and Vibration, Vol. 18, No. 3, 1971, pp. 423-427.

120. Bracewell, R., "The Fourier Transform and its Applications", McGraw-Hill Kogakusha, Tokyo, 1978, pp. 356-384.

121. Van Deusen, B., "A Statistical Technique for the Dynamic Analysis of Vehicles Traversing Rough Yielding and Non-Yielding Surfaces", NASA-CR-659, 1967.

122. Wambold, J., Park, W. and Vashlishan, R., "A New Random Data Description and Its Use in Transferring Road Roughness to Vehicle Response", Trans. ASME, Journal of Engineering for Industry, May 1974, pp. 676-681.

123. Stikeleather, L., "Review of Ride Vibration Standards and Tolerance Criteria", SAE Paper No. 760413, Presented at the SAE Earthmoving Industry Conference, April 26-28, 1976.

124. Hedrick, J. and Arsian, A., "Nonlinear Analysis of Rail Vehicle Forced Lateral Response and Stability", Trans. ASME, Journal of Dynamic Systems, Measurement and Control, Vol. 101, Sept. 1979, pp. 230-237.

125. Cooperrider, N., "Secondary Suspension Requirements for Tracked Vehicles", High Speed Ground Transportation Journal, Vol. 3, No. 2, May 1969, pp. 255-267.

126. Sankar, S., "Field Instrumentation Package for the Off-Road Motorcycle", Concordia University Internal Report (PRAI/NSERC), Summer 1982.

127. Sankar, T.S., "Random Vibrations", Glass Notes for the ENGR N733 Course, Concordia University, Summer 1981.

128. Roberts, J., "Response of Nonlinear Mechanical Systems to Random Excitation Part I: Markov Methods", Shock and Vibration Digest, Vol. 13, No. 4, April 1981, pp. 17-28.

129. Papoulis, A., "Probability, Random Variables and Stochastic Processes", McGraw-Hill, New York, 1965, pp. 515-553.

130. Fuller, A., "Analysis of Nonlinear Stochastic Systems by Means of the Fokker-Planck Equation", International Journal of Control, Vol. 9, No. 6, June 1969, pp. 603-655.

131. Wang, M. and Uhlenbeck, G., "On the Theory of Brownian Motion II", Review of Modern Physics, Vol. 17, April-July 1945, pp. 323-342.

132. Caughey, T., "Derivation and Application of the Fokker-Planck Equation to Discrete Nonlinear Dynamic Systems Subjected to White Random Excitation", Journal of the Acoustical Society of America, Vol. 35, No. 11, 1963, pp. 1683-1692.

133. Kirk, C., "Random Vibration with Nonlinear Damping", Aeronautic Journal, Vol. 77, 1973, pp. 563-569.

134. Lutes, L., "Approximate Technique for Treating Random Vibration of Hysteretic Systems", Journal of the Acoustical Society of America, Vol. 48, 1970, pp. 299-306.

135. Crandall, S., "Perturbation Techniques for Random Vibration of Nonlinear Systems", Journal of the Acoustical Society of America, Vol. 35, No. 11, November 1963, pp. 1700-1705.

136. Crandall, S., Khabbaz, G. and Manning, J., "Random Vibration of an Oscillator with Nonlinear Damping", Journal of the Acoustical Society of America, Vol. 36, No. 7, July 1964, pp. 1330-1334.

137. Khabbaz, G., "Power Spectral Density of the Response of a Nonlinear System to Random Excitation", Journal of the Acoustical Society of America, Vol. 38, No. 5, November 1965, pp. 847-850.

138. Manning, J., "Response Spectra for Nonlinear Oscillators", Trans. ASME, Journal of Engineering for Industry, Vol. 97, 1975, pp. 1223-1226.

139. Tung, C., "The Effects of Runway Roughness on the Dynamic Response of Airplanes", Journal of Sound and Vibration, Vol. 5, No. 1, 1967, pp. 164-172.

140. Booton, R., "Non-linear Control Systems with Random Inputs", IRE Trans. Circuit Theory, CT-1, March 1954, pp. 9-18.

141. Caughey, T., "Equivalent Linearization Techniques", Journal of the Acoustical Society of America, Vol. 35, No. 11, November 1963, pp. 1706-1711.

142. Iwan, W. and Patula, E., "The Merit of Different Error Minimization Criteria in Approximate Analysis", Trans. ASME, Journal of Applied Mechanics, Vol. 39, 1972, pp. 257-262.

143. Atalik, T. and Utku, S., "Stochastic Linearization of Multi-Degree of Freedom Nonlinear Systems", International Journal of Earthquake Engineering Structural Dynamics, Vol. 4, 1976, pp. 411-420.

144. Lyon, R., "Equivalent Linearization of the Hard-Spring Oscillator", Journal of the Acoustical Society of America, Vol. 32, 1960, pp. 1161-1162.

145. Iwan, W. and Yang, I., "Application of Statistical Linearization Techniques to Non-linear Multi-Degree-of-Freedom Systems", Trans. ASME, Journal of Applied Mechanics, Vol. 39, No. 2, June 1972, pp. 545-550.

146. Smith, P., "Response of Nonlinear Structures to Random Excitation", Journal of the Acoustical Society of America, Vol. 34, 1962, pp. 827-835.

147. Martins, H., "Equivalent Stochastic Linearization of Mechanical Vibration Systems with One Degree of Freedom", Maschinenbautechnik, Vol. 21, No. 1, January 1972, pp. 27-30.

148. Caughey, T., "Random Excitation of a System with Bilinear Hysteresis", Trans. ASME, Journal of Applied Mechanics, Vol. 27, 1960, pp. 649-652.

149. Wen, Y., "Equivalent Linearization for Hysteric Systems under Random Excitation", Trans. ASME, Journal of Applied Mechanics, Vol. 47, No. 1, March 1980, pp. 150-154.

150. Iwan, W. and Lutes, L., "Response of the Bilinear Hysteretic System to Stationary Random Excitation", Journal of the Acoustical Society of America, Vol. 43, 1968, pp. 545-552.

151. Roberts, J., "First Passage Time for Oscillators with Non-linear Damping", Trans. ASME, Journal of Applied Mechanics, Vol. 45, No. 1, 1978, pp. 175-180.

152. Franklin, J., "Numerical Simulation of Stationary and Non-Stationary Gaussian Random Processes", SIAM Journal of Numerical Analysis, Vol. 7, 1965, pp. 68-75.

153. Shinozuka, M. and Jan, C., "Digital Simulation of Random Processes and Its Applications", Journal of Sound and Vibration, Vol. 25, 1972, pp. 111-128.

154. Hudspeth, R. and Borgman, L., "Efficient FFT Simulation of Digital Time Sequences", ASCE Journal of Engineering Mechanics Division, Vol. 105, April 1979, pp. 223-236.

155. Iwan, W. and Yang, I., "Statistical Linearization for Nonlinear Structures", ASCE Journal of Engineering Mechanics Division, Vol. 97, December 1971, pp. 1609-1623.

156. Roberts, J., "Stationary Response of Oscillators with Non-linear Damping to Random Excitation", Journal of Sound and Vibration, Vol. 50, 1976, pp. 145-156.

157. Roberts, J., "The Response of an Oscillator with Bilinear Hysteresis to Stationary Random Excitation", Trans. ASME, Journal of Applied Mechanics, Vol. 45, 1978, pp. 923-928.

158. Karnopp, D., Crosby, M. and Harwood, R., "Vibration Control Using Semi-Active Force Generators", Trans. ASME, Journal of Engineering for Industry, Vol. 96, May 1974, pp. 619-626.

159. Dahlberg, T., "An Optimized Speed-Controlled Suspension of a 2-DOF Vehicle Travelling on a Randomly Profiled Road", Journal of Sound and Vibration, Vol. 62, No. 4, 1979, pp. 541-546.

160. Wolkovitch, J., "Techniques for Optimizing the Response of Mechanical Systems to Shock and Vibration", Trans. SAE, Paper No. 680749, 1968.

161. Sevin, E. and Pilkey, W., "Optimization of Shock Isolation Systems", Trans. SAE, Paper No. 680749, 1968.

162. van Vliet, M. and Sankar, S., "Computer-Aided Analysis and Experimental Verification of a Motorcycle Suspension", Trans. ASME, Journal of Vibration, Acoustics, Stress and Reliability in Design, Vol. 105, No. 1, January 1983, pp. 120-132.

163. van Vliet, M., Sankar, S. and Bapat, C., "Frequency and Time Domain Analysis of Off-Road Motorcycle Suspension", Shock and Vibration Bulletin, Vol. 53, No. 3, May 1983, pp. 35-49.

164. van Vliet, M. and Sankar, S., "Optimal Design of an Off-Road Motorcycle Suspension", Paper 83-DET-77, Presented at the ASME Design and Production Engineering Technical Conference, Dearborn, September 11-14, 1983 and Accepted for Publication in the Journal of Vibration, Acoustics, Stress and Reliability in Design.

165. Sankar, S. and van Vliet, M., "Computer-Aided Optimal Design of a Motorcycle Suspension", Paper CAll to be Presented at the Sixth IFToMM Congress, Theory of Machines and Mechanisms, New Delhi, India, December 15-20, 1983.

166. Judek, T., "Computer-Aided Engineering Concepts in the Design and Analysis of an Off-Road Motorcycle Suspension and Frame", Masters Thesis, Concordia University, August 1983.

167. Cooperrider, N. and Law, E., "A Survey of Rail Vehicle Testing for Validation of Theoretical Dynamic Analyses", Trans. ASME, Journal of Dynamic Systems, Measurement, and Control, Vol. 100, No. 12, December 1978, pp. 238-251.

APPENDIX I

SUPPLEMENTARY INFORMATION ON THE ANALOG COMPUTER SIMULATION

TABLE I.1: Scaling Factors

Problem Variable	Scaled Computer Variable
z	z / 0.5
$\dot{z}$	$\dot{z}$ / 15.7
$\dot{z}^2$	$\dot{z}^2$ / 246.
Δp	Δp / 300.
$\sqrt{\Delta p}$	$\sqrt{\Delta p}$ / 17.4
u_3	u_3 / 0.5
$\dot{u}_3$	$\dot{u}_3$ / 600.
$\ddot{u}_3$	$\ddot{u}_3$ / (1.6×10^6)
u_4	u_4 / 0.5
$\dot{u}_4$	$\dot{u}_4$ / 470.
$\ddot{u}_4$	$\ddot{u}_4$ / (1.41×10^6)
F_k	F_k / 30.
$F - F_k$	$(F - F_k)$ / 500.
F	F / 530.
Q_{max}	Q_{max} / 50.

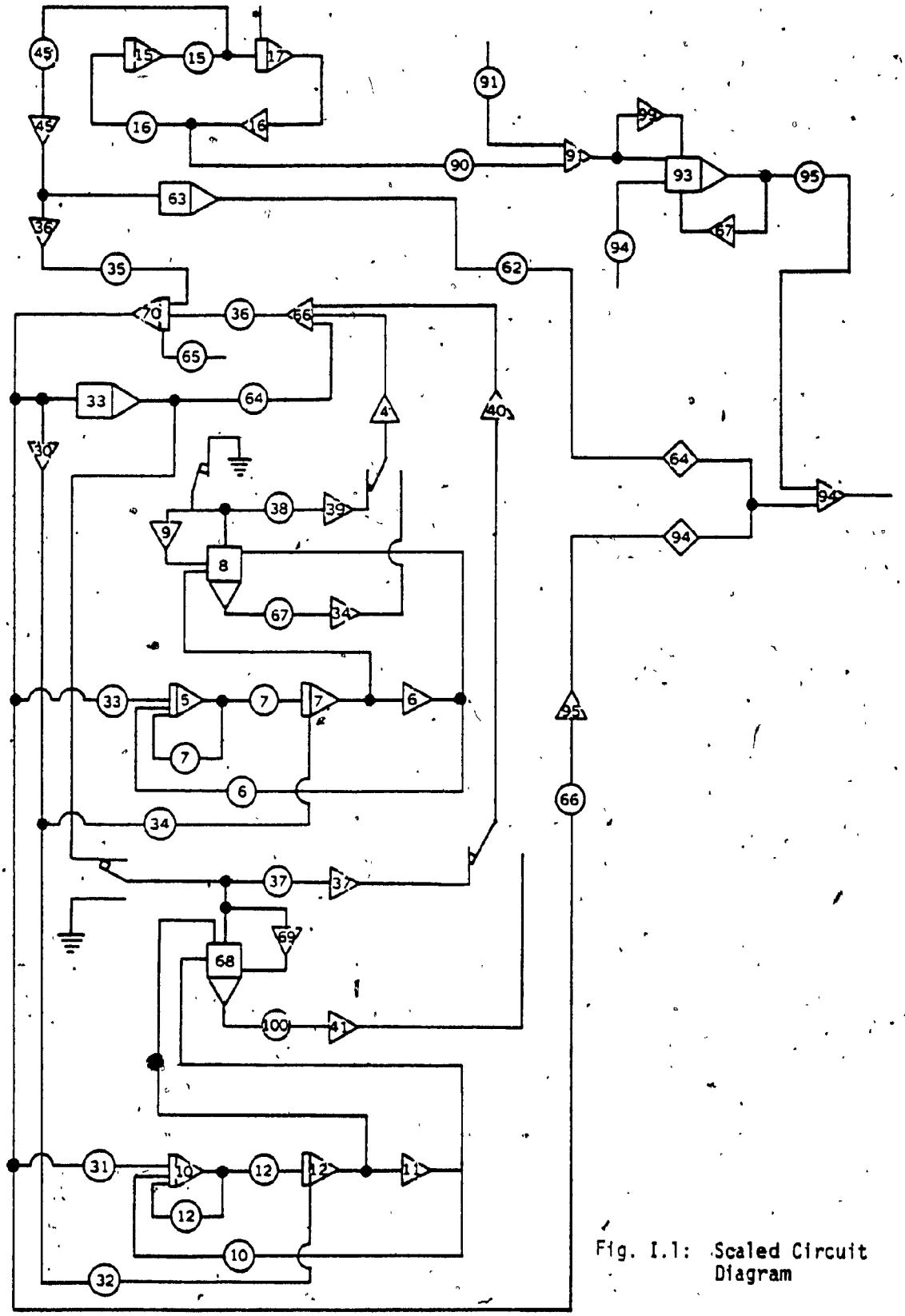

Fig. I.1: Scaled Circuit Diagram

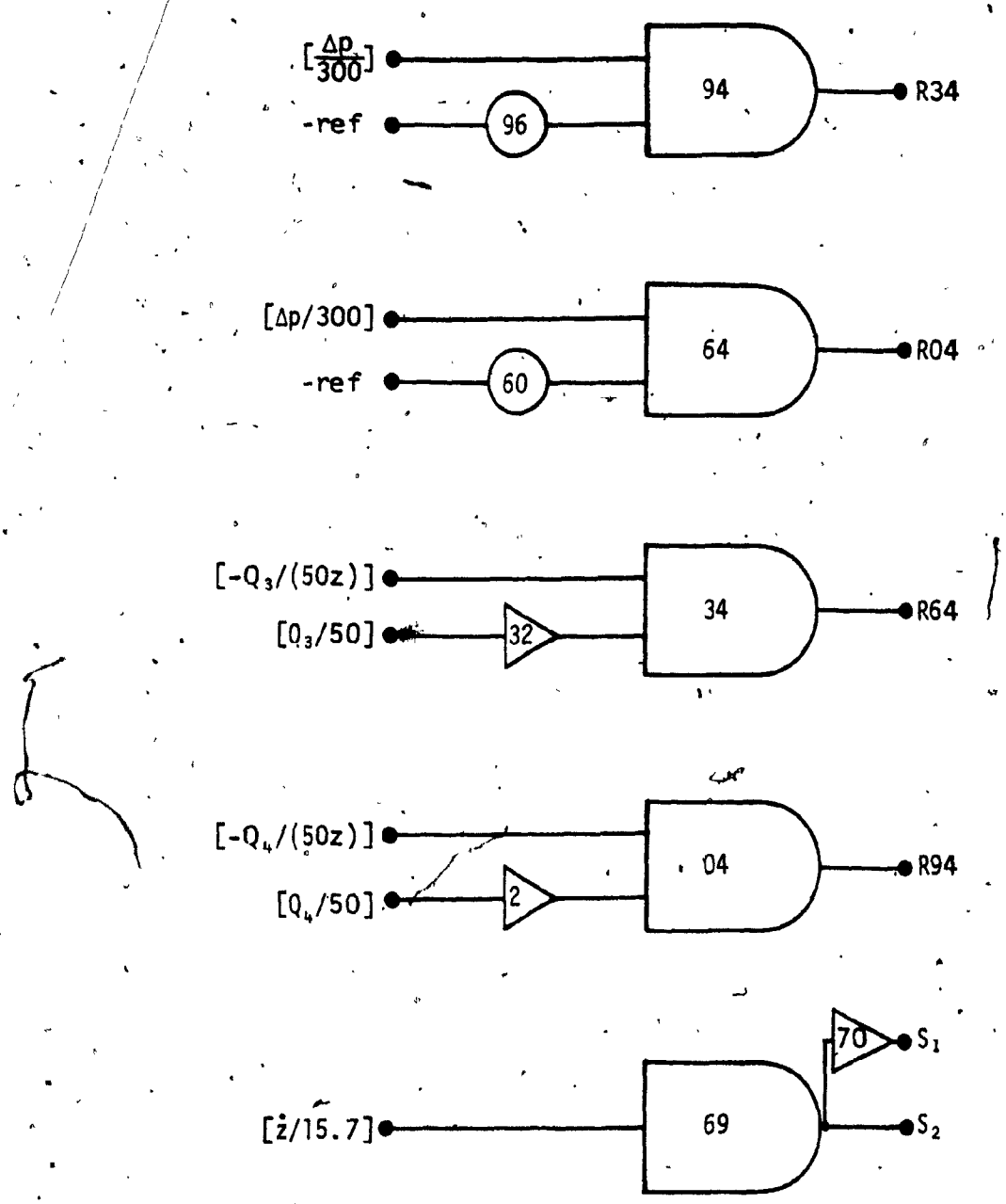

Fig. I.2: Scaled Circuit Diagram (Relays)

TABLE I.2: Potentiometer and Voltage Limiter Settings

POTENTIOMETER	COEFFICIENT	SETTING
01	Static Check	1.0000
02	Static Check	.6000
03	Static Check	.8512
05	Static Check	.5003
06	$k_3/12000\ \beta m$	.1458
10	$.5\ k_4/4700\ \beta m$	.0716
07	$12.0/\beta$	.1200
12	$94./\beta$	.9400
15	$2\pi f/\beta$	.3141
16	$2\pi f/\beta$	.3141
31	$3A/470\ \beta m$	.6492
32	$300A/k_4\ \beta$	.4530
33	$A/200\ \beta m$	.5085
34	$300A/k_3\ \beta$	.1744
35	A/β	.4562
36	$1/\beta$	1.0000
37	.4230	.4230
38	.5340	.5340
45	β Amp/157	.3185
62	.9484	.9484
64	.9810	.9810
65	$p_0/300$	.0020
60	$p_{4min}/300$	.0833
66	A300/582	.7490
67	0.1474	0.1474
90	.5/7.139	.0700
91	(V/A-1)/7.139	.9300
94	.4000	.4000
95	.6952	.6952
96	$p_{3min}/300$	.3433

.../

TABLE-I.2 (cont'd)

POTENTIOMETER	COEFFICIENT	SETTING
100	.4232	.4232
VOLTAGE		
01		+.400 -.0
71		+.500 -.0

TABLE I.3: Static Test Data

AMP NO.	FEEDBACK	OUTPUT VARIABLE	CALCULATED OUTPUT	MEASURED OUTPUT
02			.2437	.2432
04			.0681	.0681
05	$\int$	$[-\dot{u}_3/600$	-.5000	-.5002
06	Σ	$-u_3/.5$	-.8000	-.8000
07	$\int$	$u_3/.5$	.8	.8000
08	x	$[\sqrt{\Delta p}/17.4][u_3/.5]$	.4592	.4618
09	Σ	$-\sqrt{\Delta p}/17.4$	-.5740	-.5764
10	$\int$	$-\dot{u}_4/470$	.8510	.8528
11	Σ	$-u_4/.5$	.4	.4000
12	$\int$	$u_4/.5$	-.4	-.4000
15	$\int$	$-\sin(\omega t)$	.637	.6369
16	Σ	$\cos(\omega t)$	.6	-.6000
17	$\int$	$-\cos(\omega t)$	-.6	-.6000
33	$\sqrt{\ }$	$\sqrt{\Delta p}/17.4$	.574	.5767
34	Σ	$[\Delta p/300$	.0702	.0681
70	$\int$	$\Delta p/300$	.3333	.3333
36	Σ	$[\dot{z}/15.7]$	.6369	.6368
37	Σ	$\sqrt{\Delta p}/17.4$	.2429	.2436
39	Σ	$\sqrt{\Delta p}/17.4$	.3066	.3078
45	Σ	$\dot{z}/15.7$	.6369	.6367
63	$(\ )^2$	$\dot{z}^2/246$	.4065	.4056
66	Σ	$Q/50$	.6630	.6633
67	Σ		.9259	.9254
68	x	$[\sqrt{\Delta p}/17.4][u_4/.5]$	.2296	.2262
69	Σ	$-\sqrt{\Delta p}/17.4$	.5740	.5649
32	Σ	$Q_3/50$	.3079	.3080
40	Σ		.0479	.0485
41	Σ		.0479	.0485
91	Σ		.9715	.9720
93	$\div$		.9255	.9259

.../

TABLE I.3 (cont'd)

AMP NO.	FEEDBACK	OUTPUT VARIABLE	CALCULATED OUTPUT	MEASURED OUTPUT
94	Σ		.5600	.5580
99	Σ		.9718	.9720
COMPAR-ATERS				
34		Q/50	.0702(0)	0
04		Q/50	.0485(0)	0
64		Δp/300	.0486(1)	1
94		Δp/300	.0 (0)	0

APPENDIX II

LISTING OF THE COMPUTER PROGRAMS FOR OPTIMIZATION IN THE FREQUENCY AND TIME DOMAINS

```
      FREQUENCY DOMAIN OPTIMIZATION

      THIS PROGRAM OPTIMIZES THE FREQUENCY DOMAIN PERFORMANCE OF THE
      MOTORCYCLE SUSPENSION.

      PROGRAM OPTF
      DIMENSION RMAX(5),RMIN(5),XSTRT(5),X(5),PHI(6),PSI(1),WORK1(5)
      DIMENSION WORK2(5),WORK3(5),WORK4(5),XPP(16)
      DIMENSION FREQ(16)
      COMMON/VIS/K
      DATA N,IPRINT,IDATA,NCONS,F,MAXM,G,NEQUS,NSHOT,NTEST/5,1,1,5,
     10.1,300,0.01,0,3,10/
      OPEN(20,FILE ='OPTF.DAT',STATUS='NEW')
      K=1
      DO 1 I=1,5
      RMAX(I)=1.5
      RMIN(I)=.5
    1 XSTRT(I)=1.
      CALL SEEK1(N,RMAX,RMIN,NCONS,NEQUS,F,G,XSTRT,NSHOT,NTEST,MAXM,
     2IPRINT,IDATA,X,U,PHI,PSI,WORK1,WORK2,WORK3,WORK4)
      CALL IPERF(FREQ,XPP,X,XXMAX)
      WRITE(20,*) FREQ,X
      CALL ANSWER(U,X,PHI,PSI,N,NCONS,NEQUS)
      STOP
      END

      ...INEQUALITY CONSTRAINTS...

      SUBROUTINE CONST(X,NCONS,PHI)
      DIMENSION X(1),PHI(1)
      COMMON/DATA/XMMAX
      DO 3 I=1,4
    3 PHI(I)=X(I)
      PHI(5)=X(5)-.872
      RETURN
      END

      ...EQUALITY CONSTRAINTS...

      SUBROUTINE EQUAL(X,PSI,NEQUS)
      DIMENSION X(1),PSI(1)
      DO 2 I=1,NEQUS
    2 PSI(I)=X(I+1)-1.
      RETURN
      END

      ...CALCULATION OF THE PERFORMANCE INDEX...

      SUBROUTINE UREAL(X,U)
      DIMENSION X(5),XPP(16)
      REAL IFREQ(16)
      COMMON/DATA/XMMAX
      COMMON/VIS/K
      CALL IPERF(IFREQ,XPP,X,XXMAX)
      IF(K.EQ.1)GO TO 4
      GO TO 5
    4 WRITE(20,*)IFREQ,X
      K=5
    5 XMMAX=XXMAX
      FI=0.
      DO 3 J=1,15
    3 FI=(IFREQ(J)+IFREQ(J+1))*.1/2.+FI
      U=FI
      RETURN
```

```
      END
      SUBROUTINE IPERF(IFREQ,XPP,XOPT,XXMAX)
      DIMENSION FREQ(2),YO(2),TR(2),XPP(16),XOPT(5),COPT(5)
      REAL M,K,MRTA,VO,AC,XSS,IFREQ(16)
      COMMON /EPCOM9/HUSED,NQUSED,NSTEP,NFE,NJE
      COMMON /INDATA/M,K,B,AR,AS,ASACT,FRIC,FCOUL,MRTA,VO,AC,DELTAV
     1,YIN,YDOTIN,AMP,FINTEQ,BOR,PA,COPT,BCONE
      XXMAX=0.
      DO 333 I=1,5
  333 COPT(I)=XOPT(I)
      DO 61 IMC=1,16
      XPP(IMC)=.4+.1*IMC

     ...EPISODE ROUTINE PARAMETERS...

      OUT3=0.
      AMP=XPP(IMC)/24.
      FG=0.
      DO 112 KK=1,2
      K=12.*11.8
      M=93.5/32.2
      PA=2116.8
      AC=.0122
      VO=0.01525
      MRTA=38.63
      FREQ(1)=SQRT((K+(MRTA/(VO-AC*.1)-PA)*AC/.1)/M)/6.28
      FREQ(2)=8.*FREQ(1)
      FINTEQ=FREQ(KK)
      YO(1)=0.
      YO(2)=0.
      TO=0.
      X1=0.
      N=2
      HO=.1
      EPS=.01
      TOUT=1./(10.*FREQ(KK))
      JK=1
      IERROR=1
      MF=10
      INDEX=1
      AMAX=0.
      XMAX=0.
      AMIN=0.

      ...PHYSICAL PARAMETERS...

      DIRING=.853/12.
      DISLID=1.175/12.
      DDAMP=.825/12.
      DRING=1.085/12.
      RO=1.709*1.2
      ATUBE=.7854*((1.496/12.)**2.-(1.260/12.)**2.)
      ACONE=.7854*((1.0045/12.)**2.-(.9835/12.)**2.)
      AOR=.7854*(.237/12.)**2.
      APIST=((1.260/12.)**2.-(.825/12.)**2.)*.7854
      CD=.67
      DELTAV=6.28*SQRT(K/M)/50.
      FCOUL=5.5

      ...CALCULATED PARAMETERS...

      B=(APIST**3.)*RO/(2.*CD**2.)
      AS=.7854*(DISLID**2.-DRING**2.)
      BOR=(ATUBE**3.)*RO/(2.*(CD*AOR)**2.)
      BCONE=BOR*(AOR/ACONE)**2.
```

```
      AR=.7854*(DIRING**2.-DDAMP**2.)
      NN=2

      ...EPISODE DIF. EQN. SOLVER...

10    Y2DOT=-AMP*((FINTEQ*6.28)**2.)
      IF(ABS(Y2DOT).LE.COPT(4)*FCOUL/M)GO TO 54
      CALL EDRIV(NN,TO,HO,YO,TOUT,EPS,IERROR,MF,INDEX)
      YY=ABS(YO(2)-YDOTIN)
      IF(INDEX.EQ.0)GO TO 65
      PRINT*, INDEX
      GO TO 60
65    CONTINUE
      XOUT=TOUT
      JK=JK+1
      OUT3=ABS(YO(2))
       OUT33=ABS(-(B/(M*(ASACT+AR)**2.))*(YO(2)-YDOTIN)
      2*ABS(YO(2)-YDOTIN)-K*(YO(1)-YIN)/M-FRIC/M
      3-MRTA/(M*(VO-AC*(YO(1)-YIN)))+MRTA/(VO*M))
40    TOUT=TOUT+1./(10.*FREQ(KK))
      IF(TOUT.LE.10.)GO TO 10
      IF(YY.GE.XMAX)XMAX=YY
      IF(OUT3.GE.AMAX)AMAX=OUT3
      IF(TOUT.LE.(10.+3./FREQ(KK)))GO TO 10
      GO TO 60
54    YO(1)=AMP*SIN(FINTEQ*6.28*TOUT)
      YO(2)=AMP*FINTEQ*6.28*COS(FINTEQ*6.28*TOUT)
      YY=0.
      GO TO 65
60    CONTINUE
      TR(KK)=AMAX/(AMP*(FREQ(KK)*6.28))
112   CONTINUE
      XM=XPP(IMC)*(TR(1))*12.
      IF(XM.GT.XXMAX)XXMAX=XM
      D=1.
      IFREQ(IMC)=TR(1)+D*100.*(TR(2))
61    CONTINUE
55    CONTINUE
      RETURN
      END

      ...JACOBIAN (IF REQUIRED)

      SUBROUTINE PEDERV(N,T,Y,PD,NO)
      RETURN
      END

      ...DIFFERENTIAL EQUATION...

      SUBROUTINE DIFFUN(N,T,Y,YDOT)
      COMMON/INDATA/M,K,B,AR,AS,ASACT,FRIC,FCOUL,MRTA,VO,AC,DELTAV
     3,YIN,YDOTIN,AMP,FINTEQ,BOR,PA,COPT,BCONE
      DIMENSION Y(N),YDOT(N),COPT(5)
      REAL M,K,MRTA
      YIN=AMP*SIN(FINTEQ*6.28*T)
      YDOTIN=AMP*FINTEQ*6.28*COS(FINTEQ*6.28*T)
      BBCONE=BCONE
      IF(ABS(Y(1)-YIN).LT..70)BBCONE=0.
      ASACT=AS
      IF((Y(2)-YDOTIN).LE.0.)ASACT=0.
      IF(ABS(Y(2)-YDOTIN).LE.DELTAV)GO TO 35
      FRIC=FCOUL*(Y(2)-YDOTIN)/(ABS(Y(2)-YDOTIN))
      GO TO 45
35    FRIC=FCOUL*(Y(2)-YDOTIN)/DELTAV
```

```
45   CONTINUE
     YDOT(1)=Y(2)
     YDOT(2)=-(B/(M*(ASACT+AR)**2.)+BOR/M)*COPT(1)*(Y(2)-YDOTIN)
    3*ABS(Y(2)-YDOTIN) -K*COPT(3)*(Y(1)-YIN)/M-COPT(4)*FRIC/M
    4-((MRTA/((VO*COPT(5)-AC*(Y(1)-YIN))-PA)-(MRTA/(VO*COPT(5)
    5)-PA))*AC/M-COPT(2)*(BBCONE/M)*(Y(2)-YDOTIN)*ABS(Y(2)-
    6YDOTIN)
     RETURN
     END
```

```
C
C     TIME DOMAIN OPTIMIZATION
C
C     THIS PROGRAM OPTIMIZES THE TIME DOMAIN PERFORMANCE OF THE
C     MOTORCYCLE SUSPENSION.
C
      PROGRAM OPTT
      DIMENSION RMAX(5),RMIN(5),XSTRT(5),X(5),PHI(7),PSI(1),WORK1(5)
      DIMENSION WORK2(5),WORK3(5),WORK4(5)
      DIMENSION THERIT(26),XMAX(26)
      REAL IT(26)
      COMMON/VIS/K
      OPEN(21,FILE='OPT4.DAT',STATUS='NEW')
      DATA N,IPRINT,IDATA,NCONS,F,MAXM,G,NEQUS,NSHOT,NTEST/5,1,1,6,
     10.01,500,0.01,0,3,10/
      K=1
      DO 1 I=1,5
      RMAX(I)=1.5
      RMIN(I)=0.5
    1 XSTRT(I)=1.
      CALL SEEK1(N,RMAX,RMIN,NCONS,NEQUS,F,G,XSTRT,NSHOT,NTEST,MAXM,
     2IPRINT,IDATA,X,U,PHI,PSI,WORK1,WORK2,WORK3,WORK4)
      CALL ANSWER(U,X,PHI,PSI,N,NCONS,NEQUS)
      CALL IPER(IT,XMAX,THERIT,X,XXMAX)
      WRITE(21,*)THERIT,X
      STOP
      END
C
C       ...INEQUALITY CONSTRAINTS...
C
        SUBROUTINE CONST(X,NCONS,PHI)
        DIMENSION X(1),PHI(1)
        COMMON/DATA/XMMAX
        DO 3 I=1,4
    3   PHI(I)=X(I)
        PHI(5)=1.09-XMMAX
        PHI(6)=X(5)-.872
        RETURN
        END
C
C       ...EQUALITY CONSTRAINTS...
C
        SUBROUTINE EQUAL(X,PSI,NEQUS)
        DIMENSION X(1),PSI(1)
        DO 2 I=1,NEQUS
    2   PSI(I)=X(I)-1.
        RETURN
        END
C
C       ...OBJECTIVE FUNCTION...
C
        SUBROUTINE UREAL(X,U)
        DIMENSION X(1)
        DIMENSION XMAX(26),THERIT(26)
        COMMON/DATA/XMMAX
        COMMON/VIS/K
        REAL IT(26)
        CALL IPER(IT,XMAX,THERIT,X,XXMAX)
        IF(K.EQ.1)GO TO 4
        GO TO 5
    4   WRITE(21,*)THERIT,X
        K=5
    5   XMMAX=XXMAX
        FI=0.
        FTI=0.
```

```
      DO 3 J=1,25
      FI=(IT(J)+IT(J+1))*.2/2.+FI
3     FTI=FTI+(THERIT(J)+THERIT(J+1))*.2/2.
      U=500.-FTI
      RETURN
      END
C
C     ...CALCULATION OF THE PERFORMANCE INDEX...
C
      SUBROUTINE IPER(IT,XMAX,THERIT,XOPT,XXMAX)
      DIMENSION YO(2),XMAX(26),THERIT(26),COPT(5),XOPT(5)
      REAL M,K,MRTA,IT(26)
      COMMON /EPCOM9/NUSED,NQUSED,NSTEP,NFE,NJE
      COMMON /INDATA/M,K,B,AR,AS,ASACT,FRIC,FCOUL,MRTA,VO,AC,DELTAV
     1,BOR,P3,PA,ATUBE,BCONE,BBCONE,COPT
      DO 333 I=1,5
333   COPT(I)=XOPT(I)
      XXMAX=0.
      DO 61 IMC=1,26
C
C     ...EPISODE ROUTINE PARAMETERS...
C
      TO=0.
      X1=0.
      N=2
      HO=.1
      EPS=.1
      TOUT=0.01
      JK=1
      IERROR=1
      MF=10
      INDEX=1
C
C     ...PHYSICAL PARAMETERS...
C
      DIRING=.853/12.
      DISLID=1.175/12.
      DDAMP=.825/12.
      DRING=1.083/12.
      ACONE=.7854*((1.0045/12.)**2.-(.9835/12.)**2.)
      RO=1.709
      ATUBE=.7854*((1.496/12.)**2.-(1.260/12.)**2.)
      PA=2116.8
      AOR=.7854*(.237/12.)**2.
      APIST=((1.260/12.)**2.-(.825/12.)**2.)*.7854
      CD=.67
      M=73.5/(32.2)
      VO=0.01525
      MRTA=58.63
      AC=0.0122
      K=12.*11.8
      DELTAV=0.01*6.20*SQRT(K/M)/50.
      FCOUL=5.5
C
C     ...CALCULATED PARAMETERS...
C
      B=(APIST**3.)*RO/(2.*CD**2.)
      BOR=(ATUBE**3.)*RO/(2.*(CD*AOR)**2.)
      BCONE=BOR*(AOR/ACONE)**2.
      P3=MRTA/(AC*VO)
      AS=.7854*(DISLID**2.-DRING**2.)
      AR=.7854*(DIRING**2.-DDAMP**2.)
      ASACT=AS
      OUT1=0.
      OUT3=0.
```

```
      YO(1)=0.
      YO(2)=(IMC*.2+.8)*100./(2.54*12.)
      VFT=YO(2)**2.
      NN=2
      TO=0.
      XM=0.
      AM=0.
C
C     ...EPISODE DIF. EQN. SOLVER...
C
10    CONTINUE
      OUT1=YO(1)
      OUT3=-COPT(1)*(B/(M*(ASACT+AR)**2.)+COPT(2)*BBCONE/(M*
     4COPT(1))+BOR/M)*(YO(2))*ABS(YO(2))-K*COPT(3)*(YO(1))/M
     6-FRIC*COPT(4)/M-((MRTA/(M*(VO*COPT(5)
     5-AC*YO(1)))-PA/M)-(MRTA/(VO*COPT(5)*M)-PA/M))*AC
      CALL EDRIV(NN,TO,HO,YO,TOUT,EPS,IERROR,MF,INDEX)
      IF (INDEX.EQ.0) GO TO 40
      PRINT*, INDEX
      GO TO 60
40    TOUT=TOUT+.001
      IF(ABS(OUT3).GE.AM)AM=ABS(OUT3)
      IF(YO(1).LT.OUT1)GO TO 11
      JK=JK+1
      IF(JK.LE.500) GO TO 10
11    XM=YO(1)
60    CONTINUE
      THERIT(IMC)=50.*VFT/(1.09*AM)
      IT(IMC)=50.*VFT/(XM*AM)
      XMAX(IMC)=XM
      IF(XM.GE.XXMAX)XXMAX=XM
61    CONTINUE
      RETURN
      END
C
C     ...JACOBIAN (IF REQUIRED)
C
      SUBROUTINE PEDERV(N,T,Y,PD,NO)
      RETURN
      END
C
C     ...DIFFERENTIAL EQUATION...
C
      SUBROUTINE DIFFUN(N,T,Y,YDOT)
      COMMON/INDATA/M,K,B,AR,AS,ASACT,FRIC,FCOUL,MRTA,VO,AC,DELTAV
     5,BOR,P3,PA,ATUBE,BCONE,BBCONE,COPT
      DIMENSION Y(N),YDOT(N),COPT(5)
      REAL M,K,MRTA
      ASACT=AS
      BBCONE=BCONE
      IF(Y(1).LT..70)BBCONE=0.
      IF((Y(2)).LT.0.) ASACT=0.
      IF(ABS(Y(2)).LE.DELTAV)GO TO 35
      FRIC=FCOUL*Y(2)/ABS(Y(2))
      GO TO 45
35    FRIC=FCOUL*Y(2)/DELTAV
45    CONTINUE
      YDOT(1)=Y(2)
      YDOT(2)=-COPT(1)*(B/(M*(ASACT+AR)**2.)+COPT(2)*BBCONE/
     2(M*COPT(1))
     3+BOR/M)*(Y(2))*ABS(Y(2))-K*COPT(3)*(Y(1))/M-COPT(4)*FRIC/M
     4-((MRTA/(M*(VO*COPT(5)-AC*Y(1)))-PA/M)-(MRTA/(VO*COPT(5)*
     5M)-PA/M))*AC
      RETURN
```

END

APPENDIX III

LISTING OF THE COMPUTER PROGRAMS USED TO EVALUATE THE EQUIVALENT LINEARIZATION METHODS

```
C
C     SLEM :STATISTICALLY LINEARIZED ENERGY METHOD
C
      PROGRAM SHL50
      DIMENSION SO(40),FREQ(40),SI(40),TR1(40),E(40),
     *ZDOT(40),X(3),Z(40),DIFF(40),ZSM(40)
      REAL K,M,INC,INCK,KLAST,MRT
      DENOM(W)=((K-M*W**2.)**2.+(W*CEQ1)**2.)
      H2(W)=((M*W)**2.)**2./DENOM(W)
      OPEN(20,FILE='SM50.DAT',STATUS='OLD')
      OPEN(10,FILE='LBSPC2.DAT',STATUS='OLD')
      OPEN(21,FILE='SHL50.DAT',STATUS='NEW')
      DATA M,T,K,DELTA,FCOUL,MRT,VO,AC
     */2.90,0.7506,141.6,.05
     *,5.5,58.63,0.01525,.0122/
C
C     ...STATISTICAL LINEARIZATION PROCEDURE (DAMPING)...
C
      PA=MRT/VO
      PRINT*,'TYPE IN X(1)VEL2 X(2)SPRING X(3)FCOUL'
      READ*,X
      T=T*X(1)
      ZMAX=.9*VO/AC
      FCOUL=FCOUL*X(3)
      RK=K
      KLAST=K
      AC=AC*X(2)
      DO 50 I=1,40
      READ(20,*)F,TR1(I),ZSM(I)
50    READ(10,*)FREQ(I),SI(I),F
      PRINT*,'TYPE IN CEQ'
      READ*,CEQ1
85    E2Z=10.E20
      INC=1.
20    CONTINUE
      EL=E2Z
      E2Z=0.
      SUM=0.
      CEQ1=CEQ1-INC
      DO 60 J=1,40
      W=6.28*FREQ(J)
60    ZDOT(J)=SQRT(H2(W)*2.*SI(J))/W
      DO 70 I=1,40
      DIFF(I)=((ZDOT(I)*(ZDOT(I)/W))*(CEQ1-(8.*T
     **ZDOT(I)/(3.*3.14)+
     *4.*FCOUL/(3.14*ZDOT(I)))))**2.
70    E2Z=E2Z+DIFF(I)
      ERR=ABS(E2Z-EL)
      IF(ERR.LE.DELTA)GO TO 10
      IF(E2Z.LT.EL.AND.CEQ1.GT.0.)GO TO 20
      CEQ1=CEQ1+(21./10.)*INC
      INC=INC/10.
      E2Z=10.E20
      GO TO 20
10    CONTINUE
C
C     ...STATISTICAL LINEARIZATION (STIFFNESS)
C
      CLAST=CEQ1
      E2ZK=10.E20
      INCK=10.
      K=K-2.*INCK
80    CONTINUE
      ELK=E2ZK
      E2ZK=0.
```

```
      K=K+INCK
      DO 65 J=1,40
      W=6.28*FREQ(J)
65    Z(J)=.70711*SQRT(H2(W)*2.*SI(J))/(W**2.)
      DO 75 I=1,40
      IF((Z(I)/.70711).GT.ZMAX) Z(I)=ZMAX*.70711
75    E2ZK=E2ZK+ABS(.5*(Z(I)/.70711)**2.*(K-(RK+ABS(MRT*LOG((
     *VO+AC*(Z(I)/.70711))/VO)+MRT*LOG((VO-AC*(Z(I)/
     *.70711))/VO)))))**2.
      ERRK=ABS(E2ZK-ELK)
      IF(ERRK.LE.DELTA)GO TO 100
      PRINT*,'E2ZK,ELK=',E2ZK,ELK
      IF(E2ZK.LT.ELK.AND.K.GT.0.)GO TO 80
      K=K-(21./10.)*INCK
      INCK=INCK/10.
      E2ZK=10.E20
      GO TO 80
100   CONTINUE
      DELK=ABS(KLAST-K)/10.
      DELC=ABS(CLAST-CEQ1)/10.
      CLAST=CEQ1
      KLAST=K
      IF(DELK.LE.DELTA.AND.DELC.LE.DELTA)GO TO 110
      GO TO 85
110   CONTINUE
C
C     ...RESPONSE SPECTRA...
C
      E2D=0.
      E2=0.
      DO 30 I=1,40
      W=6.28*FREQ(I)
      AMP=SQRT(SI(I)*2.)/W**2.
      SO(I)=((K**2.+(W*CEQ1)**2.)*SI(I)/DENOM(W))
      E(I)=TR1(I)-SO(I)
      ED=ZSM(I)-Z(I)
      E2D=E2D+ABS(ED)
      E2=E2+ABS(E(I))
      WRITE(21,*)FREQ(I),SO(I),Z(I)
30    CONTINUE
      E2MD=E2D/40.
      E2M=E2/40.
      WRITE(21,*)'FREQ,SO,DISP'
      WRITE(21,*),'E2M=',E2M,'E2MD=',E2MD
      WRITE(21,*)'X(1)VEL2 X(2)SPRING X(3)FCOUL=',X
      STOP
      END
```

```
C
C     HLEM :HARMONICALLY LINEARIZED ENERGY METHOD
C
      PROGRAM HL50
      DIMENSION RMAX(3),RMIN(3),XSTRT(3),PHI(3),PCI(1),WORK1(3)
     *,WORK2(3),WORK3(3),WORK4(3),ACC(40),FREQ(40),DISP(40)
     *,SI(40),X(3),ACSM(40),ZSM(40)
      COMMON/DATA1/KK,D
      COMMON/DATA3/ACC,DISP
      COMMON/DATA4/FREQ,SI,C2
      OPEN(22,FILE='SM50.DAT',STATUS='OLD')
      OPEN(20,FILE='HL50.DAT',STATUS='NEW')
      OPEN(21,FILE='LBSPC2.DAT',STATUS='OLD')
      DATA N,IPRINT,IDATA,NCONS,F,MAXM,G,NEQUS,NSHOT,NTEST/
     *3,1,1,3,0.01,300,0.01,0,3,100/
      KK=1
      D=0.
      DO 11 I=1,40
      READ(22,*)F,ACSM(I),ZSM(I)
11    READ(21,*)FREQ(I),SI(I),F
      DO 1 I=1,3
      RMAX(I)=1.5
      RMIN(I)=0.5
1     XSTRT(I)=1.
      PRINT*,'TYPE IN X(1)VEL2  X(2)SPRING  X(3)FCOUL'
      READ*,X
      CALL EHL(X,ACC,DISP)
      ERMN=0.
      E2D=0.
      DO 2 I=1,40
      ACC2=ACC(I)**2.
      ERR=ACSM(I)-ACC2
      ERMN=ERMN+ABS(ERR/40.)
      ED=ZSM(I)-DISP(I)
      E2D=E2D+ABS(ED)
3     WRITE(20,*)FREQ(I),ACC2,DISP(I)
      E2MD=E2D/40.
      WRITE(20,*)'XVEL,XSPRNG,XFCOUL=',X
      WRITE(20,*)'ERMN,E2MD',ERMN,E2MD
      STOP
      END
C
C     ...RESPONSE ROUTINE...
C
      SUBROUTINE EHL(C,ACC,DISP)
      DIMENSION C(3),SI(40),ACC(40),FREQ(40),DISP(40),CEQ(40),E(40)
      REAL K,M,MRT
      COMMON/DATA4/FREQ,SI,C2
      DATA M,T,RK,DELTA,MRT,V0,AC/2.90,0.7506,141.6,
     *0.05,58.63,0.01525,0.0122/
      C1=1.
      FBRK=5.5
      FS=0.
      FCOUL=5.5*C(3)
      V0=0.01525
      MRT=58.63*C(2)
      PA=MRT/V0
C
C     ...LINEARIZATION...
C
      PRINT*,'TYPE IN FREQ**2.'
      READ*,LIM
      DO 40 J=LIM,LIM
      CS=0.
      C1=1.
```

```
      LF=1
      K=RK
      W=6.28*FREQ(J)
      AMP=SQRT(2.*SI(J))/W**2.
20    D=((K-M*W**2.)**2.+(W*(C1+CS))**2.)
      Z=(M*AMP*W**2.+AMP*W*CS)/SQRT(D)
      X=SQRT((K**2.+(W*C1)**2.)/D)*AMP
22    ZFRC=Z*(1.-FCOUL/(M*AMP*W**2.))
      IF(ZFRC.LE.0.)ZFRC=0.
      C2=8.*C(1)*T*W*Z/(3.*3.14)+4.*FCOUL*Z/(3.14*W*Z**2.)
      CSOLD=CS
      IF(LF.EQ.0)GO TO 15
      ERR=(C1-C2)
      ERREL=ERR/C2
      C1=ABS(C2+(ERR/2.))
      IF(C1.GE.10.E6)GO TO 15
      IF(ABS(Z).LE.DELTA/1000.) GO TO 15
      IF(D.GE.10.E11)GO TO 15
      IF(ABS(ERREL).LE.DELTA)GO TO 10
      GO TO 20
10    CONTINUE
      IF(C(2).EQ.0.)GO TO 16
      AK=K
      IF(Z.GE.1.25)GO TO 25
      K=RK-(MRT*LOG((VO+AC*Z)/VO)
     *+MRT*LOG((VO-AC*Z)/VO))/Z**2.
35    ERR2=ABS(AK-K)
      IF(ERR2.LE.DELTA*10.)GO TO 16
      GO TO 20
25    Z=1.25
      LF=0
      K=10E4
      PRINT*,'END STOP HIT'
      GO TO 22
30    ACC(J)=SQRT(SI(J))
      Z=0.
      GO TO 31
32    ACC(J)=0.
      Z=AMP*.70711
      GO TO 31
15    CONTINUE
16    CONTINUE
40    CONTINUE
      PRINT*,'C1,K=',C1,K
C
C     ...ACCELERATION AND DISPLACEMENT RESPONSE SPECTRA
C
      DO 45 J=1,40
      W=6.28*FREQ(J)
      D=((K-M*W**2.)**2.+(W*C1)**2.)
      ACC(J)=SQRT((K**2.+(W*C1)**2.)*SI(J)/D)
      DISP(J)=M*AMP*W**2./SQRT(2.*D)
31    CONTINUE
45    CONTINUE
      RETURN
      END
```

```
C
CC    DHLEM :DISCRETE-HARMONICALLY LINEARIZED ENERGY METHOD
C
      PROGRAM EHL50
      DIMENSION RMAX(3),RMIN(3),XSTRT(3),PHI(3),PSI(1),WORK1(3)
     *,WORK2(3),WORK3(3),WORK4(3),ACC(40),FREQ(40),DISP(40)
     *,SI(40),X(3),ACSM(40),ZSM(40)
      COMMON/DATA1/KK,D
      COMMON/DATA3/ACC,DISP
      COMMON/DATA4/FREQ,SI
      OPEN(22,FILE='SM50.DAT',STATUS='OLD')
      OPEN(20,FILE='EHL50.DAT',STATUS='NEW')
      OPEN(21,FILE='LBSPC2.DAT',STATUS='OLD')
      DATA N,IPRINT,IDATA,NCONS,F,MAXM,G,NEQUS,NSHOT,NTEST/
     *3,1,1,3,0.01,300,0.01,0,3,100/
      KK=1
      D=0.
      DO 11 I=1,40
      READ(22,*)F,ACSM(I),ZSM(I)
11    READ(21,*)FREQ(I),SI(I),F
      DO 1 I=1,3
      RMAX(I)=1.5
      RMIN(I)=0.5
1     XSTRT(I)=1.
      PRINT*,'TYPE IN X(1)VEL2  X(2)SPRING  X(3)FCOUL'
      READ*,X
      CALL EHL(X,ACC,DISP)
      ERMN=0.
      E2D=0.
      DO 2 I=1,40
      ACC2=ACC(I)**2.
      ERR=ACSM(I)-ACC2
      E2=ZSM(I)-DISP(I)
      E2D=E2D+ABS(E2)
      ERMN=ERMN+ABS(ERR/40.)
      PRINT*,FREQ(I),ACC2,ERR
2     WRITE(20,*)FREQ(I),ACC2,DISP(I)
      E2MD=E2D/40.
      WRITE(20,*)'XVEL,XSPRNG,XFCOUL=',X
      WRITE(20,*)'ERMN=',ERMN,'E2MD=',E2MD
      PRINT*,'ERMN=',ERMN
      STOP
      END
C
CC    ...RESPONSE ROUTINE...
C
      SUBROUTINE EHL(C,ACC,DISP)
      DIMENSION C(3),SI(40),ACC(40),FREQ(40),DISP(40),CEQ(40),E(40)
      REAL K,M,MRT
      COMMON/DATA4/FREQ,SI
      DATA M,T,RK,DELTA,MRT,VO,AC/2.90,0.7506,141.6,
     *0.05,58.63,0.01525,0.0122/
      C1=1.
      FBRK=5.5
      FS=0.
      FCOUL=5.5*C(3)
      VO=0.01525
      MRT=58.63*C(2)
      PA=MRT/VO
C
CC    ...LINEARIZATION...
C
      DO 40 J=1,40
      CS=0.
      C1=1.
```

```
      LF=1
      K=RK
      W=6.28*FREQ(J)
      AMP=SQRT(SI(J)*2.)/W**2.
   20 D=((K-M*W**2.)**2.+(W*(C1+CS))**2.)
      Z=(M*AMP*W**2.+AMP*W*CS)/SQRT(D)
      X=SQRT((K**2.+(W*C1)**2.)/D)*AMP
   22 ZFRC=Z*(1.-FCOUL/(M*AMP*W**2.))
      IF(ZFRC.LE.0.)ZFRC=0.
      C2=8.*C(1)*T*W*Z/(3.*3.14)+4.*FCOUL*Z/(3.14*W*Z**2.)
      CSOLD=CS
      IF(LF.EQ.0)GO TO 15
      ERR=(C1-C2)
      ERREL=ERR/C2
      C1=ABS(C2+(ERR/2.))
      IF(C1.GE.10.E6)GO TO 15
      IF(ABS(Z).LE.DELTA/1000.) GO TO 15
      IF(D.GE.10.E11)GO TO 15
      IF(ABS(ERREL).LE.DELTA)GO TO 10
      GO TO 20
   10 CONTINUE
      IF(C(2).EQ.0.)GO TO 16
      AK=K
      IF(Z.GE.1.25)GO TO 25
      K=RK-(MRT*LOG((VO+AC*Z)/VO)
     *+MRT*LOG((VO-AC*Z)/VO))/Z**2.
   35 ERR2=ABS(AK-K)
      IF(ERR2.LE.DELTA*10.)GO TO 16
      GO TO 20
   25 Z=1.25
      LF=0
      K=10E4
      PRINT*,'END STOP HIT'
      GO TO 22
   30 ACC(J)=SQRT(SI(J))
      Z=0.
      GO TO 31
   32 ACC(J)=0.
      Z=AMP
      GO TO 31
   15 CONTINUE
   16 CONTINUE
      ACC(J)=SQRT((K**2.+(W*C1)**2.)*SI(J)/D)
      DISP(J)=Z*.70711
   31 CONTINUE
   40 CONTINUE
      RETURN
      END
```

```
C
CC    SLFM :STATISTICALLY LINEARIZED FORCE METHOD
C
      PROGRAM SL50
      DIMENSION SO(40),FREQ(40),SI(40),TR1(40),E(40),
     *ZDOT(40),X(3),Z(40),DIFF(40),ZSM(40)
      REAL K,M,INC,INCK,KLAST,MRT
      DENOM(W)=((K-M*W**2.)**2.+(W*CEQ1)**2.)
      H2(W)=((M*W)**2.)**2./DENOM(W)
      OPEN(20,FILE='SM50.DAT',STATUS='OLD')
      OPEN(10,FILE='LDSPC2.DAT',STATUS='OLD')
      OPEN(21,FILE='SL50.DAT',STATUS='NEW')
      DATA M,T,K,DELTA,FCOUL,MRT,VO,AC
     */2.90,0.7506,141.6,.05
     *,5.5,50.63,0.01525,.0122/
C
CC    ...STATISTICAL LINEARIZATION PROCEDURE (DAMPING)...
C
      PA=MRT/VO
      PRINT*,'TYPE IN X(1)VEL2 X(2)SPRING X(3)FCOUL'
      READ*,X
      T=T*X(1)
      ZMAX=VO/AC
      FCOUL=FCOUL*X(3)
      RK=K
      KLAST=K
      AC=AC*X(2)
      DO 50 I=1,40
      READ(20,*)F,TR1(I),ZSM(I)
50    READ(10,*)FREQ(I),SI(I),F
      PRINT*,'TYPE IN CEQ'
      READ*,CEQ1
85    E2Z=10.E20
      INC=1.
20    CONTINUE
      EL=E2Z
      E2Z=0.
      SUM=0.
      CEQ1=CEQ1-INC
      DO 60 J=1,40
      W=6.28*FREQ(J)
60    ZDOT(J)=SQRT(H2(W)*2.*SI(J))/W
      DO 70 I=1,40
      DIFF(I)=ABS(((CEQ1*ZDOT(I)*0.70711
     *-(T*.5*ZDOT(I)**2.+FCOUL))**2.))
70    E2Z=E2Z+DIFF(I)
      ERR=ABS(E2Z-EL)
      IF(ERR.LE.DELTA)GO TO 10
      IF(E2Z.LT.EL.AND.CEQ1.GT.0.)GO TO 20
      CEQ1=CEQ1+(21./10.)*INC
      INC=INC/10.
      E2Z=10.E20
      GO TO 20
10    CONTINUE
C
CC    ...STATISTICAL LINEARIZATION (STIFFNESS)
C
      CLAST=CEQ1
      E2ZK=10.E20
      INCK=10.
      K=K-2.*INCK
80    CONTINUE
      ELK=E2ZK
      E2ZK=0.
      K=K+INCK
```

```
      DO 65 J=1,40
      W=6.28*FREQ(J)
65    Z(J)=.70711*SQRT(H2(W)*2.*SI(J))/(W**2.)
      DO 75 I=1,40
      IF((Z(I)/.70711).GT.ZMAX) Z(I)=ZMAX*.70711
75    E2ZK=E2ZK+(K*Z(I)-(RK*Z(I)+ABS((MRT/(V0-AC*Z(I)))
     *-(MRT/(V0+AC*Z(I))))*.5*AC))**2.
      ERRK=ABS(E2ZK-ELK)/10.
      IF(ERRK.LE.DELTA)GO TO 100
      IF(E2ZK.LT.ELK.AND.K.GT.0.)GO TO 80
      K=K-(21./10.)*INCK
      INCK=INCK/10.
      E2ZK=10.E20
      GO TO 80
100   CONTINUE
      DELK=ABS(KLAST-K)/10.
      DELC=ABS(CLAST-CEQ1)/10.
      CLAST=CEQ1
      KLAST=K
      IF(DELK.LE.DELTA.AND.DELC.LE.DELTA)GO TO 110
      GO TO 85
110   CONTINUE
C
C     ...ACCELERATION AND DISPLACEMENT RESPONSE SPECTRA...
C
      E2D=0.
      E2=0.
      DO 30 I=1,40
      W=6.28*FREQ(I)
      AMP=SQRT(SI(I)*2.)/W**2.
      SO(I)=((K**2.+(W*CEQ1)**2.)*SI(I)/DENOM(W))
      E(I)=TR1(I)-SO(I)
      ED=ZSM(I)-Z(I)
      E2D=E2D+ABS(ED)
      E2=E2+ABS(E(I))
      WRITE(21,*)FREQ(I),SO(I),Z(I)
30    CONTINUE
      E2MD=E2D/40.
      E2M=E2/40.
      WRITE(21,*)'FREQ,SO,DISP'
      WRITE(21,*),'E2M=',E2M,'E2MD=',E2MD
      WRITE(21,*)'X(1)VEL2 X(2)SPRING X(3)FCOUL=',X
      STOP
      END
```

```
C
C     HLFM :HARMONICALLY LINEARIZED FORCE METHOD
C
      PROGRAM PFL50
      DIMENSION RMAX(3),RMIN(3),XSTRT(3),PHI(3),PSI(1),WORK1(3)
     *,WORK2(3),WORK3(3),WORK4(3),ACC(40),FREQ(40),DISP(40)
     *,SI(40),X(3),ACSM(40),ZSM(40)
      COMMON/DATA1/KK,D
      COMMON/DATA3/ACC,DISP
      COMMON/DATA4/FREQ,SI,C2
      OPEN(22,FILE='SM50.DAT',STATUS='OLD')
      OPEN(20,FILE='PFL50.DAT',STATUS='NEW')
      OPEN(21,FILE='LBSPC2.DAT',STATUS='OLD')
      DATA N,IPRINT,IDATA,NCONS,F,MAXM,G,NEQUS,NSHOT,NTEST/
     *3,1,1,3,0.01,300,0.01,0,3,100/
      KK=1
      D=0.
      DO 11 I=1,40
      READ(22,*)F,ACSM(I),ZSM(I)
11    READ(21,*)FREQ(I),SI(I),F
      DO 1 I=1,3
      RMAX(I)=1.5
      RMIN(I)=0.5
1     XSTRT(I)=1.
      PRINT*,'TYPE IN X(1)VEL2  X(2)SPRING  X(3)FCOUL'
      READ*,X
      CALL EHL(X,ACC,DISP)
      ERMN=0.
      E2D=0.
      DO 2 I=1,40
      ACC2=ACC(I)**2.
      ERR=ACSM(I)-ACC2
      ERMN=ERMN+ABS(ERR/40.)
      ED=ZSM(I)-DISP(I)
      E2D=E2D+ABS(ED)
2     WRITE(20,*)FREQ(I),ACC2,DISP(I)
      E2MD=E2D/40.
      WRITE(20,*)'XVEL,XSPRNG,XFCOUL=',X
      WRITE(20,*)'ERMN,E2MD',ERMN,E2MD
      STOP
      END
C
C     ...RESPONSE ROUTINE...
C
      SUBROUTINE EHL(C,ACC,DISP)
      DIMENSION C(3),SI(40),ACC(40),FREQ(40),DISP(40),CEQ(40),E(40)
      REAL K,M,MRT
      COMMON/DATA4/FREQ,SI,C2
      DATA M,T,RK,DELTA,MRT,VO,AC/2.90,0.7506,141.6,
     *0.05,58.63,0.01525,0.0122/
      C1=1.
      FBRK=5.6
      FS=0.
4     FCOUL=5.5*C(3)
      VO=0.01525
      MRT=58.63*C(2)
      PA=MRT/VO
C
C     ...LINEARIZATION...
C
      PRINT*,'TYPE IN FREQ*2.'
      READ*,LIM
      DO 40 J=LIM,LIM
      CS=0.
```

```
      C1=1.
      LF=1
      K=RK
      W=6.28*FREQ(J)
      AMP=SQRT(2.*SI(J))/W**2.
   20 D=((K-M*W**2.)**2.+(W*(C1+CS))**2.)
      Z=(M*AMP*W**2.+AMP*W*CS)/SQRT(D)
      X=SQRT((K**2.+(W*C1)**2.)/D)*AMP
   22 ZFRC=Z*(1.-FCOUL/(M*AMP*W**2.))
      IF(ZFRC.LE.0.)ZFRC=0.
      C2=(C(1)*T*(W*Z*.70711)**2.+FCOUL)/(Z*W*.70711)
      CSOLD=CS
      IF(LF.EQ.0)GO TO 15
      ERR=(C1-C2)
      ERREL=ERR/C2
      C1=ABS(C2+(ERR/2.))
      IF(C1.GE.10.E6)GO TO 15
      IF(ABS(Z).LE.DELTA/1000.) GO TO 15
      IF(D.GE.10.E11)GO TO 15
      IF(ABS(ERREL).LE.DELTA)GO TO 10
      GO TO 20
   10 CONTINUE
      IF(C(2).EQ.0.)GO TO 16
      AK=K
      IF(Z.GE.1.25)GO TO 25
      K=RK+((MRT/(VO-AC*Z*.70711)-PA)-(MRT/(VO+AC*Z*.70711)
     *-PA))*.5*AC/(Z*.70711)
   35 ERR2=ABS(AK-K)
      IF(ERR2.LE.DELTA*10.)GO TO 16
      GO TO 20
   25 Z=1.25
      LF=0
      K=10E4
      PRINT*,'END STOP HIT'
      GO TO 22
   30 ACC(J)=SQRT(SI(J))
      Z=0.
      GO TO 31
   32 ACC(J)=0.
      Z=AMP*.70711
      GO TO 31
   15 CONTINUE
   16 CONTINUE
   40 CONTINUE
C
C     ...ACCELERATION AND DISPLACEMENT RESPONSE SPECTRA...
C
      DO 45 J=1,40
      W=6.28*FREQ(J)
      D=((K-M*W**2.)**2.+(W*C1)**2.)
      ACC(J)=SQRT((K**2.+(W*C1)**2.)*SI(J)/D)
      DISP(J)=M*AMP*W**2./SQRT(2.*D)
   31 CONTINUE
   45 CONTINUE
      RETURN
      END
```

```
C
C     DHLFM :DISCRETE-HARMONICALLY LINEARIZED FORCE METHOD
C
      PROGRAM ESL50
      DIMENSION RMAX(3),RMIN(3),XSTRT(3),PHI(3),PSI(1),WORK1(3)
     *,WORK2(3),WORK3(3),WORK4(3),ACC(40),FREQ(40),DISP(40)
     *,SI(40),X(3),ACSM(40),ZSM(40)
      COMMON/DATA1/KK,D
      COMMON/DATA3/ACC,DISP
      COMMON/DATA4/FREQ,SI
      OPEN(22,FILE='SM50.DAT',STATUS='OLD')
      OPEN(20,FILE='ESL50.DAT',STATUS='NEW')
      OPEN(21,FILE='LBSPC2.DAT',STATUS='OLD')
      DATA N,IPRINT,IDATA,NCONS,F,MAXM,G,NEQUS,NSHOT,NTEST/
     *3,1,1,3,0.01,300,0.01,0,3,100/
      KK=1
      D=0.
      DO 11 I=1,40
      READ(22,*)F,ACSM(I),ZSM(I)
11    READ(21,*)FREQ(I),SI(I),F
      DO 1 I=1,3
      RMAX(I)=1.5
      RMIN(I)=0.5
1     XSTRT(I)=1.
      PRINT*,'TYPE IN X(1)VEL2  X(2)SPRING  X(3)FCOUL'
      READ*,X
      CALL EHL(X,ACC,DISP)
      ERMN=0.
      E2D=0.
      DO 2 I=1,40
      ACC2=ACC(I)**2.
      ERR=ACSM(I)-ACC2
      ED=ZSM(I)-DISP(I)
      E2D=E2D+ABS(ED)
      ERMN=ERMN+ABS(ERR/40.)
2     WRITE(20,*)FREQ(I),ACC2,DISP(I)
      E2MD=E2D/40.
      WRITE(20,*)'XVEL,XSPRNG,XFCOUL=',X
      WRITE(20,*)'ERMN',ERMN,'E2MD=',E2MD
      STOP
      END
C
C     ...RESPONSE ROUTINE...
C
      SUBROUTINE EHL(C,ACC,DISP)
      DIMENSION C(3),SI(40),ACC(40),FREQ(40),DISP(40),CEQ(40),E(40)
      REAL K,M,MRT
      COMMON/DATA4/FREQ,SI
      DATA M,T,RK,DELTA,MRT,VO,AC/2.90,0.7506,141.6,
     *0.05,58.63,0.01525,0.0122/
      C1=1.
      FBRK=5.5
      FS=0.
      FCOUL=5.5*C(3)
      VO=0.01525
      MRT=58.63*C(2)
      PA=MRT/VO
C
C     ...LINEARIZATION...
C
      DO 40 J=1,40
      CS=0.
      C1=1.
      LF=1
      K=RK
```

```
      W=4.28*FREQ(J)
      AMP=SQRT(SI(J)*2.)/W**2.
   20 D=((K-M*W**2.)**2.+(W*(C1+CS))**2.)
      Z=(M*AMP*W**2.+AMP*W*CS)/SQRT(D)
      X=SQRT((K**2.+(W*C1)**2.)/D)*AMP
   22 ZFRC=Z*(1.-FCOUL/(M*AMP*W**2.))
      IF(ZFRC.LE.0.)ZFRC=0.
      C2=(C(1)*T*(W*Z*.70711)**2.+FCOUL)/(Z*W*.70711)
      CSOLD=CS
      IF(LF.EQ.0)GO TO 15
      ERR=(C1-C2)
      ERREL=ERR/C2
      C1=ABS(C2+(ERR/2.))
      IF(C1.GE.10.E6)GO TO 15
      IF(ABS(Z).LE.DELTA/1000.) GO TO 15
      IF(D.GE.10.E11)GO TO 15
      IF(ABS(ERREL).LE.DELTA)GO TO 10
      GO TO 20
   10 CONTINUE
      IF(C(2).EQ.0.)GO TO 16
      AK=K
      IF(Z.GE.1.25)GO TO 25
      K=RK+((MRT/(V0-AC*Z*.70711)-PA)-(MRT/(V0+AC*Z*.70711)
     *-PA))*.5*AC/(Z*.70711)
   35 ERR2=ABS(AK-K)
      IF(ERR2.LE.DELTA*10.)GO TO 16
      GO TO 20
   25 Z=1.25
      LF=0
      K=10E4
      PRINT*,'END STOP HIT'
      GO TO 22
   30 ACC(J)=SQRT(SI(J))
      Z=0.
      GO TO 31
   32 ACC(J)=0.
      Z=AMP
      GO TO 31
   15 CONTINUE
   16 CONTINUE
C
C     ...ACCELERATION AND DISPLACEMENT RESPONSE SPECTRA...
C
      ACC(J)=SQRT((K**2.+(W*C1)**2.)*SI(J)/D)
      DISP(J)=M*AMP*W**2./SQRT(2.*D)
   31 CONTINUE
   40 CONTINUE
      RETURN
      END
```

```
C
C     ...THIS PROGRAM USES AN INITIAL VALUE ROUTINE TO OBTAIN
C        THE STOCHASTIC RESPONSE OF A SYSTEM.IT IS USED AS THE
C        'TRUE' RESPONSE FOR COMPARING THE VARIOUS LINEARIZATION
C        METHODS.
C
C     SM : SIMULATED ('TRUE') RESPONSE
C
      PROGRAM SM50
      REAL M,KS,MRT
      DIMENSION YO(2),SO(40),FREQ(40),SI(40),TV(40),X(3),YM(40)
      COMMON/INDATA/M,T,KS,AMP,Y1,Y2,W,FCOUL,MRT,VO,AC
      COMMON/EPCOM9/HUSED,NQUSED,NSTEP,NFE,NJE
      DATA X/0.,0.,1./
      DATA M,T,KS,FCOUL,MRT,VO,AC/2.90,0.7506,141.4,5.5,58.63
     *,0.01525,0.0122/
      OPEN(20,FILE='SM50.DAT',STATUS='NEW')
      OPEN(10,FILE='LBSPC2.DAT',STATUS='OLD')
      AC=AC*X(2)
      T=T*X(1)
      FCOUL=FCOUL*X(3)
      DO 112 K=1,40
      READ(10,*)FREQ(K),SI(K),F
      N=2
      TO=0.
      HO=.001
      EPS=0.0001
      IERR=1
      MF=10
      IND=1
      YO(1)=0.
      YO(2)=0.
      YMAX=0.
      VMAX=0.
      II=1
      W=FREQ(K)*6.28
      AMP=SQRT(2.*SI(K))/W**2.
      TOUT=1./(30.*FREQ(K))
10    Y2DOT=AMP*W**2.
      CALL EDRIV(N,TO,HO,YO,TOUT,EPS,IERR,MF,IND)
      YY=ABS(YO(2))
      VM=ABS(YO(2)-Y2)
      IF(IND.EQ.0)GO TO 65
      PRINT*,IND
      GO TO 60
65    CONTINUE
      TOUT=TOUT+1./(30.*FREQ(K))
      IF(TOUT.LE.5.)GO TO 10
      IF(YY.GE.YMAX)YMAX=YY
      IF(VM.GE.VMAX)VMAX=VM
      TOUT=TOUT-.9/(30.*FREQ(K))
      TMX=5.+.5*II/(FREQ(K))
      IF(TOUT.LE.TMX)GOTO 10
      YM(II)=YMAX
      II=II+1
      YMAX=0.
      IF(II.LT.11)GO TO 10
      DO 55 I=1,II-1
      YMAX=YM(I)/(II-1)+YMAX
55    CONTINUE
      GO TO 60
50    YMAX=AMP*W
      VMAX=0.
60    CONTINUE
      SO(K)=.5*(YMAX*W)**2.
```

```
      TV(K)=YMAX/(AMP*W)
      Z=.70711*ABS(YMAX/W-AMP)
      WRITE(20,*)FREQ(K),SO(K),Z
112   CONTINUE
      WRITE(20,*)'XVEL XSPRG XFCOUL=',X
      STOP
      END
C
CC    ...JACOBIAN (IF REQUIRED)...
C
      SUBROUTINE PEDERV(N,T,Y,PD,NO)
      RETURN
      END
C
CC    DIFFERENTIAL EQUATION...
C
      SUBROUTINE DIFFUN(N,T,Y,YDOT)
      COMMON/INDATA/M,TP,KS,AMP,Y1,Y2,W,FCOUL,MRT,VO,AC
      DIMENSION Y(N),YDOT(N)
      REAL M,KS,MRT,KA
      PA=MRT/VO
      DELTAV=10.E-5
      Y1=AMP*SIN(W*T)
      Y2=AMP*W*COS(W*T)
      IF(ABS(Y2-Y(2)).LT.DELTAV)GO TO 30
      FRIC=FCOUL*(Y(2)-Y2)/ABS(Y2-Y(2))
      GO TO 40
30    FRIC=FCOUL*(Y(2)-Y2)/DELTAV
40    CONTINUE
      Z=Y(1)-Y1
      IF(AC.EQ.0.)GO TO 45
      IF(ABS(Z).GT.VO/AC)Z=VO*ABS(Z)/(Z*AC)
45    CONTINUE
      YDOT(1)=Y(2)
      YDOT(2)=-(TP/M)*(Y(2)-Y2)*ABS(Y(2)-Y2)
     *-(KS/M)*(Y(1)-Y1)-FRIC/M
     *-((MRT/(M*(VO-AC*(Z))-PA/M)))*AC
      FK=KS*(Y(1)-Y1)
      RETURN
      END
```

APPENDIX IV

VALIDATION OF MATHEMATICAL MODELS

A major objective of this investigation is to establish a computer aided design methodology for motorcycle suspensions. The methodology uses mathematical models developed from fundamental engineering principles validated by laboratory testing. Validation is an important aspect of any engineering investigation. In investigations with computer simulation, the degree of credibility of the mathematical models is directly related to the extent that they have been validated.

Validation can be undertaken at various levels. At the lowest level, a qualitative correlation is observed between trends obtained by analytical prediction and experiment. As a typical example, one such trend would be that an increase in orifice area leads to a decrease in damping force. Cooperrider and Law [167] lend credibility to this level of validation:

> 'The value of qualitatively validated analysis should not be underestimated. Such models are invaluable in making design changes and in devising successful experiments because they provide information about the sensitivity of the vehicle behavior to parameter changes, and also provide a framework for interpreting the test results'.

A second level of validation utilizes a limited amount of quantitative results. It typically entails the correlation of a single, usually critical, value from the analysis with results from experiment.

The use of a range of inputs in a variety of operating conditions leads to the highest level of validation. The highest level entails a fairly complete quantitative correlation of analytical and experimental results. Such a validation should include a wide band width in the frequency domain in addition to the comparison of response histories in the time domain. This level of validation is necessary in order to place confidence in the quantities predicted by a mathematical analysis.

In this investigation the peak to peak damper force, measured at mid-stroke, is used to validate the damper force models. An example of the second level of validation in this investigation would be the use of a single excitation amplitude and frequency to validate the damper force models in Tables 3.1 and 3.2. Instead, a range of excitations was used. The degree of credibility of the damper force models, reflected in Tables 3.1 and 3.2 not withstanding qualitative differences in the shape of the F-D diagrams away from midstroke, sufficient confidence was felt for the inclusion of the damper force modeling procedure in the formulation of the suspension system model.

The modeling process is validated throughout the thesis. In addition to the validation presented in Tables 3.1 and 3.2, the modeling process is validated by comparing simulated and experimental time histories for the frequency and time domains as presented in Figs. 4.8 and 4.9. In the frequency domain the close correlation near resonance indicates validated damper behavior. The good correlation at low frequencies validates the seal stiction values. In the time domain the agreement in the transient region validates (indirectly) the damping force whereas the steady-state behavior validates the value of seal stiction. Additional validation is performed after optimization, as presented in Figs. 7.14 and 7.15 and Table 6.3. The close agreement between theory and experiment in all these results validates the modeling procedure to a high level. This validation in the frequency and time domains can be classified as an indirect validation procedure, which is an accepted practice. Cooperrider and Law [167] note, when summarizing techniques for obtaining suspension characteristics:

> '... indirect means for quickly finding suspension charcteristics should be the goals of these developments'.